

Processing Composite Sandwich Structures using Out-of-Autoclave Technology

by

James Kratz

B. Eng., Carleton University, 2007

Department of Mechanical Engineering
McGill University, Montreal

A thesis submitted to
McGill University
in partial fulfillment of the requirements of the degree of
Master's of Engineering



August 2009

© James Kratz 2009

Abstract

Currently, out-of-autoclave (OOA) technology is being used to design and manufacture composite structural components at lower costs. OOA technology enables composites to be produced using only vacuum pressure, eliminating the cost of purchasing and operating an autoclave. The key to OOA prepreg is that they are specially designed to remove air that is entrapped during the lay-up process. The in-plane and through thickness permeability of the prepreg were characterized to determine which bagging configuration would produce the best honeycomb sandwich structure. The bagging configuration that produced the lowest skin porosity was determined to be one ply of non-perforated release film with edge breathing around the perimeter of the panel. The resin content of the prepreg is such that any resin loss from the skin will create dry spots, pinholes, and porosity. The edge breathing allows the air inside the prepreg and core to be removed by the vacuum, and the non-perforated release film presents resin starvation and subsequently reduces porosity. Caution should be used when debulking out-of-autoclave sandwich panels, since removing all the air from the core reduces the amount of skin compaction available during cure. The skin compaction is needed to suppress void growth, and the optimal internal core pressure was experimentally determined to be between 35-55 kPa. The resin was fully characterized such that when the internal core pressure has reached the optimal range, the resin can flow and close off the air passages.

Five representative panels were manufactured using two low temperature cure film adhesives. The optimal curing temperature to minimize porosity of the composite skin was determined to be 100°C. Climbing drum peel tests were used to evaluate the mechanical performance of the panels.

Sommaire

Présentement, la technologie hors autoclave (OOA) est utilisée pour la conception et la fabrication à moindre coût des composants structuraux en composite. La technologie OOA permet de produire des composites en utilisant uniquement la pression générés lors des procédés d'ensachage sous vide, en éliminant par le fait même les coûts relatifs à l'achat et à l'exploitation d'un autoclave. L'avantage des matériaux pré-imprégnés destinés à des cuissons hors autoclave est qu'ils sont spécialement conçus pour éliminer les bulles d'air emprisonnées au cours de la préparation. Afin de déterminer la configuration d'ensachage optimale pour la production de structure en sandwich avec noyau en nid d'abeille, l'épaisseur du matériel pré-imprégné ainsi que la perméabilité à travers le plan ont été caractérisées. Les conditions d'ensachage ayant menées à la plus faible porosité correspondent à l'utilisation combinée d'une couche non perforée de pellicule antiadhésive et d'une bordure permettant l'extraction des produits gazeux. La pellicule antiadhésive non perforée permet de prévenir les pertes de résine, tandis que la bordure permettant l'extraction des produits gazeux permet d'évacuer l'air contenu dans le noyau et les couches pré-imprégnés. L'utilisation d'une pellicule non perforée s'est avérée nécessaire puisque la teneur en résine du matériel pré-imprégné est telle que toute perte de résine crée des régions dites sèches (non imprégnée), produit des trous ou défauts à la surface du laminé et augmente la porosité.

Il convient d'être prudent lors du dégazage des panneaux en sandwich hors autoclave puisque la suppression de tout l'air contenue dans le noyau réduit le niveau de compaction disponible durant la cuisson. L'application d'une force de compaction adéquate doit être effectuée lors de la cuisson afin de réduire la formation de vides à l'intérieur du laminé. Une étude expérimentale a permise déterminer que des résultats optimaux peuvent être obtenus lorsque la

pression interne du noyau se situe entre 35 et 55 kPa. Grâce à une caractérisation complète de la résine, les paramètres du cycle de cuisson ont pu être ajustés de façon à ce que la résine puisse circuler et fermer les passages d'air lorsque la pression interne atteint la fourchette optimale.

Cinq panneaux représentatifs ont été fabriqués en utilisant deux couches de pellicule adhésive à cuisson à basse température. Une température de cuisson de 100 °C a été identifiée comme étant la condition optimale pour minimiser la porosité du composite. À 80 °C, la viscosité de la résine ne permet pas l'imprégnation complète des fibres sèches. De plus, la porosité augmente drastiquement lorsque la cuisson s'effectue à plus de 120 °C. Grâce au test de pelage par tambour ascendant, il a été déterminé que, à 100 °C, l'AF 163 produit un composite de meilleure qualité que le FM300-2 en ce qui a trait au joints entre le laminé et les cellules du noyau en nid d'abeille.

Acknowledgments

I would like to express my gratitude to all those people who supported me through my master's program. I am grateful to my parents, who always provided moral support, and paid my tuition throughout university.

I would like to thank my thesis supervisor, Professor Pascal Hubert, for all the insightful guidance and strong support throughout my master's degree. I truly appreciate the opportunity to work as a part of an exceptional composite research lab.

A big thank you goes to Bombardier Aerospace and Bell Helicopter Textron Canada for donating the materials, and providing financial support for this project. I would like to specifically thank Khassan Mourtazov for going the extra mile to acquire the prepreg and honeycomb core.

I truly appreciate being able to use the machining and testing facilities at Bell Helicopter for the climbing drum peel testing. I would like to thank Phil Barsalou for coordinating this opportunity, and for all the help during the machining and testing.

The guidance I received from Jonathan Laliberté saved me a considerable amount of time and frustration. Thank you for helping machine the permeability fixture, configuring the LabView data acquisition system, and teaching me how to use all the TA Instruments.

I am thankful for the wonderful friendships that I have made with my colleagues in FDA 015. I truly appreciate the private lesson by Dr. Loleï Khoun on how to fit a cure kinetics and rheology model to experimental data. I appreciate the help of Tim Centea with the glass transition temperature model. Finally, I would like to thank Mihran Khachkhechyan and Xavier Gagné Brulotte for helping with the abstract translation.

Table of Contents

ABSTRACT	II
SOMMAIRE	III
ACKNOWLEDGMENTS	V
TABLE OF CONTENTS	VI
LIST OF TABLES.....	IX
LIST OF FIGURES	X
NOMENCLATURE.....	XIII
1 INTRODUCTION.....	1
1.1 RESEARCH OBJECTIVES AND THESIS ORGANIZATION	7
2 LITERATURE REVIEW	9
2.1 OUT-OF-AUTOCLAVE PREPREG	10
2.2 PREPREG AIR PERMEABILITY MEASUREMENTS	15
2.3 INTERNAL CORE PRESSURE OF HONEYCOMB SANDWICH PANELS	18
2.3.1 <i>Prepreg Air Permeability</i>	20
2.4 LITERATURE REVIEW SUMMARY	23
3 RESIN CHARACTERIZATION	25
3.1 MATERIAL	26
3.2 THERMAL STABILITY OF THE MATERIAL	26
3.2.1 <i>Equipment</i>	26
3.2.2 <i>Performance Verification</i>	27
3.2.3 <i>Testing Procedure</i>	28
3.2.4 <i>Results and Discussion</i>	29
3.3 CURE KINETICS	30
3.3.1 <i>Equipment</i>	30
3.3.2 <i>Experimental Procedure</i>	33
3.3.3 <i>Resin Cure Kinetics Model</i>	34

3.4	RHEOLOGY.....	40
3.4.1	<i>Small-Amplitude Oscillatory Shear</i>	40
3.4.2	<i>Equipment</i>	42
3.4.3	<i>Experimental Procedure</i>	45
3.4.4	<i>Experimental Results and Discussion</i>	47
3.4.5	<i>Resin Viscosity Modeling</i>	49
3.5	THE GLASS TRANSITION TEMPERATURE	52
3.5.1	<i>Dynamic Mechanical Analysis</i>	53
3.5.2	<i>Experimental Procedure</i>	55
3.5.3	<i>Experimental Results</i>	56
3.5.4	<i>Glass Transition Temperature Model</i>	57
3.6	SUMMARY	60
4	PREPREG CHARACTERIZATION	61
4.1	PREPREG PERMEABILITY TEST SYSTEM.....	61
4.1.1	<i>Through Thickness Permeability Test Fixture</i>	63
4.1.2	<i>In-Plane Permeability Test Fixture</i>	65
4.1.3	<i>Measurement System Validation</i>	66
4.1.4	<i>Pressure Sensor Calibration</i>	68
4.2	PERMEABILITY TESTING PROCEDURE	69
4.2.1	<i>Through Thickness</i>	70
4.2.2	<i>In-Plane</i>	70
4.3	TEST MATRIX	71
4.3.1	<i>Through Thickness Permeability Tests</i>	72
4.3.2	<i>In-Plane Permeability Tests</i>	72
4.4	PERMEABILITY RESULTS AND DISCUSSION	74
4.4.1	<i>Through Thickness Permeability Results and Discussion</i>	75
4.4.2	<i>In-Plane Permeability Results and Discussion</i>	76
4.5	VOID CONTENT RESULTS AND DISCUSSION	80
4.6	SUMMARY	83
5	REPRESENTATIVE SANDWICH PANELS.....	85
5.1	MATERIALS	85
5.2	TEST MATRIX	86
5.3	SANDWICH PANEL MANUFACTURING PROCEDURE.....	87
5.4	VOID CONTENT ANALYSIS	89

5.5	HOT WATER SUBMERSION TEST.....	91
5.5.1	<i>Results and Discussion</i>	92
5.6	CLIMBING DRUM PEEL TESTING.....	93
5.6.1	<i>Test Coupon Preparation</i>	93
5.6.2	<i>Experimental Procedure</i>	94
5.6.3	<i>Results and Discussion</i>	96
5.7	SUMMARY.....	99
6	CONCLUSION	100
6.1	FUTURE WORK.....	101
	REFERENCES	102
	APPENDIX A – DMA TEST DATA	108
	APPENDIX B – PERMEABILITY TEST DATA	114

List of Tables

TABLE 2.1: COMMERCIALLY AVAILABLE OOA PREPREGS.	11
TABLE 3.1: TGA PERFORMANCE VERIFICATION SUMMARY.....	28
TABLE 3.2: THERMAL STABILITY TEST MATRIX	29
TABLE 3.3: MTM45-1 CURE KINETICS TEST MATRIX	33
TABLE 3.4: PERFORMANCE VERIFICATION SUMMARY	44
TABLE 3.5: RHEOLOGY TEST MATRIX	45
TABLE 3.6: GLASS TRANSITION TEMPERATURE TEST MATRIX.....	56
TABLE 4.1: THE THROUGH THICKNESS TEST MATRIX.....	72
TABLE 4.2: IN-PLANE PERMEABILITY TEST MATRIX	74
TABLE 4.3: IN-PLANE PERMEABILITY TEST RESULTS	78
TABLE 4.4: COMPARISON OF THROUGH THICKNESS AND IN-PLANE PERMEABILITY	84
TABLE 5.1: SANDWICH PANEL TEST MATRIX	86
TABLE 5.2: SUMMARY OF HOT WATER SUBMERSION TESTS	93
TABLE 5.3: REPRESENTATIVE PANEL PROPERTIES.....	97

List of Figures

FIGURE 1.1: FULLY IMPREGNATED CONVENTIONAL PREPREG LAYED-UP ON A TOOL WITH ENTRAPPED AIR. [1].....	2
FIGURE 1.2: SCHEMATIC OF A LAYUP AND KEY VACUUM BAG CONSUMABLES [3].....	2
FIGURE 1.3: SCHEMATIC OF THE AUTOCLAVE COMPONENTS [3].	3
FIGURE 1.4: TWO PLYS OF OOA PREPREG SHOWING THE UN-IMPREGNATED FIBRES WHICH CREATE THE EVACUATION CHANNELS. [2]	4
FIGURE 1.5: THE SCALED COMPOSITES SPACESHIPONE AND WHITEKNIGHTONE [5].....	5
FIGURE 1.6: COMMON MATERIALS USED TO FABRICATE A COMPOSITE HONEYCOMB STRUCTURE [6].....	6
FIGURE 2.1: TWO PLYS OF EVAC AND OST PREPREG. [2]	12
FIGURE 2.2: SCHEMATIC OF HOW ENTRAPPED AIR IS EVACUATED WITH EDGE BREATHING. [2]	13
FIGURE 2.3: A PLY OF ACG’S ZPREG [15].	14
FIGURE 2.4: A PLY OF GURIT’S SPRINT MATERIAL. [28]	15
FIGURE 2.5: FALLING PRESSURE APPROACH TO MEASURING THE PERMEABILITY OF A POROUS MEDIUM.	16
FIGURE 2.6: EXPERIMENTAL SET-UP FOR MEASURING THE THROUGH THICKNESS AIR PERMEABILITY DURING PROCESSING CONDITIONS. [8]	18
FIGURE 2.7: FREE BODY DIAGRAM OF THE PRESSURE DIFFERENTIAL IN HONEYCOMB SANDWICH PROCESSING.	19
FIGURE 2.8: PROCESSING CONDITIONS UNDER INVESTIGATION.	20
FIGURE 2.9: FLOW CHART OF THE RESEARCH PRESENTED IN THIS THESIS.	24
FIGURE 3.1 THE THERMAL GRAVIMETRIC ANALYZER.	27
FIGURE 3.2: TGA PERFORMANCE VERIFICATION WITH CALCIUM OXALATE.....	28
FIGURE 3.3: THERMAL STABILITY OF THE MTM45-1 RESIN.	29
FIGURE 3.4: DSC (RIGHT), AND A CUTAWAY OF THE Q100 DSC CELL (LEFT) [39].	31
FIGURE 3.5: BASELINE VERIFICATION OF THE DSC BEFORE AND AFTER CLEANING AND CALIBRATION.....	32
FIGURE 3.6: HEAT FLOW FROM A DYNAMIC SCAN AT 20°C/MIN UP TO 250°C.....	34
FIGURE 3.7: ARRHENIUS PLOT TO DETERMINE THE ACTIVATION ENERGY E_a	37
FIGURE 3.8: ISOTHERMAL PROGRESSION OF THE CURE RATE WITH INCREASING DEGREE OF CURE FOR MTM45-1. THE EXPERIMENTAL DATA (SYMBOLS) IS COMPARED WITH THE MODEL PREDICTIONS (CONTINUOUS LINES).	37
FIGURE 3.9: THE EVOLUTION OF THE DEGREE OF CURE DURING THE CURE CYCLE. THE EXPERIMENTAL DATA (SYMBOLS) IS COMPARED WITH THE MODEL PREDICTIONS (CONTINUOUS LINES).	38
FIGURE 3.10: ISOTHERMAL SCAN AT 120°C.	39
FIGURE 3.11: TEMPERATURE CYCLE GUIDELINE.	39
FIGURE 3.12: DYNAMIC RESPONSE OF A VISCOELASTIC MATERIAL [42].	41
FIGURE 3.13: THE COMPLEX MODULUS COMPOSED OF THE STORAGE AND LOSS MODULUS [43].	42

FIGURE 3.14: RHEOMETER WITH CLOSE-UP OF THE PARALLEL PLATE GEOMETRY.	43
FIGURE 3.15: OSCILLATORY FREQUENCY SWEEP WITH PDMS.	44
FIGURE 3.16: OSCILLATORY STRESS SWEEP OF MTM45-1.	47
FIGURE 3.17: DYNAMIC VISCOSITY RESPONSE OF MTM45-1.	48
FIGURE 3.18: ISOTHERMAL VISCOSITY RESPONSE OF MTM45-1.	48
FIGURE 3.19: ISOTHERMAL VISCOSITY RESULTS FOR MTM45-1. THE EXPERIMENTAL DATA (SYMBOLS) IS COMPARED TO THE MODEL PREDICTIONS (CONTINUOUS LINES).	51
FIGURE 3.20: DYNAMIC VISCOSITY RESULTS FOR MTM45-1. THE EXPERIMENTAL DATA (SYMBOLS) IS COMPARED TO THE MODEL PREDICTIONS (CONTINUOUS LINES).	51
FIGURE 3.21: DSC AND DMA PLOTS TO DETERMINE THE T_g OF A GLASS REINFORCED EPOXY [46].	52
FIGURE 3.22: RECTANGULAR SPECIMEN INSTALLED IN THE 3-POINT BENDING FIXTURE OF THE DMA.	54
FIGURE 3.23: DMA TEST AT 2°C/MIN OF 2 PLYS OF MTM45-1/CF2426A, ORIGINALLY CURED AT 120°C.	56
FIGURE 3.24: EVOLUTION OF THE ONSET OF THE GLASS TRANSITION TEMPERATURE.	57
FIGURE 3.25: COMPARISON OF THE T_g MODEL AND THE EXPERIMENTAL DATA.	58
FIGURE 3.26: CURE CYCLE WITH POST CURE AT RAMP RATE OF 0.5°C/MIN, PREVENTING PART DISTORTION.	59
FIGURE 3.27: CURE CYCLE WITH POST CURE AT RAMP RATE OF 2°C/MIN THAT WILL LEAD TO PART DISTORTION.	60
FIGURE 4.1: EXPERIMENTAL SET-UP SCHEMATIC.	62
FIGURE 4.2: THROUGH THICKNESS CORE PRESSURE MEASUREMENT TEST SCHEMATIC.	63
FIGURE 4.3: CLOSE-UP OF THE PREPREG AND SEALANT TAPE PRE-TEST.	64
FIGURE 4.4: CLOSE-UP OF THE ½ SANDWICH POST-TEST.	65
FIGURE 4.5: IN-PLANE CORE PRESSURE MEASUREMENT TEST SCHEMATIC.	66
FIGURE 4.6: JIG LEAK TEST USING SHEET METAL IN PLACE OF PREPREG.	67
FIGURE 4.7: LEAK TEST PERFORMANCE VERIFICATION OF THE PRESSURE POTS.	68
FIGURE 4.8: PRESSURE TRANSDUCER CALIBRATION SET-UP.	69
FIGURE 4.9: THE PERMEABILITY FIXTURE CONFIGURED FOR THROUGH THICKNESS TESTING.	70
FIGURE 4.10: THE PERMEABILITY FIXTURE AFTER AN IN-PLANE TEST.	71
FIGURE 4.11: THROUGH THICKNESS AIR PERMEABILITY TEST OF 4 PLYS OF MTM45-1/CF2426A, 1 PLY OF RELEASE FABRIC, AND FULL VACUUM APPLIED AT ROOM TEMPERATURE.	76
FIGURE 4.12: IN-PLANE AIR PERMEABILITY TEST OF 4 PLYS OF MTM45-1/CF2426A WITHOUT EDGE BREATHING, 2 PLYS OF P3 RELEASE FILM, AND FULL VACUUM APPLIED AT ROOM TEMPERATURE.	77
FIGURE 4.13: AN IN-PLANE PERMEABILITY TEST OF 4 PLYS OF MTM45-1/CF2426A WITH EDGE BREATHING, 2 PLYS OF P3 RELEASE FILM, AND FULL VACUUM APPLIED AT THE START OF THE DWELL.	77
FIGURE 4.14: ROOM TEMPERATURE DEBULKING IN-PLANE PERMEABILITY RANGES.	80
FIGURE 4.15: PROCESS FLOW FOR THE IMAGE ANALYSIS OF THE COMPOSITE SKIN.	81
FIGURE 4.16: VOID CONTENT AS A FUNCTION OF THE INTERNAL CORE PRESSURE.	82

FIGURE 4.17: THE RELATIONSHIP BETWEEN THE RESIN CHARACTERIZATION, PREPREG PERMEABILITY, AND THE FINAL PART PERFORMANCE OF THE SANDWICH STRUCTURE.	84
FIGURE 5.1: THE STEPS IN THE SANDWICH STRUCTURE LAYUP PROCESS.	88
FIGURE 5.2: REPRESENTATIVE SANDWICH PANEL (LEFT), SHOWING THE MICROSCOPY LOCATIONS, AND THE FIBRE AND RIBBON DIRECTIONS (RIGHT).....	89
FIGURE 5.3: VOID CONTENT IN THE SKIN OF THE SANDWICH PANELS.	90
FIGURE 5.4: CROSS SECTION OF THE BAG SIDE IN THE CENTRE OF PANEL 1, SHOWING THE RESIN RICH REGIONS BETWEEN THE FIBRE TOWS.	91
FIGURE 5.5: CROSS SECTION OF THE BAG SIDE IN THE CENTRE OF PANEL 5, SHOWING THE VOIDS.....	91
FIGURE 5.6: HOT WATER SUBMERSION TEST SETUP.	92
FIGURE 5.7: CLIMBING DRUM PEEL TEST SETUP.	95
FIGURE 5.8: COMPLETED CLIMBING DRUM PEEL TEST.	95
FIGURE 5.9: TYPICAL CLIMBING DRUM PEEL TEST DATA.	96
FIGURE 5.10: THE AVERAGE AND ONE STANDARD DEVIATION OF THE CLIMBING DRUM PEEL TESTS.	97
FIGURE 5.11: EXAMPLE OF CORE FAILURE AND ADHESIVE FAILURE FROM THE SAME DRUM PEEL COUPON.	98

Nomenclature

A	Cross-sectional area
A	Arrhenius constant
A	Viscosity constant
A_{μ}	Viscosity constant
B	Viscosity constant
C	Cure kinetics diffusion constant
dH/dt	Heat flow
dP/dx	Pressure gradient
E_A	Activation energy
E_{μ}	Viscosity activation energy
G'	Storage modulus
G''	Loss modulus
G^*	Complex modulus
H_I	Isothermal heat of reaction
H_R	Residual heat of reaction
H_T	Total heat of reaction
K	Permeability
m	Cure kinetics material constant
n	Cure kinetics material constant
P_1	Instantaneous pressure on the high pressure side
$P_{1,i}$	Initial pressure on the high pressure side
P_2	Instantaneous pressure on the low pressure side
P_{bag}	Vacuum pressure on the bag side of the prepreg skin
P_{cell}	Internal core pressure
Q	Volumetric flow rate
R	Universal gas constant
t	Time
T	Absolute temperature

T_g	Glass transition temperature
T_{g0}	Glass transition temperature of the uncured resin
$T_{g\infty}$	Glass transition temperature of the fully cured resin
V_1	Volume of the high pressure side
α	Degree of cure
α_g	Degree of cure at gelation
α_{c0}	Critical degree of cure at absolute zero temperature
α_{cT}	Critical resin degree of cure with temperature
$d\alpha/dt$	Cure rate
δ	Phase angle
γ	Strain amplitude
λ	Glass transition temperature constant
μ	Viscosity
η^*	Complex viscosity
ω	Frequency
τ	Shear stress

1 Introduction

Composite materials have been used to manufacture aircraft structures since the mid-1970s. The popularity of composites has only increased due to their high strength and stiffness to weight ratios, allowing manufacturers to reduce the weight of their aircraft. A composite is a material comprised of two or more chemically different materials; however, the majority of aerospace composites are fibre reinforced plastics [1]. Carbon fibres are predominantly used as the reinforcement material, and an epoxy matrix is used to maintain the shape of the composite part. The fibre reinforcement is usually supplied to the manufacturer pre-impregnated with the epoxy resin, this is known as prepreg.

Whereas metals are supplied as standard shapes, and then machined into the desired component, composites allow for integrated manufacturing. The prepreg is cut to the desired shape, stacked, placed on a tool (mould), and then cured at elevated temperature, under pressure. The mechanical and physical properties of the composite are determined during processing, and are governed by the number of plies, the orientation of these plies, and the cure cycle. This is advantageous because the composite structure can be highly optimized, the part count can be decreased, and the number of manufacturing steps reduced [1]. However, since the properties of the material are dependent on the process, this requires manufacturers to understand how the material behaves throughout the manufacturing process.

The three major steps in the manufacturing process are the layup, vacuum bagging, and curing of the composite part. The layup consists of stacking

the prepreg layers onto the mould. During the layup, air is entrapped between the plies (Figure 1.1). Conventional prepreg shown in Figure 1.1, is fully impregnated, making it difficult to remove the entrapped air. Major air pockets are removed from the skin by debulking (applying vacuum pressure) the prepregs stack every 3-5 plies [1]. Any residual air is removed by the vacuum bag, or dissolved into the resin by the compaction pressure during cure [1].

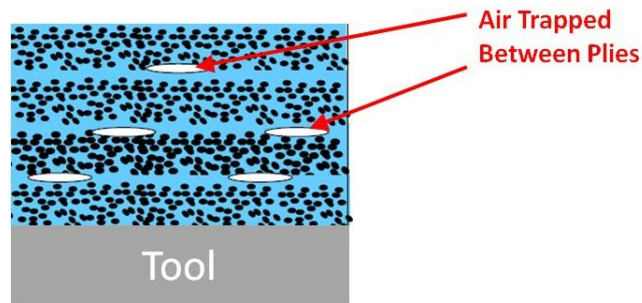


Figure 1.1: Fully impregnated conventional prepreg layed-up on a tool with entrapped air. [1]

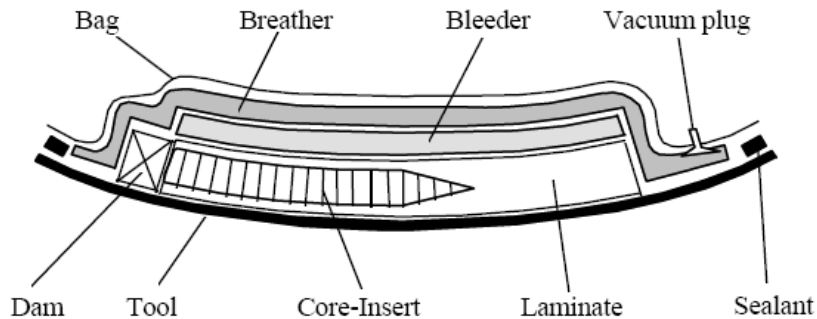


Figure 1.2: Schematic of a layup and key vacuum bag consumables [3].

When the layup is complete, a vacuum bag is installed. The term vacuum bag refers to the consumable materials that are placed over the prepreg stack, not just the nylon vacuum bagging film. A typical autoclave cure vacuum bag is shown in Figure 1.2. Directly above the prepreg stack is a bleeder. The bleeder is used to absorb excess resin [1]. If the prepreg is a no-bleed system (no excess resin), a release film can be used instead of the bleeder either to restrict the resin

flow or to allow a specified percentage of resin to be absorbed by the breather. The breather provides an air path for entrapped air and any volatiles that are released during the cure cycle. Furthermore, the breather serves to evenly distribute vacuum pressure, and prevent any bag wrinkling from appearing on the bag side surface of the composite part [1]. Finally, the vacuum bag is secured to the tool using sealant tape, and a vacuum plug is used to connect the vacuum source to the bag. With the vacuum bag in place, the composite part is cured. The cure cycle involves heating the resin under an applied pressure. As the temperature increases, the viscosity decreases allowing the resin to flow into any un-impregnated regions. After a period of time, the cross-linking of the resin overpowers the viscosity, and the resin behaves like a gel (which means the resin cannot flow). It is important to maintain good pressure in order to achieve a high fibre volume fraction and low void content in the composite part. The conventional approach to applying pressure and heat is to use an autoclave – a pressurized oven (Figure 1.3).

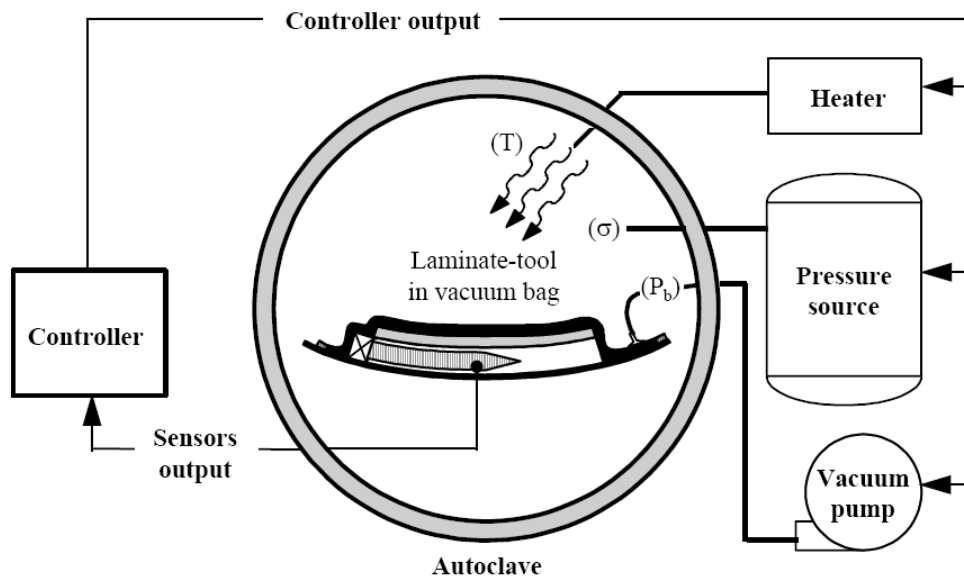


Figure 1.3: Schematic of the autoclave components [3].

Composite parts cured inside an autoclave have excellent quality. The fibre volume fraction is usually optimal, and the void content is low. However, this quality comes with a high price tag. There exists a large infrastructure investment and operating cost for the autoclave. Due to the large cost acquisition cost of an autoclave, composite parts are sized to fit inside the autoclave. In order to build large composite structures, such as a wing or a fuselage, smaller parts are manufactured and then assembled; this extra step is expensive and time consuming. Vacuum pressure and ovens have no size constraint, and therefore can be used to build large, one-piece, composite structures.

Recent developments in prepreg technology have led to the development of an out-of-autoclave (OOA) prepreg that can be cured with only vacuum pressure, compared to 6-7 bar of positive pressure in an autoclave. The OOA prepreg is capable of removing air that is entrapped during the lay-up process because the prepreg is partially impregnated, as shown in Figure 1.4. The partial impregnation creates a porous medium, termed evacuation (EVaC) channels, which will remove any entrapped air before the resin becomes liquid and infuses the fibres [2]. Unlike autoclave curing, the air must be removed during vacuum bag curing because the reduced consolidation pressure cannot dissolve all the air; the maximum possible pressure is 1 bar.

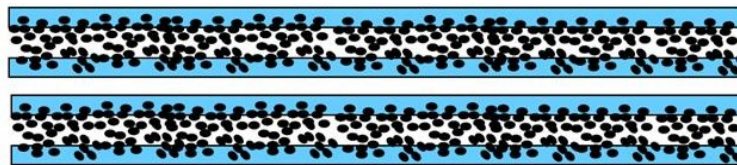


Figure 1.4: Two plies of OOA prepreg showing the un-impregnated fibres which create the evacuation channels. [2]

The cost to manufacture high quality composite parts will be significantly reduced if an equivalent performance can be achieved with OOA prepreg, vacuum pressure, and an oven. One area where OOA prepreg has successfully

been used is in prototype manufacture. Autoclave tooling must maintain their shape in the high temperature and pressure environment of an autoclave. The high cost of purchasing and machining tooling cannot be amortized over multiple parts with prototypes. OOA prepreg can be cured at lower temperatures, allowing for the use of low cost wood or polymer based tooling [4]. An example of an aircraft fabricated with OOA prepreg and vacuum bag curing is the 2004 Ansari X-prize winner, SpaceShipOne and WhiteKnightOne shown together in Figure 1.5, built by Scaled Composites [5].



Figure 1.5: The Scaled Composites SpaceShipOne and WhiteKnightOne [5].

Honeycomb structures are commonly used to reduce weight in fuselage panels, and aerodynamic surfaces on aircraft. A composite skin is bonded to both sides of the honeycomb, usually with the aid of a film adhesive, as shown in Figure 1.6. The film adhesive is an extra layer of resin, usually designed with a higher fracture toughness than the prepreg resin, and it forms a fillet at the cell walls. Ideally, the perimeters of the honeycomb cells are directly in contact with the prepreg skins, and are not separated by a layer of resin. With autoclave cure, the prepreg skins were commonly pre-cured prior to bonding, to prevent the skin

from dimpling due to the high autoclave pressures. The lower consolidation pressure used with OOA prepreg and vacuum bag curing reduce the possibility of skin dimpling, and allow for the honeycomb structure to be cured in one manufacturing step.

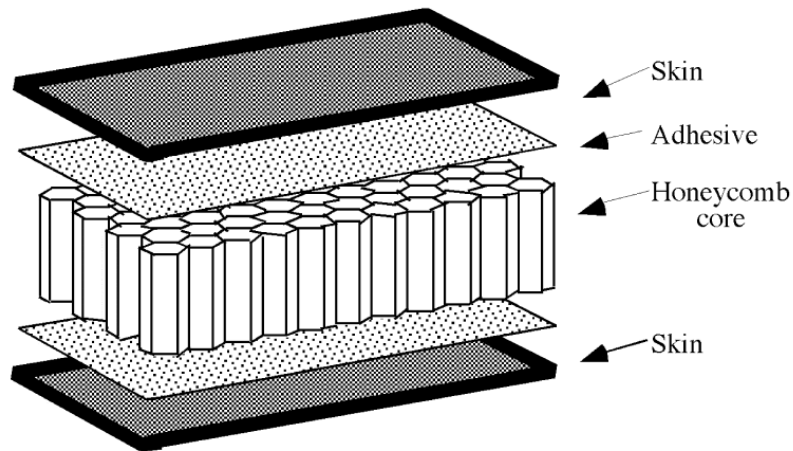


Figure 1.6: Common materials used to fabricate a composite honeycomb structure [6].

When manufacturing sandwich structures with a honeycomb core, an additional volume of air is present. Depending on the cell size and density of the honeycomb core, it can be comprised of 90-98% air [7]. The air can have a dramatic impact on the resulting part quality. For example, if the air remains entrapped in the core, it will expand upon heating, and cause the composite skin to lift off the honeycomb core, reducing the fracture toughness between the skin and core [8]. On the other hand, if all the air is removed from the core, the porosity of the composite skin will increase. The internal core pressure will determine the skin compaction pressure, which if insufficient, has been observed to cause voids in vacuum bag laminates [9]. Given this, an optimal internal core pressure exists to provide the sufficient skin compaction, and ensure a high quality bond between the skin and core.

1.1 Research Objectives and Thesis Organization

In light of the potential cost savings associated with OOA technology, this research project was conceived. The objective of this research project is twofold. The first objective is to understand the critical parameters which affect sandwich structure quality. The second objective is to determine if OOA technology can be used to manufacture a composite sandwich structure with equivalent quality to the autoclave technique. In order to achieve these objectives, a fundamental approach was used to characterize the resin and prepreg. With a solid understanding of the material behaviour, representative sandwich panels were constructed to evaluate the skin quality and mechanical performance. The thesis is organized in the following chapters:

Chapter 2: A review of the current literature on prepreg air permeability is presented. The relationship between the internal core pressure and the final part quality is discussed. Finally, the processing variables which effect sandwich structure quality are explored.

Chapter 3: The thermochemical and rheological behaviour of the resin are characterized. A cure kinetics model was developed, which serves as the basis for the viscosity and glass transition temperature models. Mathematical relations are presented, which describe the state of the resin after any time-temperature history.

Chapter 4: The air permeability of the prepreg is characterized for different processing conditions, such as vacuum pressure, cure cycle, and bagging arrangement. A test fixture was designed and manufactured to measure the air permeability of the prepreg to identify how the processing variables influence part quality. The internal core pressure during cure is related to the porosity of the sandwich skin.

Chapter 5: The outcome of the tests described in Chapter 4 were used to design cure cycles to manufacture representative sandwich structures. The representative structures were inspected for quality, and

mechanically tested according to standard test methods to determine their performance.

Chapter 6: The conclusions of this research project are presented, along with proposed future work which could further expand on the knowledge gained during this research.

2 Literature Review

Out-of-Autoclave (OOA) prepregs are a relatively new class of materials. The first commercially available OOA prepreg system came to market in the early 2000's [2]. The major difference between OOA prepreg and conventional autoclave prepreg is the selective impregnation, increasing the permeability of the prepreg. The increased permeability allows entrapped air to be removed. The benefit of characterizing the in-plane permeability of autoclave prepreg used to manufacture monolithic and sandwich laminates was the subject of many papers from the Polymeric Composites Laboratory in the Department of Chemical Engineering at the University of Washington in the 1990's. Despite their success improving the quality of autoclave cured composites, no prepreg permeability investigations arose in the literature until the mid 2000's. In 2007, a group from Ecole Polytechnique Fédérale de Lausanne (EPFL) studied the through thickness permeability of a marine OOA prepreg. The prepreg was used to build one-piece composite sandwich hulls for racing yachts.

This chapter summarizes the literature available on OOA sandwich structures. First, the different types of commercially available OOA prepregs will be summarized. Second, the technique used to characterize the air permeability of prepregs will be presented. Third, the effect of different processing parameters on the quality of honeycomb sandwich structures will be outlined. Finally, this chapter will conclude with a short summary of the current literature, and describe where this research contributes to the literature.

2.1 Out-of-Autoclave Prepreg

A significant effort has led to the development of out-of-autoclave (OOA) prepregs in recent years [2, 4, 10-15]. The two distinct features of OOA prepreg are the partial impregnation of the fibre reinforcement, and a low temperature curing resin. The OOA prepreg is initially cured at low temperatures until sufficient resin strength is developed in order to ensure that the part can be de-moulded without being damaged. Once de-moulded, a freestanding postcure at higher temperatures is required to fully develop the physical and mechanical properties of the resin. This technique was successfully used by the marine and wind turbine industries to manufacture large, one-piece composite boat hulls and wind turbine blades [15].

The aerospace industry has observed the potential of OOA technology, and many material suppliers have responded with the development of aerospace grade OOA prepregs. A summary of the commercially available OOA prepregs is presented in Table 2.1. Included in the summary table is the cure temperature range of the material system, the wet and dry glass transition temperature (T_g), and the method used to measure the wet and dry T_g . The T_g is commonly used to compare the performance of different resin systems, and to select a resin for a specific application. The T_g is the maximum operating temperature of the resin in certain conditions. The dry T_g is measured without moisture, and the wet T_g is measured after the sample has been conditioned with moisture. For example, ACG MTM 45-1 and MTM 46 have the same cure temperatures, and dry T_g , but the MTM 46 resin is more susceptible to moisture ingress because of a lower wet T_g . However, MTM 46 has an out life six times greater than MTM 45-1, so storage complexities can be reduced for a reduction in wet resin performance [16]. Many factors contribute to the selection of a resin system, and Table 2.1 should only be considered a summary of the available OOA resin systems, and a comparison of one physical property – the T_g . The reported T_g was measured by the manufactures using either the DMA (Dynamic Mechanical Analysis) or TMA

(Thermal Mechanical Analysis) method. The ACG MTM 45-1 was selected for this work because it is part of a shared materials database.

Table 2.1: Commercially available OOA prepregs.

Material Supplier	Resin System	Cure Temp (°C)	T _g Wet (°C)	T _g Dry (°C)	Method	Ref
ACG	MTM 44-1	130-180	150	190	DMA Onset	[17]
	MTM 45-1*	80-180	150	190	DMA Onset	[18]
	MTM 46	80-180	130	190	DMA Onset	[16]
	VTM 260	65-120	-	100	DMA Onset	[19]
Cytec	Cycom 5215*	66-177	166	180	DMA Onset	[19]
	Cycom 5320	93-177	154	-	DMA Onset	[20]
	Cycom 754	50-90	-	118	Unspecified	[22]
Gurit	EP142-C510-50	100-180	-	196	TMA**	[23]
	SPRINT ST 95	85-125	-	123	DMA**	[23]
Hexcel	M36	130-180	-	211	DMA**	[25]
	M9	85-150	-	135	DMA**	[26]

* NCAMP Qualification Program Material

** The specific technique used to evaluate the T_g is not reported

In an effort to reduce material characterization costs, NASA, the FAA, and the aerospace industry have collaborated to develop a materials database on five resin systems. Of the five resin systems, there are two OOA prepreg systems, ACG MTM45-1 and Cytec 5215. The NCAMP (National Center for Advanced Materials Performance) qualification program allows companies to fabricate test panels and the results are collected by NCAMP. The results are available in a shared materials database. Since OOA materials are part of this database, it shows that industry is moving towards OOA composite manufacturing.

OOA prepreg with vacuum bag cure is very similar to the resin film infusion (RFI) process. In RFI, a layer of resin film is placed beneath a layer of dry reinforcement, vacuum and heat are applied, and the liquid resin flows through

the reinforcement. With OOA prepregs, the resin infusion process is started by the prepreg manufacturer, and is completed by the end user without having to handle dry reinforcement and resin film layers. In the two most common types of prepreg, hot resin is melted onto the reinforcement surface to create a partially infused two side tacky, or one side tacky prepreg, as shown in Figure 2.1.

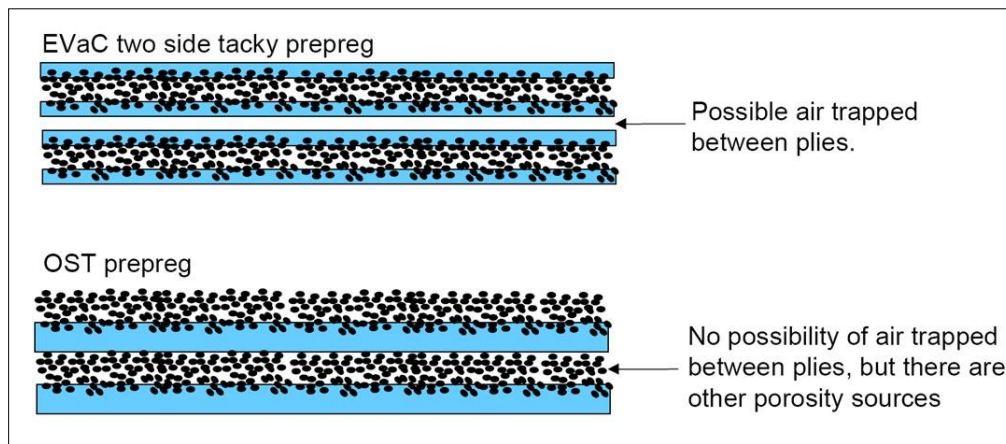


Figure 2.1: Two plies of EVaC and OST prepreg. [2]

The un-impregnated regions of the two side tacky prepreg have been termed Engineered Vacuum Channels (EVaC) by the prepreg industry [2]. The EVaC channels create a vacuum in the centre of the prepreg, allowing any entrapped air between the plies to diffuse through the matrix and be extracted by the vacuum, as shown in Figure 2.2. The ease with which the air can travel into these EVaC channels depends on the viscosity of the resin and the air flow path. As the temperature increases, the resin softens, allowing entrapped air to flow with greater ease into the EVaC channels. However, if the viscosity becomes sufficiently low, the resin will flow into the EVaC channels, blocking the air removal path. This will result in a composite part with a high void content.

The effectiveness of the EVaC channels can be increased by using edge breathing. An impermeable release film is usually placed on top of the prepreg

stack to prevent the consumables from sticking to the composite part. This release film severely restricts the air flow in the through thickness direction. In light of this, edge breathing must be used with an appropriately sized dam to remove the entrapped air in the in-plane direction (Figure 2.2). The dam (tacky tape) is placed at the same height as the laminate to prevent the pinching of the air paths of the top plies of the the laminate. If the corners are pinched or rounded, the air breathing through the edges will be impeded [2].

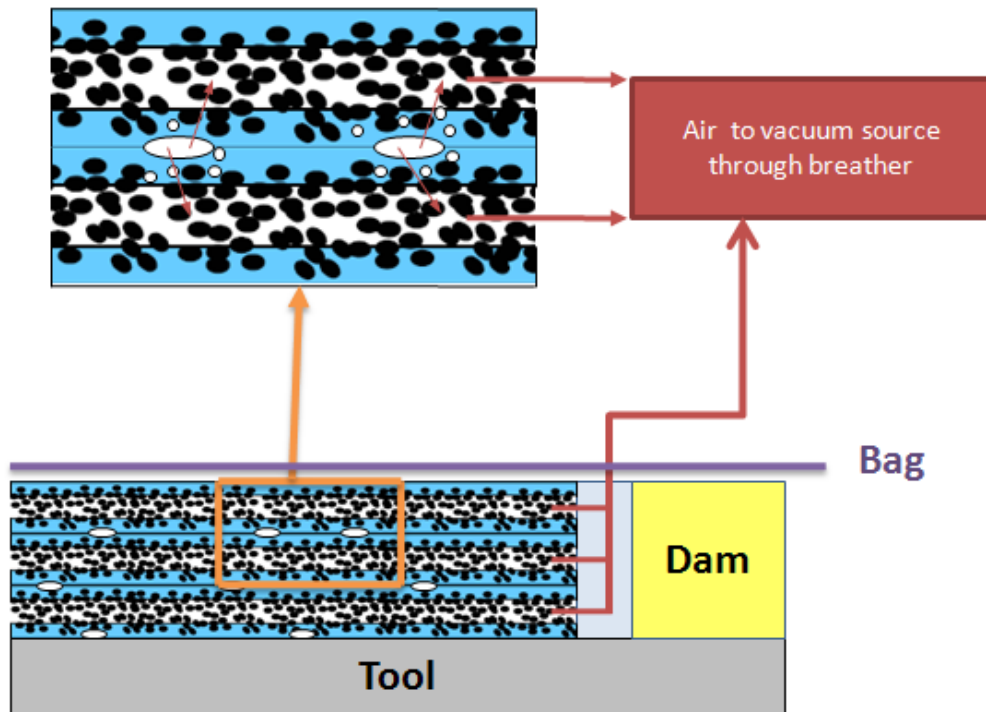


Figure 2.2: Schematic of how entrapped air is evacuated with edge breathing. [2]

All OOA preregs share the partial impregnation, but the method of selective impregnation depends on the supplier. The most common selective impregnation technique is two side tacky, but the Advanced Composites Group (Heanor, Derbyshire, UK) and Gurit (Newport, Isle of Wight, UK) have developed patented techniques. The Advanced Composites Group (ACG) developed the alternative prepreg impregnation technique known as Zpreg[®]. Here, the resin is applied as a series of parallel stripes between two layers of dry fabric

reinforcement, as shown in Figure 2.3. The dry areas in the reinforcement facilitate air extraction in the in-plane, and through thickness directions. During cure, the elevated temperature and vacuum pressure complete the consolidation because the resin viscosity becomes very low, and the resin stripes flow in a controlled manner [15]. One problem with the Zpreg® technology is that very reactive resins can gel too quickly, or toughened resins will not reach a sufficiently low viscosity. In both cases the resin is unable to completely wet-out the fabric [15]. Another issue with Zpreg® arises during the manufacturing of sandwich structures. When Zpreg® is placed directly over a honeycomb core, the resin can flow into the honeycomb cells without fully impregnating the fabric, and create dry spots in the sandwich skin [27].

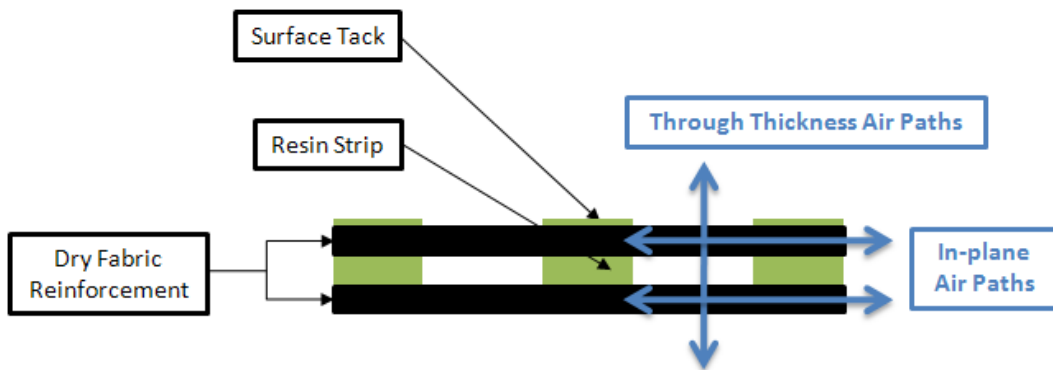


Figure 2.3: A ply of ACG's ZPREG [15].

Gurit has developed a material system, known as SPRINT, where a layer of fibre reinforcement is placed on either side of a resin film [28]. A schematic of the SPRINT material is shown in Figure 2.4, and similar to other OOA prepregs, the dry regions allow for easy air removal from the material stack. A light surface tack is applied to one side of both the ZPREG and SPRINT materials to ensure the material stays in place on the mould, and during the layup process.

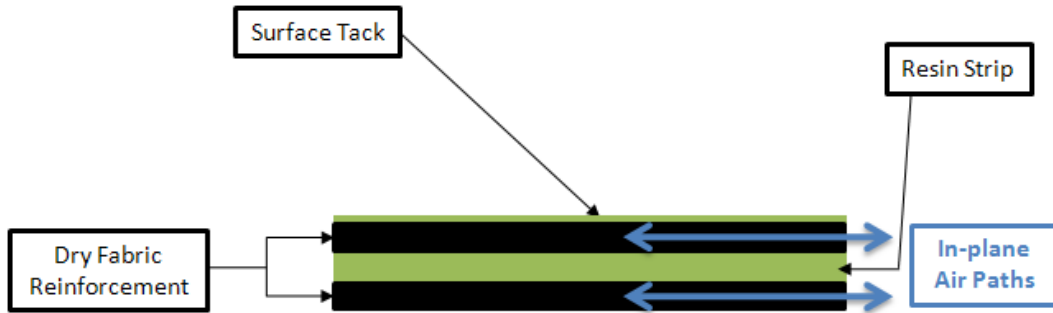


Figure 2.4: A ply of Gurit's SPRINT material. [28]

2.2 Prepreg Air Permeability Measurements

The importance of prepreg air permeability was originally considered for autoclave processing of laminates [29-32]. The usefulness of permeability measurements is described as “a simple technique to describe the ability of the prepreg to vent off volatiles during the consolidation and curing processes, and higher air permeation may result in the production of void free composites [29].” The ability of the prepreg to vent-off volatiles and entrapped air becomes even more important during the debulking of a prepreg stack to be cured with only vacuum pressure. The size of the composite part will determine the length of time required to remove the air from the prepreg stack and honeycomb core. The degree of impregnation of the fibre reinforcement will affect the air passages in the prepreg. These air passages will allow air flow, and therefore the air permeability of the prepreg can be determined. The permeability K is most often described by Darcy's law:

$$Q = \frac{KA}{\mu} \frac{dP}{dx} \quad (2.1)$$

Where Q is the volumetric flow rate, μ is the viscosity of the moving fluid (air in this case), A is the cross-sectional area through which the flow travels, and

dP/dx is the pressure gradient. Using a falling pressure approach, the air will travel from the high pressure side to the low pressure side of the porous medium as shown in Figure 2.5.

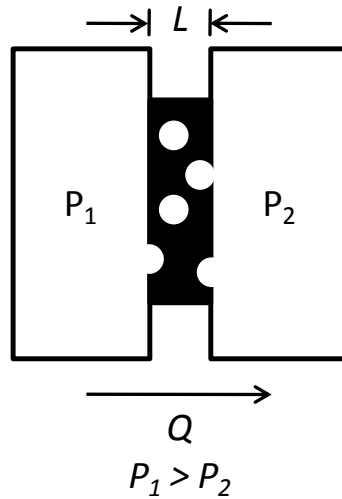


Figure 2.5: Falling pressure approach to measuring the permeability of a porous medium.

Previous studies conducted on the permeability of prepreg have led to the development of the following semi-empirical relation [8, 29-33]:

$$\ln \left[\frac{(P_2 + P_{1,i})(P_2 - P_1)}{(P_2 - P_{1,i})(P_2 + P_1)} \right] = \frac{KAP_2}{LV_1\mu} t \quad (2.2)$$

where P_2 is instantaneous pressure on the side of the porous medium at lower pressure, P_1 is instantaneous pressure on the side of the porous medium at higher pressure, $P_{1,i}$ is the initial pressure on the high pressure side, V_1 is the volume of the high pressure side, and t is the time. If the permeability is measured at elevated temperatures, the viscosity of the air can be described by Sutherland's law:

$$\mu = 1.71 \times 10^{-5} \frac{kg}{m \cdot s} \left(\frac{T}{273 K} \right)^{\frac{3}{2}} \left(\frac{383.4 K}{T + 110.4 K} \right) \quad (2.3)$$

where T is the temperature of the air in Kelvin.

Tavares et al. developed an air permeability test fixture to measure the through thickness permeability of ACG VTM 264 vacuum cure unidirectional prepreg during processing conditions [8]. A schematic of the experimental set-up is shown in Figure 2.6. The mould was made from steel with a 3cm deep cavity where the honeycomb core would rest. The prepreg skin was placed over the core, and extended onto the mould surface. A sealant was used between the first ply and the metallic tool, and a polyimide tape was used to seal the edges of the skin to ensure all the air passed through the thickness of the prepreg. The permeability measurements included all the consumables that would be used while curing the prepreg. In order to determine the air permeability a vacuum pump applied a constant pressure on the same side of the skin as the consumables. Meanwhile, the pressure on the core side of the prepreg decreased at a constant rate that depended on the permeability of the prepreg. In order to repeat or extend the test, the vacuum pump was turned-off and a valve was opened to allow air into the core side of the prepreg, and the pump restarted as soon as the valve was closed [8]. Difficulties were observed with the pressure measurements during the opening of the valve to extend the test [8].

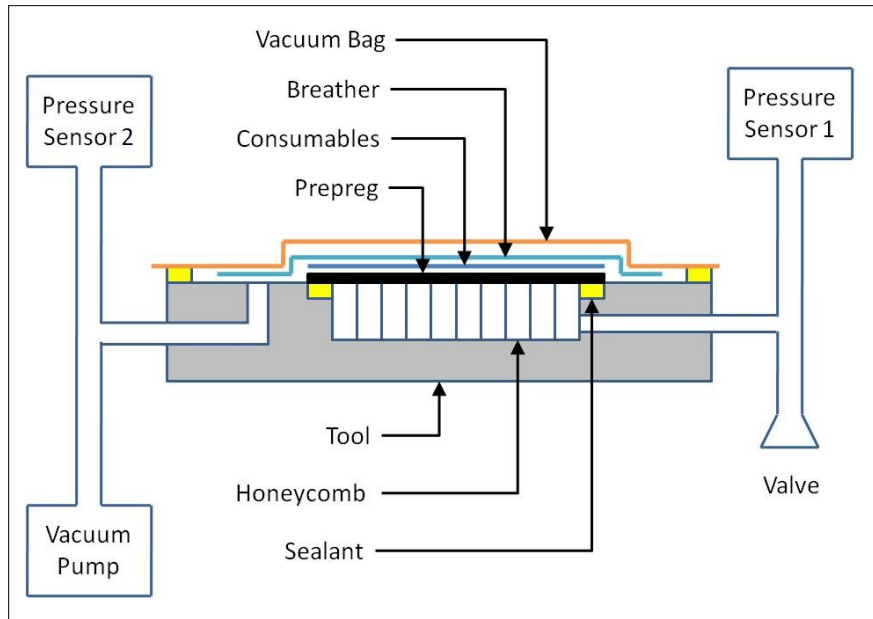


Figure 2.6: Experimental set-up for measuring the through thickness air permeability during processing conditions. [8]

2.3 Internal Core Pressure of Honeycomb Sandwich Panels

The air entrapped inside the core is a crucial factor when manufacturing honeycomb structures. The original work on permeability was developed with the intention of pushing air into the core during autoclave cure to avoid skin dimpling and core crush [33]. Core crush is the compression of the core due to the pressure applied by the autoclave. Core crush is mainly caused by the low in-plane stiffness of the honeycomb core. Skin dimpling is also caused by high autoclave pressure. The high pressure deforms the uncured prepreg skin into the honeycomb cells, and the surface resembles that of a golf ball – dimpled. Efforts were made to inflate the core during autoclave curing to avoid or reduce core crush and skin dimpling. The time required to inflate the core was based on the air permeability of the prepreg. This technique was successfully used to reduce the core crush and skin dimpling, but the porosity of the skin was greatly increased [33]. This increase in porosity indicates that the presence of air

dominates the generation of voids, as opposed to the volatiles released from the resin.

Aside from entrapped air in between the prepreg layers, there exists a large volume of air entrapped in the honeycomb cells. The entrapped air in the core will flow into the skin if a path exists. If the air path is closed, the air will expand during heating, and cause the composite skin to lift-off the cells. Figure 2.7 shows the entrapped air (represented as P_{cell}) that will expand during cure, and the vacuum level (represented as P_{bag}) in the vacuum bag. The pressure differential of expanding air inside the honeycomb cells and the vacuum pressure will determine the total consolidation pressure ($P = P_{bag} - P_{cell}$) during the cure cycle. This consolidation pressure will influence the final fibre volume fraction of the skin.

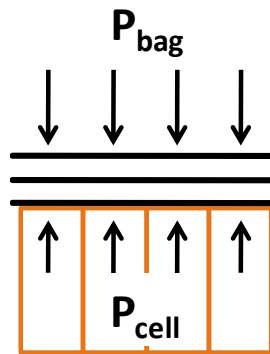


Figure 2.7: Free body diagram of the pressure differential in honeycomb sandwich processing.

The internal core pressure can be controlled to create a void free composite skin and a good quality bond between the skin and the core. The two material properties that can be used control the pressure inside the honeycomb cells are the prepreg air permeability and the resin rheology. The following sections describe in detail the effect of the processing parameters on the internal core pressure.

2.3.1 Prepreg Air Permeability

Since the prepreg is porous, the vacuum pump will extract the air from inside the honeycomb cells, through the prepreg skin, and into the bag, where it is removed. After a certain period of time, the pressure inside the cells will be equal to the applied vacuum pressure. That period of time will depend on the permeability of the prepreg. A detailed discussion of how to calculate the air permeability of a prepreg was presented in section 2.2. The factors that influence the air permeability of the prepreg stack, and subsequently the pressure inside the honeycomb cells, are presented in Figure 2.8. The following sections describe the influence of these factors.

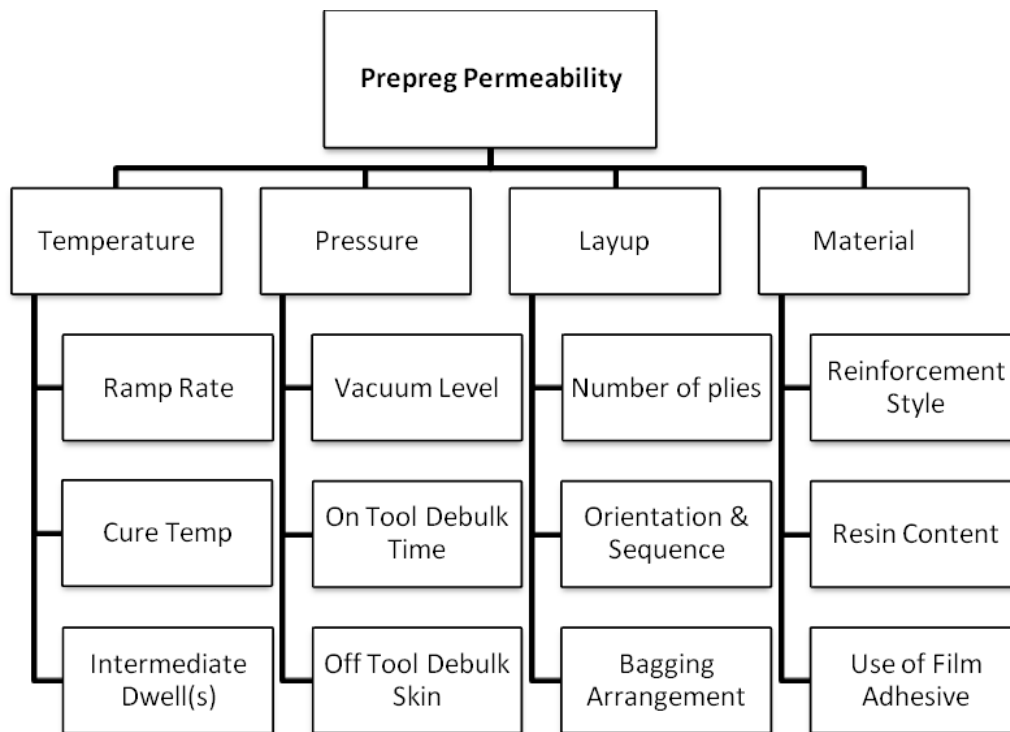


Figure 2.8: Processing conditions under investigation.

2.3.1.1 Temperature

The rheological behaviour of the resin is dependent on its chemistry and the temperature cycle. The chemistry is controlled by the material supplier;

therefore the only variable is the temperature. The resin behaviour during a specific temperature cycle (ramp rate and dwell) will determine the minimum viscosity of the resin and the gel time. The lower the viscosity, the easier it will be for the resin to infuse any dry spots in the fabric. However, as the resin closes off air passages, the air permeability of the prepreg will change, and careful attention must be taken to evacuate the core prior to closing off the air passages. Since the resin is viscoelastic, minor resin flow will occur at room temperature, but it will permanently change the architecture of the prepreg. The permeability of the prepreg will depend on the air passages that remain after the resin impregnates the fabric. The use of an intermediate dwell will allow extra time for the resin to flow, and may improve the infusion of the resin into the interlaminar voids remaining from the impregnation process [34]. The closing of the pores will change the permeability of the prepreg, and thus affect the ability of the vacuum to extract any entrapped air. A detailed analysis of the rheological behaviour of the resin is presented in Chapter 3, section 4.

The rheological behaviour plays another important role in developing the joint between the skin and the core. Studies have shown that the size of the fillet between the skin and the core affects the fracture toughness, and the size of the fillet is determined by the amount of resin flow [35-36].

2.3.1.2 Pressure

The amount of vacuum pressure and the duration of application, and whether the skin is de-bulked prior to layup will dramatically influence the cell pressure. De-bulking the skin prior to lay-up will collapse interlaminar and intralaminar air passages, dramatically reducing the ability of the vacuum to extract the entrapped air [32]. In light of this, debulking the skin prior to lay-up will unnecessarily complicate matters and will not be investigated.

2.3.1.3 Lay-up

The number of plies and the orientation of the plies will affect the permeability [30]. Furthermore, the bagging configuration will determine if the air travels in the through thickness direction, or the in-plane direction. If a peel ply is used, the air flow will primarily be in the through thickness direction, and a bleed configuration occurs allowing the resin to flow out of the laminate [27]. However, if an impermeable material (solid release film) is used, the air will primarily flow in-plane, resulting in a no-bleed configuration [37]. Opposed to flowing into the peel ply and breather, the excess resin should be available for fillet formation at the skin/bond interface [35]. Furthermore, a no-bleed bagging configuration may decrease void content, and may improve surface finish. However, the extra resin may increase the weight of the structure and decrease the fibre volume fraction.

2.3.1.4 Material

The fibre architecture, resin content, and use of a film adhesive will change the air permeability of the prepreg. A unidirectional tape, as opposed to a 5 harness satin, will change the amount of interlaminar and intralaminar voids/air passages available for air/volatile extraction. The amount of resin in the prepreg will influence the amount of resin available for bonding the skin to the core material, and may also affect the surface finish. If the resin content of the material is insufficient to create a strong joint at the skin to core interface, the use of a film adhesive may be necessary to increase the mechanical performance. However, the film adhesive does not have any fabric reinforcement to provide an air passage, and may impede the air flow out of the cells, dramatically reducing permeability of the layup [8].

2.4 Literature Review Summary

The techniques to measure the in-plane air permeability of prepreg were developed to reduce the defects in honeycomb sandwich structures during autoclave processing. These techniques were applied by other researchers to measure the through thickness air permeability of sandwich panels during processing conditions. Interesting observations from this work include that low internal core pressure increases the porosity of the skin, and high internal core pressure reduces the fracture toughness of the bond between the skin and the core. The context of this work was a large one-piece composite racing yacht hull, where a peel ply was used to allow air to flow in the through thickness direction. The through thickness permeability of the prepreg is not as dominant as the in-plane permeability when manufacturing aerospace sandwich panels. The use of caul plates and release films to distribute the pressure and improve the bag-side surface finish eliminates the through thickness permeability. This research applies the permeability concepts previously developed, and expands the literature to include the processing of aerospace sandwich structures, as shown in Figure 2.9. This research project aims to determine the in-plane permeability of the prepreg skin of a sandwich panel during different processing conditions. This information will be used to evaluate different cure cycles to determine the effect of internal core pressure on the mechanical performance of a honeycomb sandwich panel.

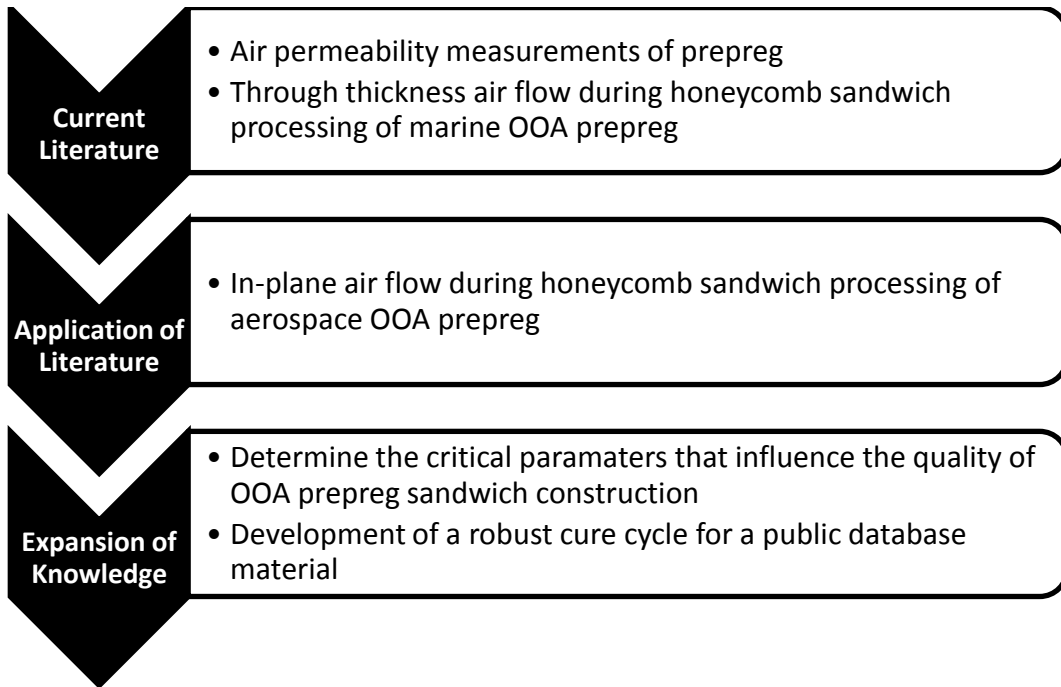


Figure 2.9: Flow chart of the research presented in this thesis.

3 Resin Characterization

The focus of this chapter is to understand how the resin behaves during each step of the cure cycle. The first step towards designing a cure cycle is to understand the thermal stability of the material, in order to avoid excessively degrading the material during cure. Once the upper temperature limit of the material is known, a cure kinetics model can be developed to provide the degree of cure of the resin after any cure cycle. The cure kinetics model is used for all other models, such as viscosity and glass transition temperature. As the temperature increases during the cure cycle, the viscosity decreases and a competition begins between the softening and cross-linking of the polymer. The rheological performance of the resin will be used to select the optimal temperature ramp rate and dwell temperature. The resin viscosity can be controlled to keep the air paths in the prepreg open, in order to remove entrapped air prior to the resin flowing. Once the resin has cured, the glass transition temperature of the resin can be determined by oscillating a sample while increasing the temperature.

The following sections of this chapter will outline the materials and detailed characterization of the resin. The first step is to determine the thermal stability of the resin, followed by the cure kinetics, rheology, and glass transition temperature. The test procedures will be outlined, the models developed based on the experimental results, and the implications of the modeling discussed for each step of the characterization.

3.1 Material

The material used in this project was MTM45-1/CF2426A carbon epoxy prepreg from the Advanced Composites Group (ACG). The prepreg contained 36% resin content by weight, the reinforcement weave was a 5 harness stain, and the size of the tows was 6K (6,000 carbon fibres per tow). Neat resin was supplied as an unsupported film for the thermal characterization. The chemistry of the epoxy resin is formulated for an initial cure at low temperatures (80-100°C), while equivalent performance to second generation autoclave prepreg can be achieved with a freestanding postcure at 180°C [4].

3.2 Thermal Stability of the Material

Thermally degrading the resin during heating should be avoided. When the resin degrades, volatiles are released and must be evacuated or dissolved, otherwise voids will form in the skin, reducing part quality. The following sections outline the equipment and procedure used to test the materials, and the results and implications of the tests.

3.2.1 Equipment

A TA Instruments Q500 Thermal Gravimetric Analyzer (TGA) was used to measure the thermal stability of the resin. The TGA (Figure 3.1) comes equipped with a loading tray where the sample pans are stored. The loading tray also places the sample pan onto the hook, which is connected to a load cell. The furnace moves up to enclose the suspended sample pan and maintain a gas environment. Two gases are available for testing the samples, nitrogen and compressed air. Resins contain organic compounds, and the inert nitrogen prevents the sample from reacting chemically. Furthermore, this allows any weight loss arising from escaping volatiles or solvents present in the resins to be measured. Once the resin is tested through the desired temperature range, the gas is switched to air. The oxygen in the air reacts with the resin and burns the remaining resin from the pan.



Figure 3.1 The Thermal Gravimetric Analyzer.

3.2.2 Performance Verification

The TGA can be calibrated for temperature and mass when required. To determine if a calibration was needed, the performance of the TGA was verified using calcium oxalate. The thermal degradation of calcium oxalate occurs in increments and temperatures that are well established [38]. A sample weighing approximate 10 mg is placed in a sample pan, and heated at a constant rate of 20°C/min, up to 1000°C, in a nitrogen environment. The result of the performance verification test is shown in Figure 3.2.

A comparison of the known and measured thermal degradation of calcium oxalate is presented in Table 3.1. The difference between the known and measured transitions is less than 0.5% for the first and second transitions, and 1.9% for the third transition. The increased error in the third transition is not of major concern because the range of interest for this work is between room temperature and 180°C. Therefore, the performance of the TGA was deemed acceptable, and no calibrations were performed.

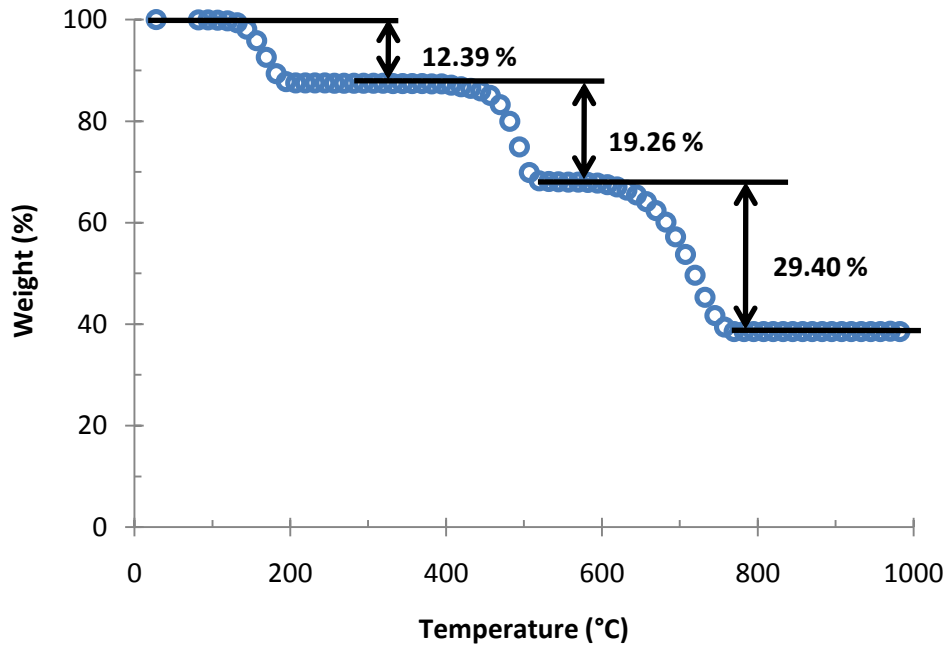


Figure 3.2: TGA performance verification with calcium oxalate.

Table 3.1: TGA Performance Verification Summary

	Transition 1	Transition 2	Transition 3
Known	12.44	19.34	29.98
Measured	12.39	19.26	29.40
Difference	-0.4 %	-0.4 %	-1.9 %

3.2.3 Testing Procedure

The first step was to tare the platinum pans. The testing procedure used was a standard ramp at 20°C/min in a nitrogen environment until 350°C, when the gas was switched to air and heating continued until 800°C. Three runs were performed to validate consistency of the results.

Table 3.2: Thermal Stability Test Matrix

Material	Ramp Rate (°C/min)	Gas Switch Temp (°C)	No. Tests
MTM45-1	20	350	3
Total			3

3.2.4 Results and Discussion

The averaged results of the three TGA experiments are shown in Figure 3.3. The MTM45-1 is stable until 110°C, and then degrades slowly until 175°C, when it starts to exhibit substantial mass loss. The TGA tests are conducted under atmospheric pressure, therefore the results may be underestimating the mass loss during manufacturing, where the resin will be exposed to vacuum, increasing the ease which volatiles can be released from the resin [2,4]. If the volatiles that are escaping from the resin are not extracted from the prepreg, voids will occur. Since the resin starts to behave as a gel at 140°C (see section 3.4.4), it is impossible to extract the escaping volatiles above 140°C. The best solution to avoid voids arising from the volatiles is to initially cure the composite parts below 110°C.

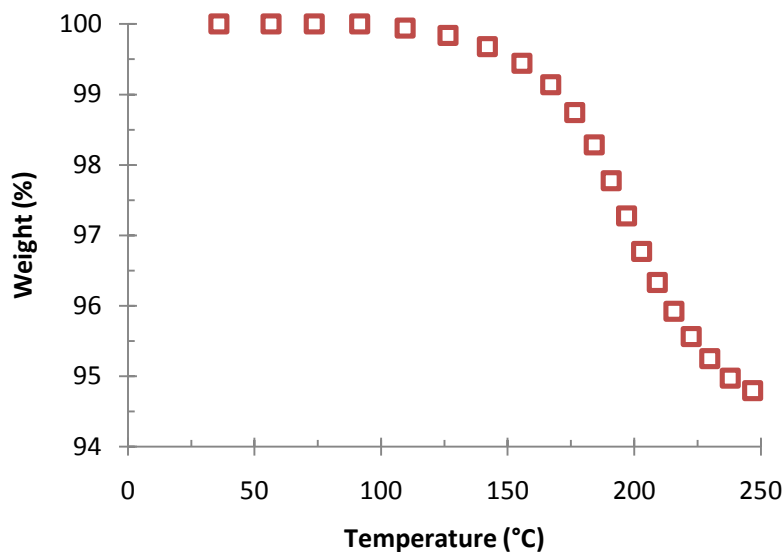


Figure 3.3: Thermal stability of the MTM45-1 resin.

3.3 Cure Kinetics

An accurate cure kinetics model is the cornerstone for designing cure cycles for thermosetting composites. The extent of the reaction, known as the degree of cure, is used as the basis for important physical property models, such as the viscosity and the glass transition temperature. To create a cure kinetics model, experiments with small amounts of resin are conducted, and then a mathematical relation is used to fit the data by linear regression. With this equation, the degree of cure of the resin can be determined after any time-temperature history. More importantly, cure cycles can be designed to meet a certain performance criteria without having to worry about scraping an expensive composite structure. The following sections describe the equipment and experimental procedure used to perform the tests. With the test data collected, the steps used to fit an equation to the data are explained. Finally, a design guide is developed to relate the time required to cure a part in order to achieve the maximum degree of cure, at various temperatures within the processing window.

3.3.1 Equipment

A TA Instruments Q100 Dynamic Scanning Calorimeter (DSC) was used to measure the heat flow of the neat resin in dynamic and isothermal conditions. A cutaway of the test cell is shown in Figure 3.4. The test sample is placed in a pan on the sample platform, and an empty pan is placed on the reference platform. Area thermocouples (grey disks under the platform) measure the respective temperatures, and the cell thermocouple (pink bulb between the platforms) measures the cell temperature. These three temperature values are used to determine the heat flow into, or out of the specimen. The heat flow and cell temperature are the output values from the DSC used to create a cure kinetics model.

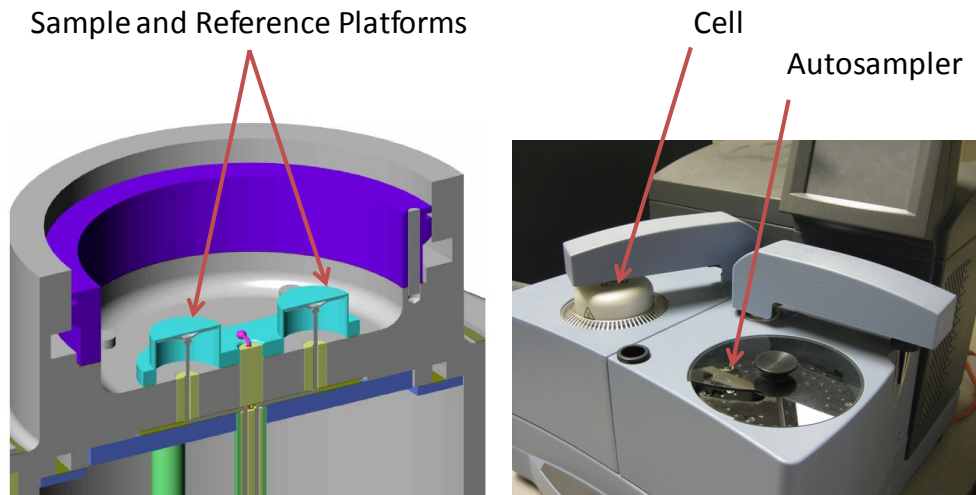


Figure 3.4: DSC (right), and a cutaway of the Q100 DSC cell (left) [39].

The DSC is equipped with an autosampler, dramatically increasing the efficiency of the test sequence. The autosampler consists of a tray where the test samples are placed, and a robotic arm that places the sample and reference pans on their respective platforms. Careful attention was taken to ensure the correct sample was placed in the associated position in the autosampler tray. If an error was made in either the placement of the sample or the recording of the sample mass with the test number, the heat flow would be incorrect.

3.3.1.1 Calibration of the DSC

The performance of the DSC is verified by increasing the temperature of an empty cell. If the DSC is not contaminated or in need of calibration, there should be no heat flow measured if there is no sample in the cell. Unfortunately, the baseline of the empty cell showed that a thermal drift was present. The DSC was calibrated, but the thermal drift remained, indicating the cell was contaminated. The cell was cleaned by heated to 550°C at 20°C/min. The lid remained open during the cleaning procedure to avoid contamination. Once the cell cooled to room temperature, it was brushed with a fiberglass brush and lightly blasted with dry compressed air to remove any residual contaminants. After cleaning,

the DSC was calibrated, and the subsequent baseline improved. The difference in the thermal drift of the baseline runs before and after the cleaning and calibration procedure is shown in Figure 3.5.

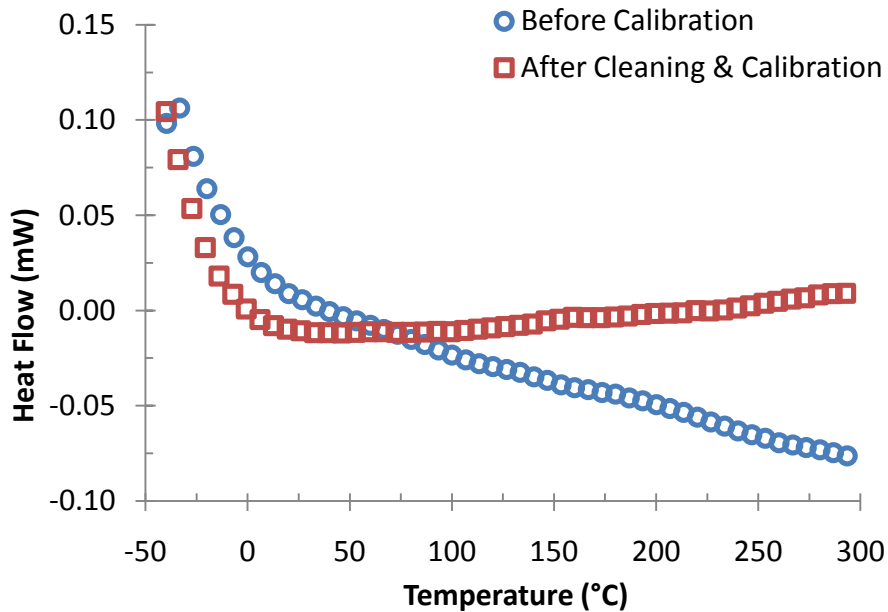


Figure 3.5: Baseline verification of the DSC before and after cleaning and calibration.

The effect of thermal drift significantly impacts the dynamic DSC scans, which are used to determine the total heat of reaction of the resins in section 3.3.3. The operating temperature of the tests is from 25°C to 250°C, where the data from the DSC can be considered accurate to within 0.9%, compared to 4.9%, had the instrument not been cleaned and calibrated prior to use. Considering that this data is used to build the cure kinetics model, from which all the other thermo-mechanical models are based, it is important to know the accuracy of the data collected.

The odd behaviour of the heat flow signal at the beginning of the baseline tests in Figure 3.5 was discussed with the instrument manufacturer. The thermal drift below freezing was attributed to a slight misalignment of the DSC lid [40].

Since the tests are being conducted above 25°C, where the baseline is very good, no further action was taken.

3.3.2 Experimental Procedure

Dynamic scans at 2°C/min up to 250°C were conducted to determine the total heat of reaction of the resin. Isothermal tests were performed between 80°C and 180°C to determine the isothermal heat of reaction. Following the isotherm, the sample was cooled to room temperature and then ramped at 2°C/min to determine the residual heat of reaction. To ensure consistency of the results, four repeats were performed for the dynamic tests, and two repeats for the isothermal tests. A summary of the test matrix is provided in Table 3.3.

Table 3.3: MTM45-1 Cure Kinetics Test Matrix

Type	Temp (°C)	Time (min)	Ramp (°C/min)	Residual Temp (°C)	No. Tests
Dyn	250	-	2	-	4
Iso	80	2000	2	250	2
Iso	100	800	2	250	2
Iso	120	400	2	250	2
Iso	140	200	2	250	2
Iso	160	180	2	250	2
Iso	180	100	2	250	2
Total					16

To prepare the test samples, the resin was removed from the freezer and thawed to room temperature. The sample mass should be between 5-10 mg, and the sample was placed in a hermetically sealed aluminum pan. To determine the exact mass of the sample, the empty pan was weighed on a Sartorius scale (resolution 0.01 mg), and then the scale was zeroed. The resin was placed in the pan and re-weighed to determine its mass. The sample pan was sealed, and placed in the appropriate position in the DSC autosampler. Prior to weighing the

pan, the scale was verified using dead weights of 5 mg and 10 mg from the TMA accessory kit. The scale reading was 1.6 % below the 5 mg dead weight, and 0.5 % below the 10 mg dead weight. With less error closer to 10 mg, the samples were prepared such that their mass was between 8-10 mg.

3.3.3 Resin Cure Kinetics Model

The degree of cure of the resin describes the extent of the chemical reaction. By conducting a few experiments over the processing window, a mathematical equation was used to describe the degree of cure of the resin after any time-temperature history. The first step was to convert the heat flow values obtained from the DSC to heats of reaction. The total heat released during a complete reaction was determined using the dynamic tests shown in Table 3.3. From these tests, the total heat of reaction was determined as the area between the heat flow and baseline curves (Figure 3.6). The baseline curve is a linear line between the start and end of the reaction. Using this technique, the average total heat of reaction for the MTM45-1 was 368.91 J/g with a standard deviation of 3.39 J/g.

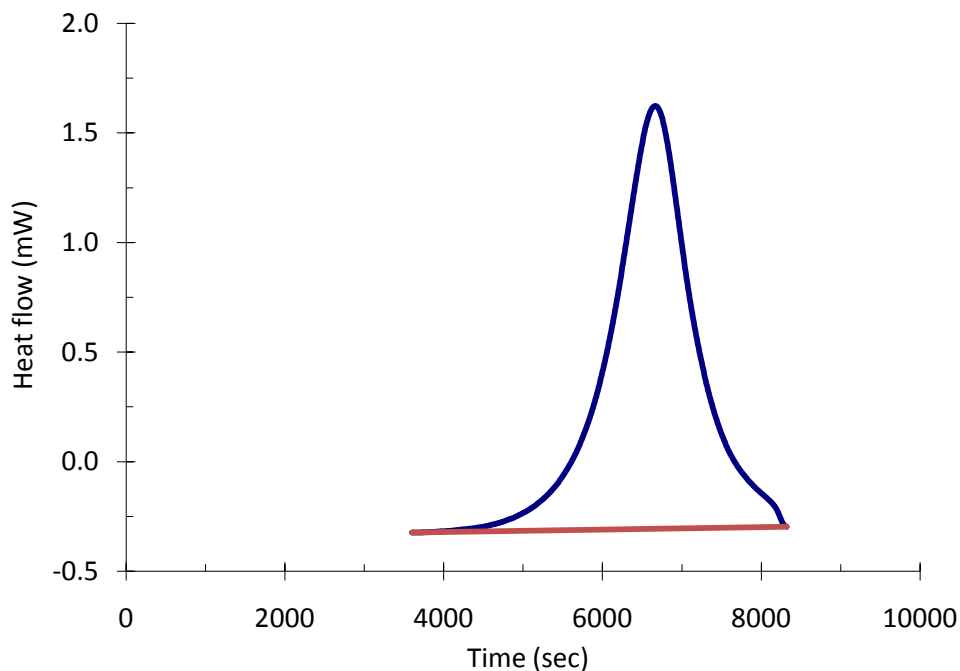


Figure 3.6: Heat flow from a dynamic scan at 20°C/min up to 250°C.

The degree of cure (α), was determined for the isothermal tests in Table 3.3 by comparing the isothermal (H_I) and residual (H_R) heats of reaction with the total heat of reaction (H_T). The theoretical degree of cure α was calculated as follows:

$$\alpha = \frac{H_T - H_R}{H_T} \quad (3.1)$$

The degree of cure obtained with equation (3.1) was used to set the baseline for the isotherm, in the same manner as Figure 3.6, such that:

$$H_I = H_T - H_R \quad (3.2)$$

With the baseline in place, the experimental cure rate ($d\alpha/dt$) of the isothermal reaction was determined. The cure rate was assumed to be proportional to the heat flow (dH/dt), and was calculated as follows:

$$\frac{d\alpha}{dt} = \frac{1}{H_T} \frac{dH}{dt} \quad (3.3)$$

The experimental cure rate was used to fit constants to a diffusion controlled autocatalytic equation developed by Cole [41]. The equation that describes the curing behaviour of the MTM45-1 resin is:

$$\frac{d\alpha}{dt} = A \exp\left(\frac{-E_A}{RT}\right) \frac{\alpha^m (1 - \alpha)^n}{1 + \exp(C(\alpha - (\alpha_{CO} + \alpha_{CT} T)))} \quad (3.4)$$

where A is the experimentally determined Arrhenius constant for MTM45-1, E_A is the activation energy, R is the universal gas constant, T is the absolute temperature, m and n are material constants, C is the diffusion constant, α_{CO} is the critical degree of cure at absolute zero temperature, and α_{CT} accounts for the

increase in critical resin degree of cure with temperature. The constants were experimentally determined to be:

$$\begin{array}{ll}
 A = 2.28 \times 10^4 \text{ s}^{-1} & C = 54.26 \\
 E_a = 60628 \text{ J/mol} & \alpha_{CO} = -1.076 \\
 m = 0.526 & \alpha_{CT} = 4.44 \times 10^{-3} \text{ K}^{-1} \\
 n = 0.946 &
 \end{array}$$

The activation energy comes from the Arrhenius equation:

$$\frac{d\alpha}{dt} = A \exp\left(\frac{-E_A}{RT}\right) \quad (3.5)$$

which was re-written as:

$$\ln\left(\frac{d\alpha}{dt}\right) = \ln A - \frac{E_A}{RT} \quad (3.6)$$

and E_A is the slope of $\ln(d\alpha/dt)$ versus $1/T$ (Figure 3.7) for low degrees of cure ($\alpha < 0.1$). The other constants were determined using a weighted least-squares curve fit with the experimental data.

The cure kinetics model is in good overall agreement with the experimental data. The model slightly over-predicts cure rate and the degree of cure when $\alpha > 0.75$ for the 160°C and 180°C isothermal holds in Figure 3.8. Conversely, the model under-estimates the degree of cure for 80°C isotherm, until $\alpha = 0.5$, as seen in Figure 3.9. Imperfect behaviour can be tolerated at the extreme ends of the processing window, especially when the temperature window is as large as 100°C.

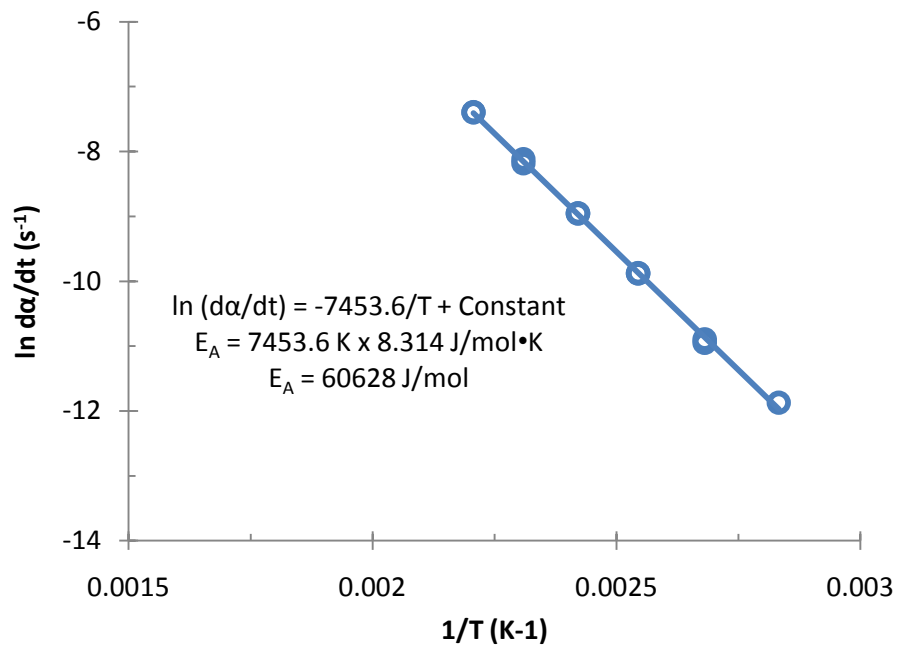


Figure 3.7: Arrhenius plot to determine the activation energy E_a .

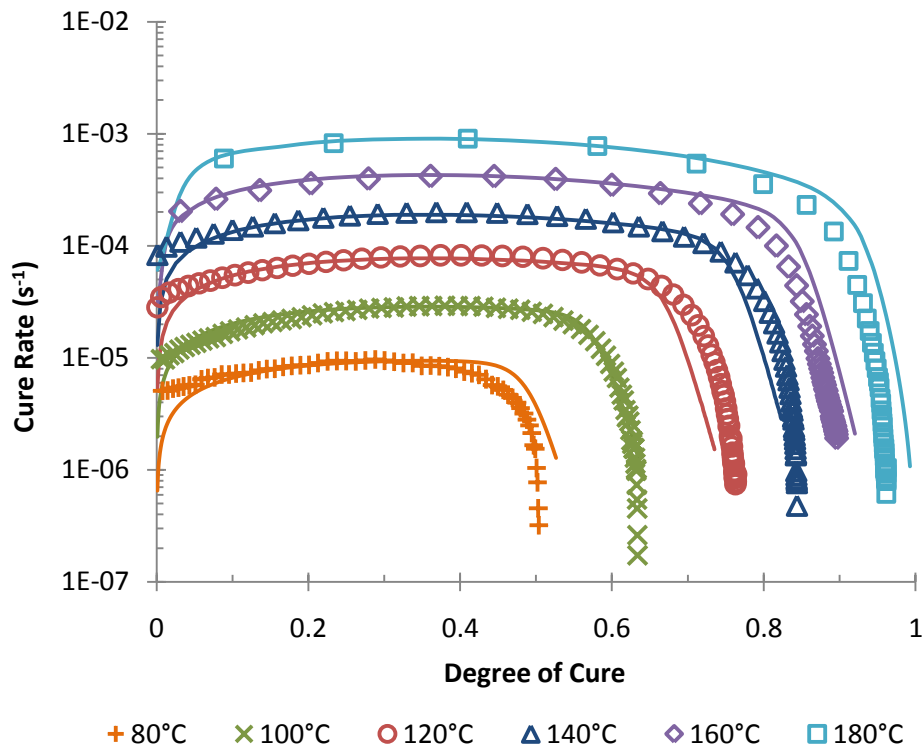


Figure 3.8: Isothermal progression of the cure rate with increasing degree of cure for MTM45-1. The experimental data (symbols) is compared with the model predictions (continuous lines).

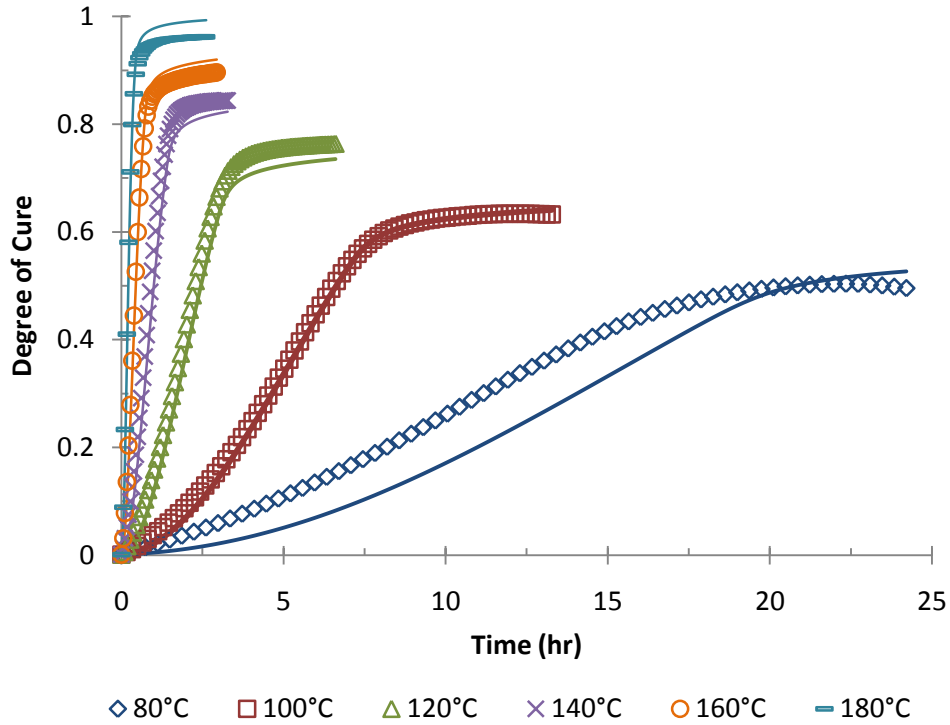


Figure 3.9: The evolution of the degree of cure during the cure cycle. The experimental data (symbols) is compared with the model predictions (continuous lines).

From a cure cycle design standpoint, the key information from the cure kinetics model is the length of the dwell at a specific temperature. There is a maximum degree of cure that can be achieved for each dwell temperature, and a minimum amount of time required to achieve that degree of cure. When the degree of cure becomes constant (i.e. $da/dt = 0$), the time and degree of cure are determined as shown in Figure 3.10. The same process was used for all the isothermal scans, and the results are plotted in Figure 3.11.

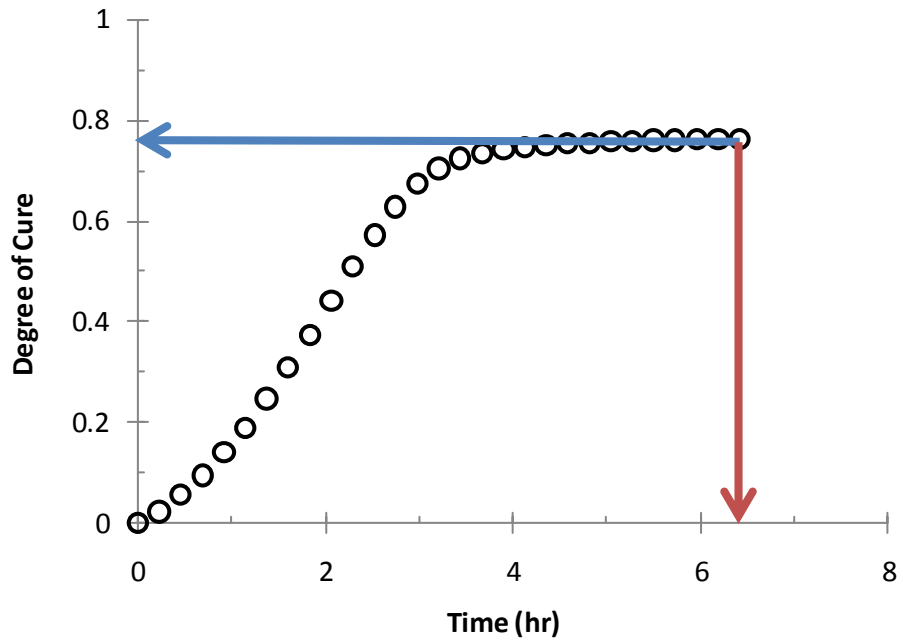


Figure 3.10: Isothermal scan at 120°C.

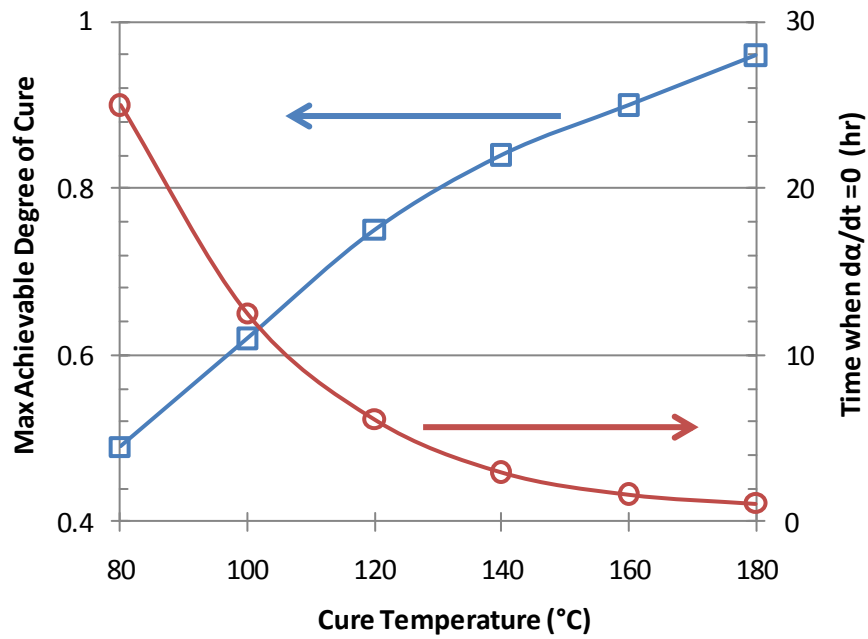


Figure 3.11: Temperature cycle guideline.

3.4 Rheology

The viscosity is the most important parameter to help control the void content in the skin of sandwich structures. The two parameters that control the viscosity during a cure cycle are the temperature ramp rate, and the dwell temperature. The ramp rate will identify the temperature where the minimum viscosity occurs, and if the minimum viscosity changes at different ramp rates. The dwell temperature will determine how long the resin behaves like a fluid and can flow into any dry fibre regions. Furthermore, the rheology of the resin can be coupled with the cure kinetics model to predict the viscosity as a function of the degree of cure. With this model, the degree of cure of the resin can be predicted at the minimum viscosity and the gel point for any temperature cycle. The following sections describe the equipment, procedures, and models used to characterize the rheological behaviour of the resin.

3.4.1 Small-Amplitude Oscillatory Shear

A rheometer is used to measure the viscosity of the resin. The technique the rheometer uses to calculate the material properties is explored prior to outlining the equipment and procedures used to characterize the resin. The Rheometer motor measures rotational displacement and torque, and outputs material functions. The torque is converted into shear stress depending on the area of the test geometry. Furthermore, the modulus can be determined by dividing the shear stress by the strain amplitude. Unfortunately, the material is viscoelastic, and there exists a lag, described by the phase angle δ , between the applied strain and the measured stress, as shown in Figure 3.12.

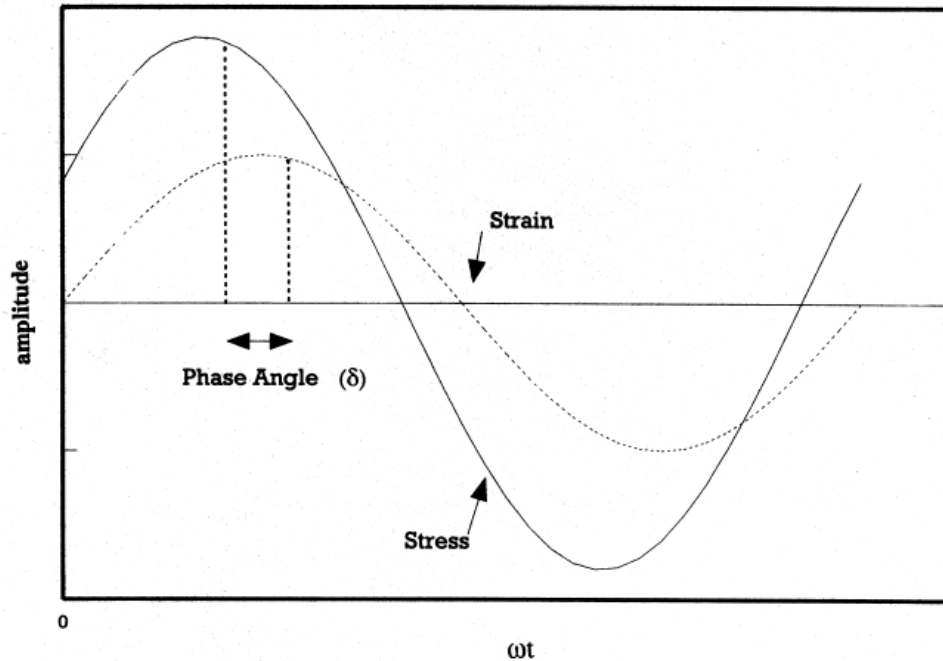


Figure 3.12: Dynamic response of a viscoelastic material [42].

The modulus is comprised of an elastic (in-phase) component known as the storage modulus G' , and a viscous (out-of-phase) component known as the loss modulus G'' , and they are defined as follows:

$$G' = \frac{\tau}{\gamma} \cos \delta \quad (3.7)$$

$$G'' = \frac{\tau}{\gamma} \sin \delta \quad (3.8)$$

where τ is the shear stress, and γ is the strain amplitude. For a material with an in-plane and out-of-plane component of modulus, a complex modulus G^* is developed as shown in Figure 3.13.

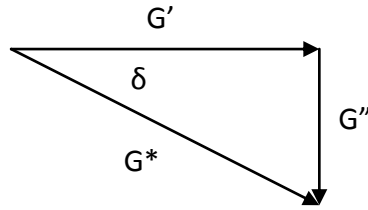


Figure 3.13: The complex modulus composed of the storage and loss modulus [43].

The viscosity that is measured from these experiments is oscillatory, and is therefore called the complex viscosity [44], and the magnitude of the complex viscosity η^* is determined as follows:

$$|\eta^*| = \frac{G^*}{\omega} \quad (3.9)$$

where ω is the frequency. The steady-shear viscosity (dependant of shear rate) cannot be measured because of the nature of thermosetting materials; the material is physically changing over time as the temperature is increased. Furthermore, the resin is provided as a film and can only be tested in a parallel plate geometry, which has a non-uniform stress distribution in the radial direction. However, the Data Analysis software that is used with the Rheometer allows the user to plot the steady-shear viscosity. For this case, the software assumes that the fluid is Newtonian, which is incorrect because Newtonian fluids have a viscosity that is independent of shear rate; unlike most thermosetting polymers. In light of this, the complex viscosity will be used to describe the rheological behavior of the resin, and should not be considered equivalent to the steady-state shear viscosity.

3.4.2 Equipment

The rheological behaviour of the neat resin was characterized using an AR 2000 Rheometer by TA Instruments. The Rheometer is equipped with an Environmental Test Chamber (ETC) used to control the temperature of the

specimen. Dynamic and isothermal tests were used to monitor the change in complex viscosity of the resin by inducing a small amplitude oscillatory strain in the resin sample between two 25 mm parallel plates. The Rheometer and a close-up of the resin in between the 25 mm parallel plates are shown in Figure 3.14.



Figure 3.14: Rheometer with close-up of the parallel plate geometry.

3.4.2.1 Performance Verification

The Rheometer cannot be calibrated in the same manner as the other characterization equipment. The performance is verified using a known standard, and if the rheometer fails the performance verification, maintenance by the instrument manufacturer is the only option. PDMS putty was used to verify the oscillatory performance. The PDMS putty has a well established angular frequency where G' equals G'' . When the storage modulus is equal to the loss modulus, this is known as the G-crossover point. A performance verification test was performed prior and after the resin film tests to determine if

any change in instrument performance had occurred. The results of these tests are shown in Figure 3.15.

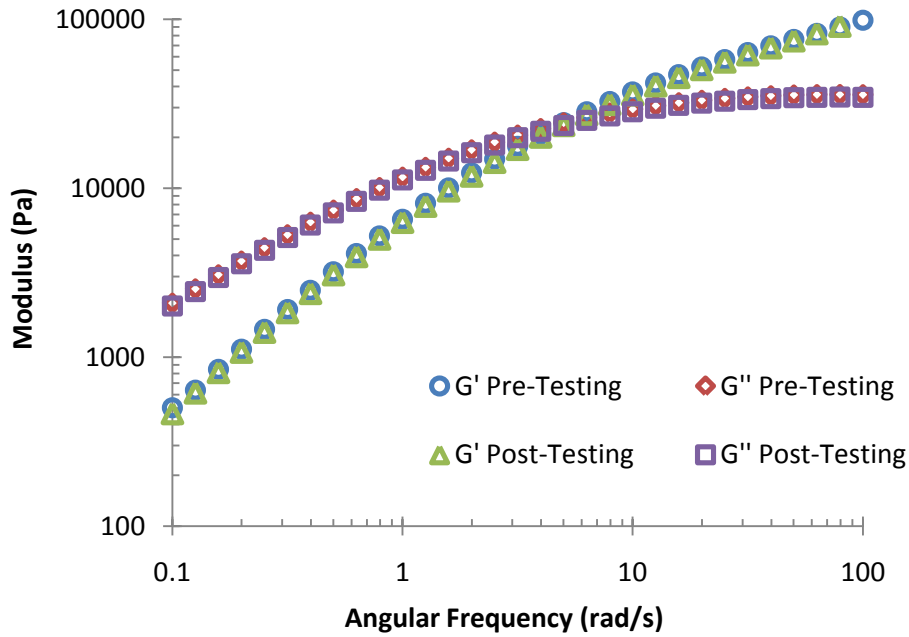


Figure 3.15: Oscillatory frequency sweep with PDMS.

The oscillatory frequency sweeps used to measure the PDMS angular frequency and G-crossover point look very similar. A comparison of the theoretical and measured values at the G-crossover point is shown in Table 3.4. The performance of the Rheometer was within tolerance before and after the experimental tests in section 3.4.4.

Table 3.4: Performance Verification Summary

Criteria	Reference	Tolerance	Pre-Test	Error	Post-Test	Error
G-crossover (Pa)	24990	±8%	23430	-6.2%	24380	-2.4%
Angular Frequency (rad/s)	5.09	±5%	4.98	-2.2%	4.98	-2.2%

3.4.3 Experimental Procedure

Two types of rheology test were conducted: dynamic temperature ramps and isothermal dwells. The dynamic tests were performed at temperature ramp rates between 1-4°C/min and the isothermal dwells were carried out between 80-180°C. The complete test matrix is provided in Table 3.5. The rheology tests were conducted at a controlled strain of 0.1% and constant frequency of 1 Hz, until the termination criteria, a complex viscosity > 10000 Pa-s, was met. A frequency sweep was conducted on the resin to ensure that the tests were in the linear viscoelastic region of the material (see section 3.4.3.1 for more information).

Table 3.5: Rheology Test Matrix

Type	Temp (°C)	Ramp (°C/min)	No. Tests
Dyn	-	1	3
Dyn	-	2	3
Dyn	-	3	3
Dyn	-	4	3
Iso	80	20	3
Iso	100	20	3
Iso	110	20	3
Iso	120	20	3
Iso	130	20	3
Iso	140	20	3
Iso	180	20	3
Total			33

The disposable parallel plate attachment was installed in the Rheometer, and the 25 mm disposable plates were secured to the attachment and draw rod. Careful attention was taken not to over-tighten the draw rod; finger tight was

acceptable. The Rheometer was then calibrated. This consisted of mapping the air-bearing, calibrating the system inertia and setting the zero-gap. All the calibrations were performed using the control software. Three plies of resin film were punched-out from a resin strip, and carefully placed on the lower plate. The upper plate was then lowered to the appropriate height. It was verified that there were no spaces between the sample and the top plate, and that the edges of the sample were flush with the plates. The environmental test chamber doors were closed and the whole system was heated to 30°C prior to conducting the experiment.

3.4.3.1 The Linear Viscoelastic Region

As noted in the previous section, the strain was controlled at 0.1% for the rheology tests. Prior to testing the resin, an oscillatory stress sweep was performed at 30°C and 80°C to determine the linear viscoelastic region (LVR). The LVR is defined as the range-of-deformation where the stress generated is linear in strain [44]. The small-amplitude oscillatory shear material functions are only valid if the rheology tests are conducted in the LVR of the material. The controlled variable during the LVR test was the motor torque, which was varied from the lower to upper limit. The resulting data was plotted as a function of the strain in order to determine the value of % strain to use during the testing of the resin. In Figure 3.16, the storage modulus is constant at 30°C, where the viscosity is very high, and the resin behaves elastically throughout the test. When the temperature is increased to 80°C, nonlinear behaviour is observed at the beginning and end of the test because the strain rate is no longer in the LVR of the material. The test itself takes approximately 30 minutes to complete, and 80°C was selected as the upper temperature where no curing of the resin would occur to influence the results. Based on these tests, a strain of 0.1%, which is in the middle of the 2 arrows in Figure 3.16, was selected.

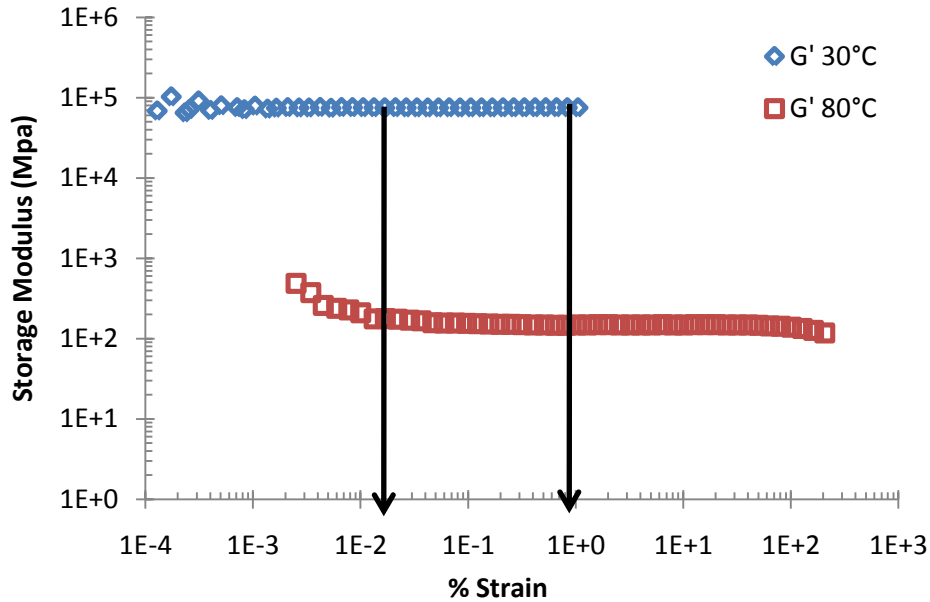


Figure 3.16: Oscillatory stress sweep of MTM45-1.

3.4.4 Experimental Results and Discussion

The dynamic rheological behavior of the resin is presented in Figure 3.17. The change in viscosity of the resin is independent of the ramp rate until 120°C. The ramp at 1°C/min has the most noticeable difference in minimum viscosity compared to the ramps between 2-4°C/min. Based on this information, a ramp rate of 2°C/min was chosen for the core pressure tests (Chapter 4) and the representative panels (Chapter 5) in order to reduce the process variables. The isothermal rheological behavior of the resin is presented in Figure 3.18. The graph shows the time available for the resin to flow, until a dramatic increase in complex viscosity occurs in a short period of time, known as gelation. For multi-step cure cycles, the resin does not gel at 80°C within the first few hours. This slow curing behaviour is advantageous if a higher dwell temperature is used after an intermediate hold at 80°C. After the intermediate dwell, the resin will continue to flow and infuse any dry regions of the fabric during the ramp to the final dwell temperature.

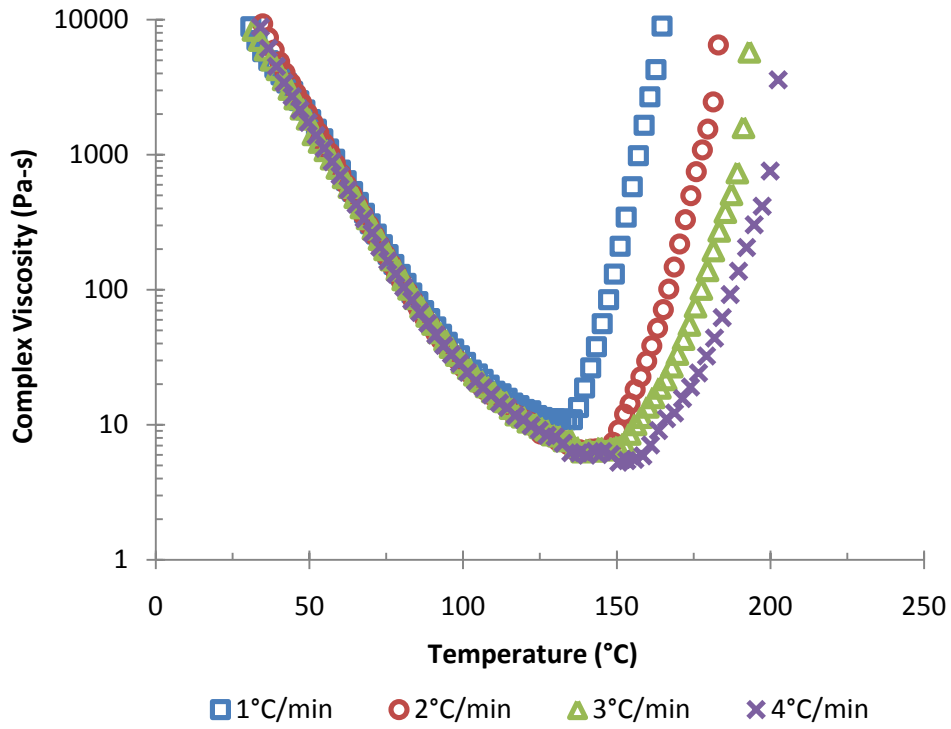


Figure 3.17: Dynamic viscosity response of MTM45-1.

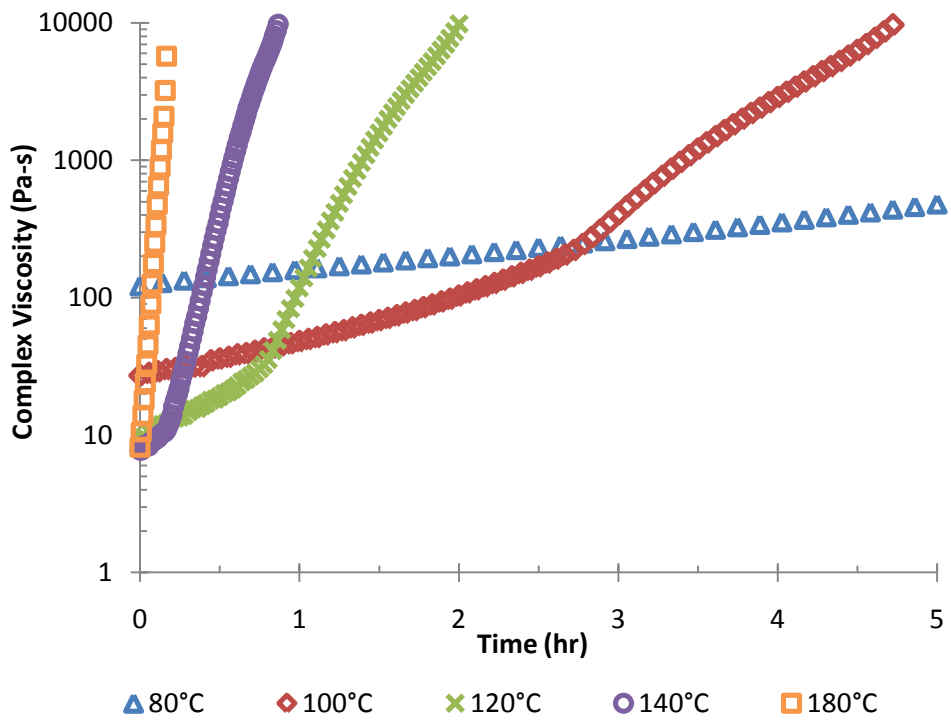


Figure 3.18: Isothermal viscosity response of MTM45-1.

3.4.5 Resin Viscosity Modeling

The viscosity of the resin can be described at any point with the cure kinetics model and the temperature history. The viscosity model used in this work to describe the MTM45-1 was developed by *Kenny et al.* [45]. The model includes the degree of cure at gelation (α_g), which was determined to be 0.40 from the dynamic and isothermal viscosity tests. The value of $\alpha_g = 0.40$ was determined by taking an average of the G-crossover point (i.e. $\tan(\delta) = 1$) from each experiment. The equation is as follows:

$$\mu = A_{\mu} \exp\left(\frac{E_{\mu}}{RT}\right) \left[\frac{\alpha_g}{\alpha_g - \alpha}\right]^{(A+B\alpha)} \quad (3.10)$$

where, E_{μ} is the viscosity activation energy, A_{μ} , A, and B are experimentally determined constants using linear regression, and R is the universal gas constant, and T is the absolute temperature. Careful attention should be taken not to confuse the viscosity activation energy E_{μ} with the E_A of the cure kinetics model. The constants were experimentally determined to be:

$$\begin{aligned} A &= 5 & \alpha_g &= 0.40 \\ B &= -5 \end{aligned}$$

The rate of change of the viscosity decreases at 100°C. In order for the model to accurately predict the viscosity during the temperature ramp and gelation, two different values for E_{μ} and A_{μ} were used as follows:

25°C < T < 100°C

$$A_{\mu} = 1.8 \times 10^{-10} \text{ Pa}\cdot\text{s}$$

$$E_{\mu} = 79500 \text{ J/mol}$$

T > 100°C

$$A_{\mu} = 3.0 \times 10^{-5} \text{ Pa}\cdot\text{s}$$

$$E_{\mu} = 42000 \text{ J/mol}$$

The viscosity activation energy E_{μ} was determined following the same approach outlined in section 3.3.3. The $\ln \mu$ was plotted versus $1/T$ from room temperature until the viscosity began increasing. The slope and intercept of the linear trendline were used to determine E_{μ} and A_{μ} respectively. One set of values for E_{μ} and A_{μ} was measured from room temperature until 100°C, and for above 100°C.

The results from the model in equation (3.10) are plotted with the corresponding isothermal experimental data in Figure 3.19. The model is in good agreement with the experimental data. The model nicely captures the gelation between 100-140°C, but minor disagreement is present for the 80°C isotherm. This error is related to the cure kinetics model, which does not capture the evolution of the degree of cure as well at 80°C compared to 100-180°C. The viscosity model is very closely matched to the dynamic experimental data, as shown in Figure 3.20. The model captures the ramp and gelation, but slightly overpredicts the minimum viscosity. The model accurately predicts the temperature where minimum viscosity occurs, but the predicted value is slightly above the experimental data. This model is valid until gelation, which is a degree of cure above 0.40 for MTM45-1.

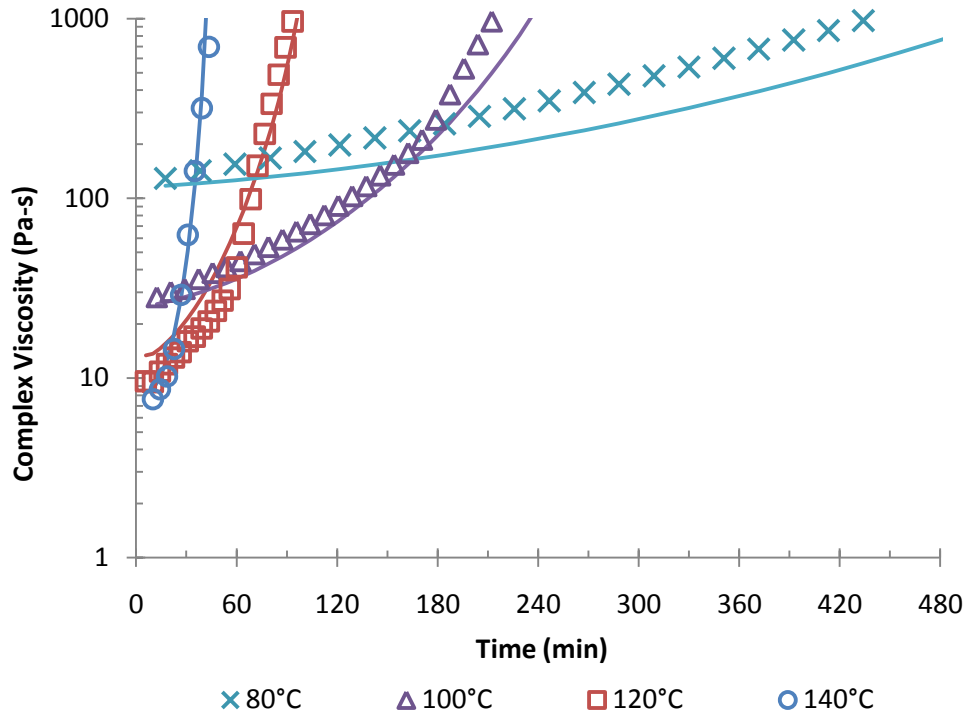


Figure 3.19: Isothermal viscosity results for MTM45-1. The experimental data (symbols) is compared to the model predictions (continuous lines).

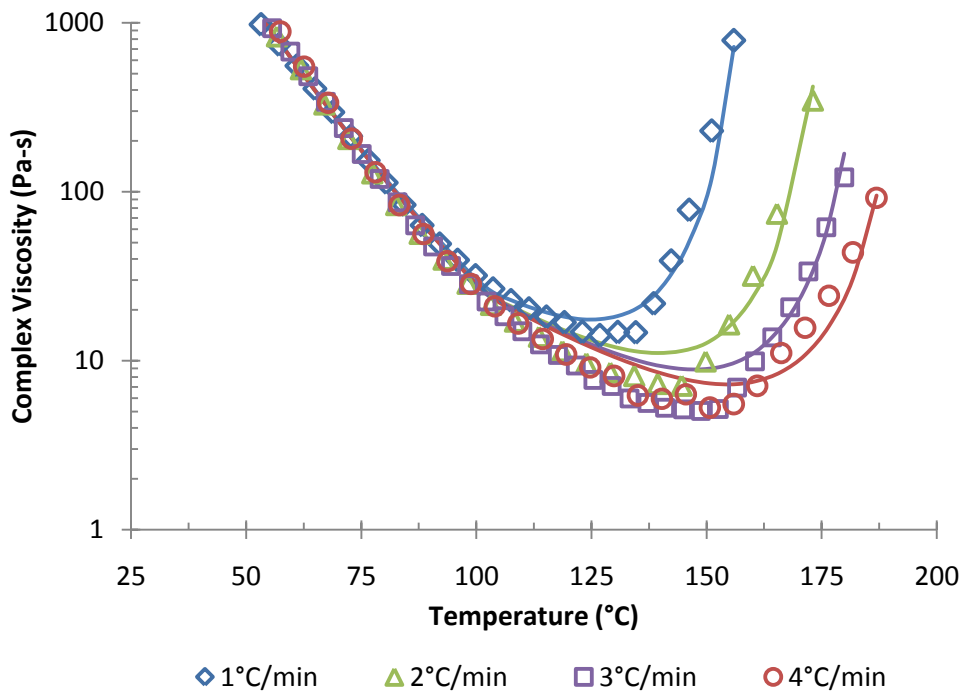


Figure 3.20: Dynamic viscosity results for MTM45-1. The experimental data (symbols) is compared to the model predictions (continuous lines).

3.5 The Glass Transition Temperature

The glass transition temperature (T_g) is an important physical property that defines the upper operating temperature of a polymeric based structure. The T_g represents the temperature when the polymer goes from a hard glassy state to a rubbery state [42]. The most common ways to measure the T_g are with differential scanning calorimetry (DSC described in section 3.3.1) or dynamic mechanical analysis (DMA described in section 3.5.1). A comparison of DSC and DMA measurement techniques for T_g are presented in Figure 3.21. The DSC measures physical changes in the resin, one of which is the change in heat capacity of a cured polymer [42]. The DSC value for T_g is usually 10-20°C below that of the DMA [42]. The DMA is more sensitive to changes in T_g because the DMA applies a periodic mechanical force to a specimen as the temperature is increased. The DMA is basically an axial Rheometer, and all the material functions presented in section are 3.4.1 valid. The only difference is that the modulus is not the shear modulus (G), but the elastic modulus (E).

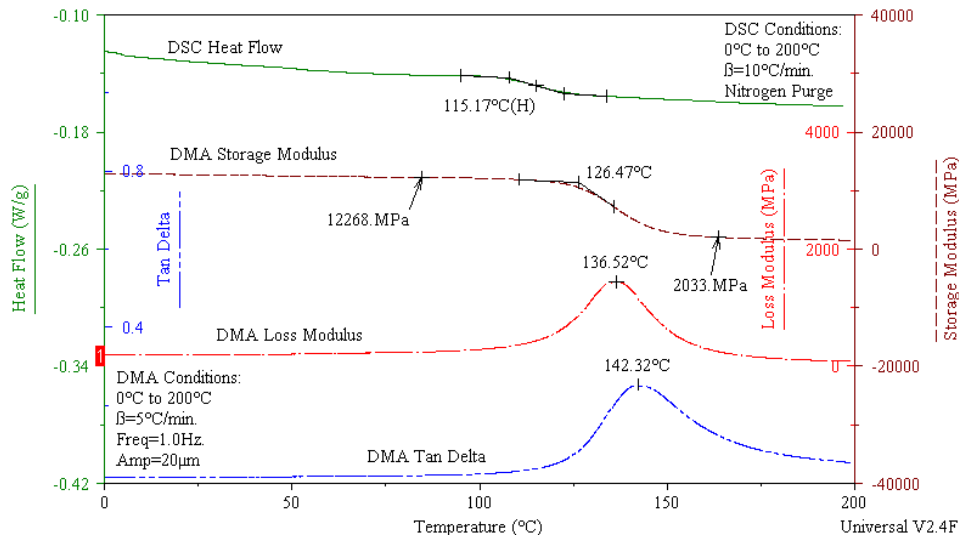


Figure 3.21: DSC and DMA plots to determine the T_g of a glass reinforced epoxy [46].

The three DMA signals in Figure 3.21 are the storage modulus E' , the loss modulus E'' , and the trigonometric tangent of delta. The storage modulus is a measure of how much energy can be recovered (the elastic response according to Hooke's law), and when the storage modulus begins to decrease, this temperature represents the value of T_g – onset. The loss modulus is the amount of energy lost to friction and internal motions (viscous response) [42], and the temperature at the peak of this curve is known as the T_g – peak of E'' . Finally, $\tan \delta$ is a ratio of the elastic and viscous responses. The temperature when the material is most efficiently absorbing energy to molecular rearrangements and internal friction is known as the T_g – peak of $\tan \delta$ [42-45]. There is no standard for which of the three values of T_g should be reported, except that the user should be consistent and indicate which method was used [47].

For the purposes of this project, T_g is defined as the onset of the storage modulus decrease, or when the resin loses the ability to support load. The following sections describe the equipment used, how it was calibrated, the experimental procedure, and the results of the DMA tests.

3.5.1 Dynamic Mechanical Analysis

A TA instruments Q800 DMA (dynamic mechanical analyzer) was used to oscillate a 2-ply composite beam to determine the T_g . The DMA is shown in Figure 3.22, with a close-up of the 3-point bending fixture and the thermocouple that measures the temperature of the specimen. The 3-point bending fixture was chosen because it does not impart any shear stresses into the specimen, unlike with the single or dual cantilever fixtures [42]. There are 2 thermocouples in the furnace, one measures the air temperature, and the other measures the specimen temperature. The specimen thermocouple is adjustable, and was positioned as close to the specimen as possible, without interfering with the test.

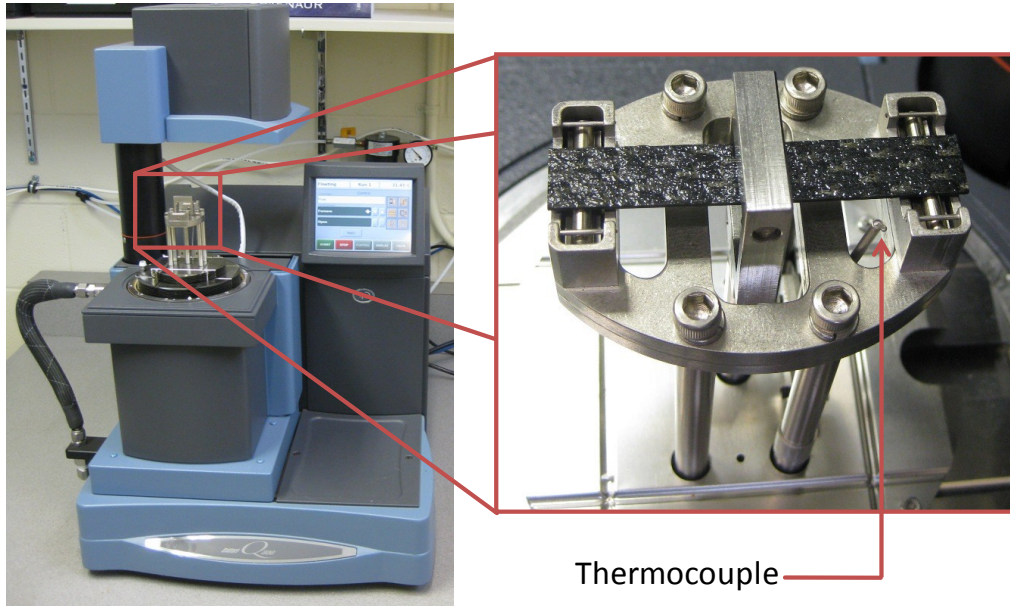


Figure 3.22: Rectangular specimen installed in the 3-point bending fixture of the DMA.

3.5.1.1 DMA Calibration and Temperature Verification

All of the calibrations can be performed with the assistance of the calibration wizard in the Q800 DMA software. The manufacturer recommends calibrating the instrument every month; therefore the calibrations were performed before verifying the performance. The two main calibrations are for the instrument itself, and the clamp being used. First the instrument electronics, force and dynamic calibrations were performed. Afterwards, the 3-point bending clamp was calibrated for mass and compliance. Upon completion of the calibrations, the temperature performance was verified using a rectangular polycarbonate sample. The same temperature ramp rate and test conditions were used in the temperature verification as for the experiments. The measured T_g of the polycarbonate was 148.9°C, compared to the known value of 150°C [48]. This difference of 0.73% was factored out by placing the observed temperature of 148.9°C and the correct temperature of 150°C into the temperature calibration table of the DMA. With the calibrations complete and performance known, the confidence in the accuracy of the tests was established.

3.5.2 Experimental Procedure

The procedure for the DMA tests was the multi-frequency strain mode, and the temperature ramp/frequency-sweep test. There is no option for a single frequency, therefore the multi-frequency was simply set to one value, 1 Hz. A preload of 0.5 N was used to ensure the clamp remained in contact with the specimen at all times. A sinusoidal amplitude of 100 μm was applied to the specimen, and the force track was set to 125%. The force track is used to keep the preload applied to the specimen in addition to the force required to apply the 100 μm displacement. A temperature ramp rate of 2°C/min was selected to minimize the temperature lag between the specimen and furnace, and the test was started from room temperature. The final temperature was set to 250°C for all the specimens to ensure that the T_g would not be missed at the higher degrees of cure.

The specimens for the first four tests were cured as a traveler coupon at the same time as the representative sandwich panels in Chapter 5. The final specimen, cured at 180°C was cured separately. The traveler coupons were 100 mm x 100 mm and consisted of two plies of prepreg, which were layed up symmetrically. The final cured thickness of the specimens was 0.89 ± 0.02 mm. The traveler coupons were cut to a width of 10 mm and a length of 60 mm using a Struers low speed precision water cooled saw with a diamond coated cutting blade. Special attention was taken to ensure that the edges were parallel to eachother, and that the 0° tows were parallel to the edges on the top and bottom of the specimen. Each test level was performed twice as shown in the test matrix (Table 3.6). The degree of cure shown in Table 3.6 was predicted using the cure kinetics model and the temperature data recorded during cure.

Table 3.6: Glass Transition Temperature Test Matrix

Cure Temp (°C)	Degree of Cure	No. Tests
80	0.51	2
100	0.65	2
120	0.72	2
140	0.82	2
180	0.99	2
Total		10

3.5.3 Experimental Results

An example of the data collected from the DMA is shown in Figure 3.23. As mentioned earlier, the T_g in this work is determined using the onset of the change in storage modulus. The onset is the intersection of the lines before and after the modulus decrease, which was determined to be 142.59°C for this test. The peaks of tan delta and the loss modulus are shown in Figure 3.23, and are approximately 20°C above the storage modulus onset value for T_g . The data and analysis for the 10 tests are available in appendix A.

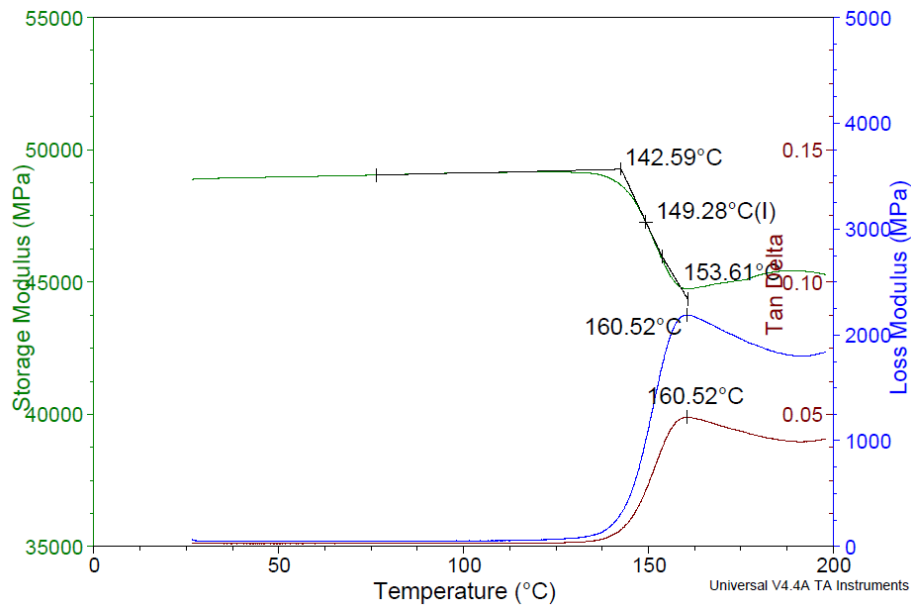


Figure 3.23: DMA test at 2°C/min of 2 plies of MTM45-1/CF2426A, originally cured at 120°C.

The T_g is a physical property of the resin, and as such, it is related to the degree of cure of the material. Therefore it comes as no surprise that the onset of the T_g is increasing with the cure temperature (Figure 3.24). An interesting trend is that the T_g is consistently 20°C above the cure temperature. The T_g is one of the physical properties that will determine if a material system is suitable for a specific application. Therefore, the information presented in Figure 3.24 will be useful to determine the minimum degree of cure needed to meet the T_g requirements of the structure. From a comparative standpoint, the T_g of the fully cured MTM45-1 is equivalent to the second generation aerospace grade epoxies, which have dry T_g 's between 185-200°C [50-51].

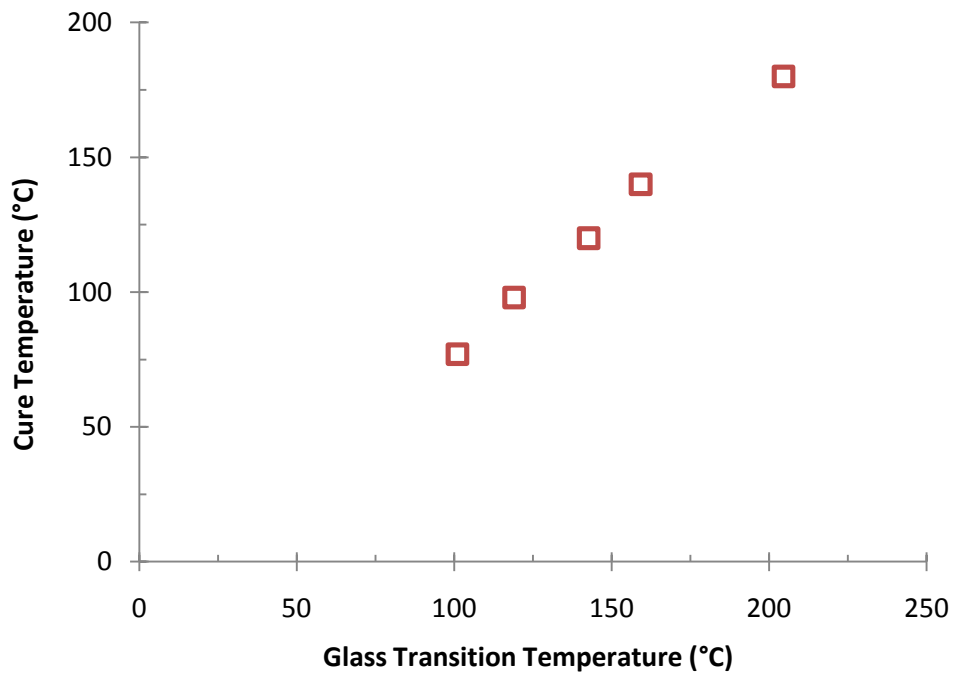


Figure 3.24: Evolution of the onset of the glass transition temperature.

3.5.4 Glass Transition Temperature Model

The T_g can be described by the degree of cure of the resin. The experimental data was used to determine the single parameter of the model developed by DiBenedetto [49]. The equation is as follows:

$$\frac{T_g - T_{g0}}{T_{g\infty} - T_{g0}} = \frac{\lambda \alpha}{1 - (1 - \lambda)\alpha} \quad (3.11)$$

where T_{g0} is the glass transition temperature of the uncured resin, $T_{g\infty}$ is the glass transition temperature of the fully cured resin, α is the degree of cure, and λ is the experimentally determined constant. The T_g of the uncured resin was measured with the DSC, and observing the transition similar to that shown in Figure 3.21. The values that were experimentally determined are as follows:

$$\begin{aligned} T_{g0} &= -8.6^\circ\text{C} & \lambda &= 0.83 \\ T_{g\infty} &= 210^\circ\text{C} \end{aligned}$$

There exists a good agreement between the model and the experimental data, as observed in Figure 3.25. Equation (3.11) describes the T_g of the resin at any degree of cure.

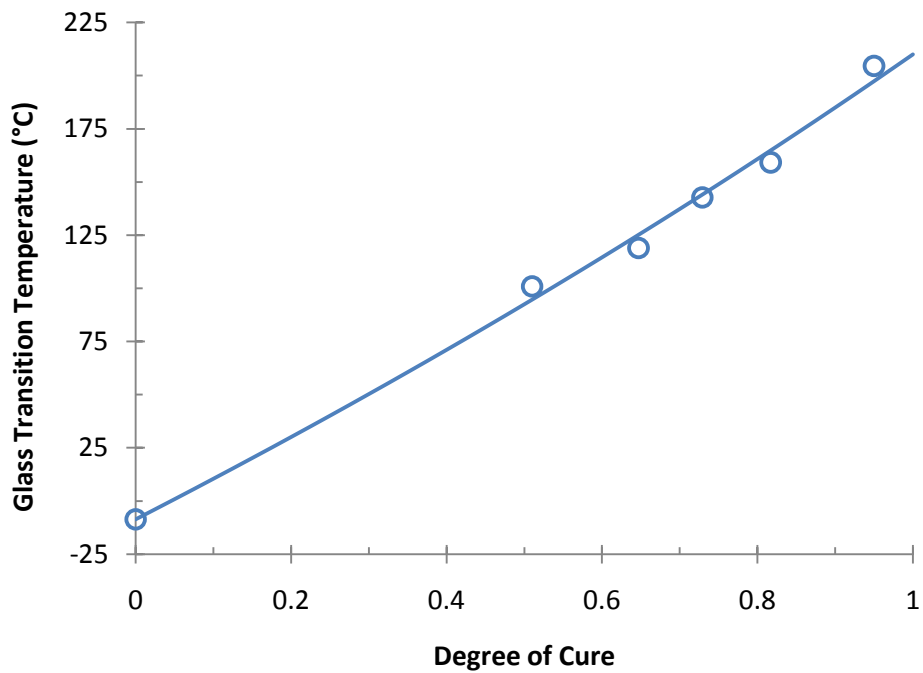


Figure 3.25: Comparison of the T_g model and the experimental data.

An accurate model of the T_g is important during the freestanding postcure of the composite structure. If the T_g is crossed during postcure, permanent deformation of the part could occur, especially on large contoured structures. If the deformation is substantial, the part could be scrapped. A simulation of the thermal history was performed of a part initially cured at 100°C with temperature ramps at 2°C/min. If the temperature ramp rate of the post cure is 0.5°C/min, above the initial cure temperature, the T_g will not cross the postcure temperature (Figure 3.26), and minimal stress relaxation will occur. However, if the temperature rate during the post cure is the same as the initial cure cycle, the T_g will cross the post cure temperature curve (Figure 3.27), causing a decrease in the modulus, and the stress relaxation could possibly permanently deform the composite structure.

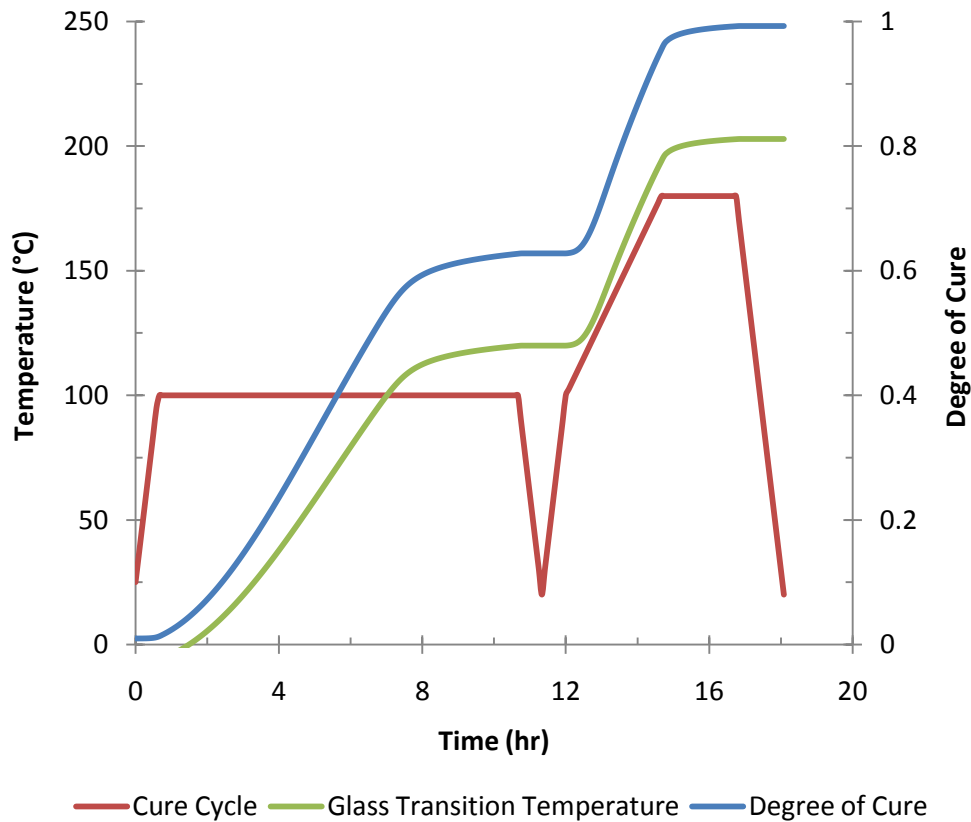


Figure 3.26: Cure cycle with post cure at ramp rate of 0.5°C/min, preventing part distortion.

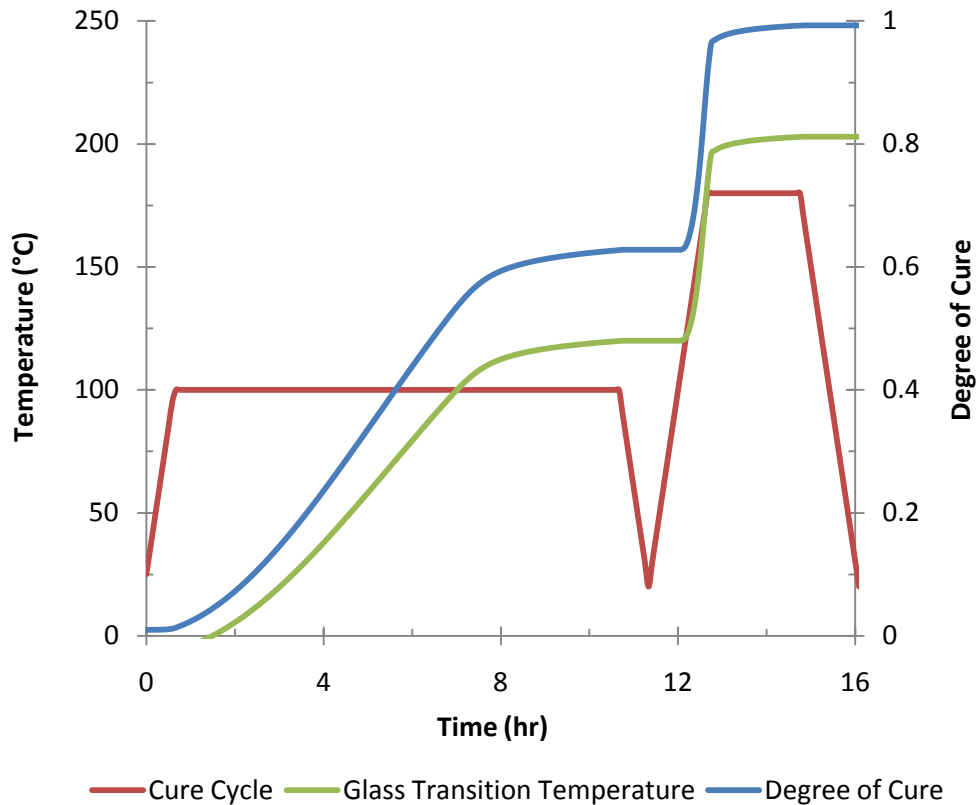


Figure 3.27: Cure cycle with post cure at ramp rate of 2°C/min that will lead to part distortion.

3.6 Summary

The MTM45-1 resin was characterized. The resin was observed to be thermally stable up to a temperature of 110°C. Above this temperature volatiles will be released, which can lead to voids. A cure kinetics model was developed, which describes the degree of cure of the resin based on any time-temperature history. The cure kinetics model was then used to develop a viscosity and glass transition temperature model. The viscosity model accurately predicts the gelation of the resin, which can be used to determine when the resin will stop flowing during cure. Finally, the glass transition temperature of the resin was modeled as a function of the degree of cure. Using these models, a process engineer can select the appropriate initial and post cure temperature to meet the design requirements of a composite structure manufactured with MTM45-1 resin.

4 Prepreg Characterization

The focus of this chapter is to investigate how the air inside the honeycomb core changes during the manufacturing of a sandwich panel. Since the prepreg is porous, the air permeability can be characterized for different flow directions. The two flow directions are through thickness and in-plane, and the flow direction is determined by the consumables and configuration used to build the vacuum bag. The following sections describe the test system used to characterize the prepreg air permeability, the prepreg permeability experimental procedure, the tests performed, and a discussion of the results.

4.1 *Prepreg Permeability Test System*

A test system to measure the prepreg air permeability was designed and manufactured based on the work of *Tavares et al.* [8]. The test system was used to measure the pressure inside the honeycomb cells during different cure cycles, and with different bagging arrangements. The permeability was calculated using a falling pressure approach (Equation 2.2). The direction of the air flow in the prepreg will change depending on the type of consumables used. The through thickness air flow will occur when a porous release fabric is used, such as a peel ply, and the through thickness permeability can be measured. Conversely, if an impermeable release film is used, the air flow will be limited to the in-plane direction, and the in-plane permeability can be measured.

A single test system was designed and built to measure both in-plane and through thickness permeability. In order to monitor the changes in permeability and core pressure during the cure cycle, the experiments were performed in an

oven. Unfortunately, the pressure sensors that were used are rated to 82°C, and the tests conducted in this project were as high as 180°C. As a result, the pressure sensors were not directly mounted to the permeability test fixture because of their temperature operating range. The most practical solution was to keep the pressure sensors at room temperature, and connect them to the test fixture using vacuum hoses. The schematic of the test set-up is shown in Figure 4.1.

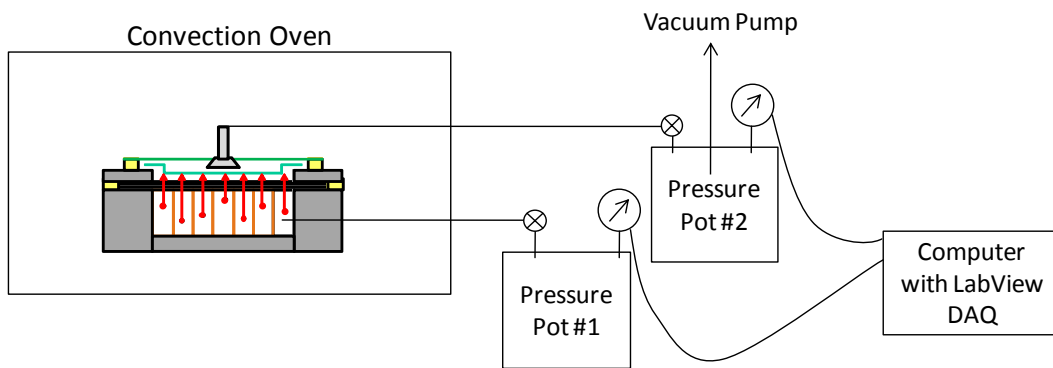


Figure 4.1: Experimental set-up schematic.

The vacuum hoses were connected to the test fixture and pressure pots using quick disconnect vacuum fittings. A miniature ¼ turn ball valve was used in between the pressure pot and the quick disconnect fitting. This configuration allowed full vacuum to be achieved in pressure pot 2, and 5% vacuum in pressure pot 1 prior to starting the test. The mild vacuum was applied in pressure pot 1 to ensure that a seal between the lid and pressure pot existed. This procedure also ensured that all the air flow travelled through the prepreg, and no ambient air was leaking into the pressure pot. The pressure sensors were connected to a National Instruments Data Acquisition box, which was connected to a PC, and the data was recorded using LabView. The following sections describe how the test system was configured to measure the through thickness and in-plane permeability of the prepreg.

4.1.1 Through Thickness Permeability Test Fixture

Through thickness air flow occurs when a porous media is placed on top of the prepreg stack. A schematic of the test fixture used to monitor the pressure inside the honeycomb cells during cure is shown in Figure 4.2. A pressure sensor is connected to the cavity where the honeycomb is contained, and the pressure inside the honeycomb cells is recorded as P_{cell} . Simultaneously, the vacuum pressure on the bag side of the prepreg skin is measured, and designated as P_{bag} . The prepreg stack is placed above the honeycomb core, and the entrapped air inside the honeycomb cavity (represented by the red dots in Figure 4.2) is pulled through the prepreg by the vacuum pressure applied on the bag side. The honeycomb core rests on a suspended aluminum plate that was wrapped with Kevlar fabric, and the hole connecting the cavity to the pressure sensor is located underneath this plate. The Kevlar was used to ensure an even distribution of pressure in between the cells, and was wrapped around the edges to ensure an air path existed between the walls of the cavity and the pressure sensor.

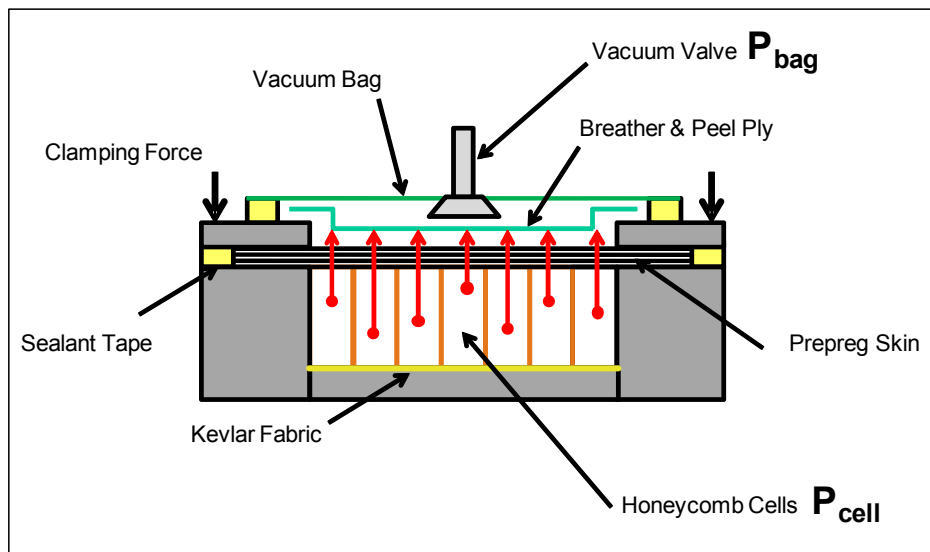


Figure 4.2: Through thickness core pressure measurement test schematic.

To ensure all the air travels through the prepreg, the prepreg overhangs the test cavity by 25 mm, and sealant tape is placed against the cut edge of the prepreg stack, as shown in Figure 4.3. An aluminum picture frame is used to ensure a tight seal between the test fixture and the prepreg. Alignment pins were used to ensure the opening of the picture frame was aligned with the cavity in the test fixture. The applied force compresses the prepreg and sealant tape in between the picture frame and top surface of the test fixture. A close-up view of the expanded sealant tap and the infusion of the compressed sealant tape into the carbon fibres post-testing is shown in Figure 4.4. Figure 4.4 does not show the smoothness of the sealant tape, but there are no porosities or channels formed in the prepreg during cure. Based on the edge sealing, the air entrapped inside the core can only travel in the through thickness direction. The potential for minor air leaks into the vacuum bag does exist; however, it does not influence the pressure readings. The air can leak into the bag where the sealant tape secures the bag to the aluminum fixture. However, the low flow rate of ambient air into the bag can easily be removed by the high flow rate pump. The end result is that no increase in pressure on the bag side was observed.

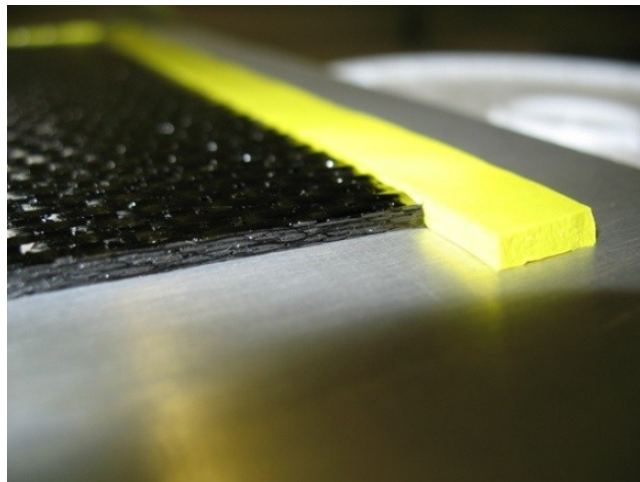


Figure 4.3: Close-up of the prepreg and sealant tape pre-test.

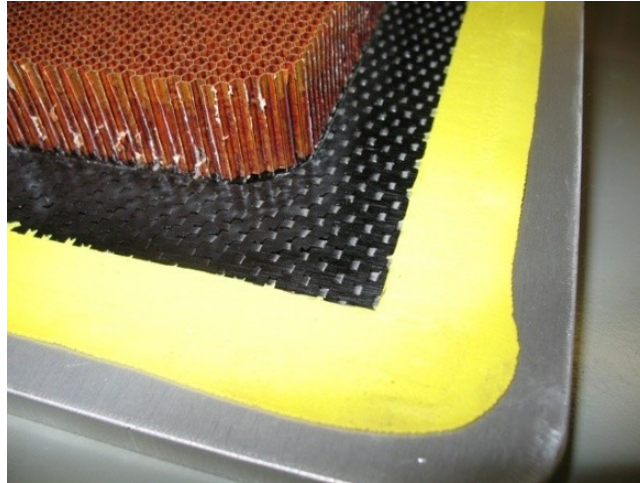


Figure 4.4: Close-up of the $\frac{1}{2}$ sandwich post-test.

4.1.2 In-Plane Permeability Test Fixture

Most commercially available prepregs contain the optimal amount of resin, and therefore the resin should not flow out of the prepreg during cure. In order to achieve this, an impermeable material is placed directly on top of the prepreg stack, and a dam is placed around the perimeter. The impermeable membrane can be a polymer release film, or an appropriately shaped piece of sheet metal, known as a caul plate. The surface finish of the final part is much better when a release film or caul plate is used, as opposed to a porous release fabric. With these impermeable materials, the air flow in the prepreg will occur in the in-plane direction. Edge dams prevent the resin from flowing out of the prepreg sides. Any semi-rigid material can be used, such as cork, thin flat metal strips, or sealant tape. In-order for vacuum to reach the edges of the prepreg during autoclave curing, glass tows were commonly placed between the perimeter of the prepreg and the edge dam [1].

The permeability test system in Figure 4.2 was modified to allow for the in-plane permeability testing, and the schematic of the system is shown in Figure 4.5. The major difference is the lack of sealant tape and aluminum picture frame used to seal the edges of the prepreg. However, sealant tape is used as a dam,

and to support the fibreglass cloth used to provide the edge breathing. The fibreglass cloth and breather ensures an air path is present between the perimeter of the prepreg and the vacuum source. The air passages remain open until the resin reaches sufficiently low viscosity to infuse the fibreglass. The resin will impregnate the fibreglass until it reaches the sealant tape. Now the sealant tape becomes the dam that keeps the resin inside the prepreg.

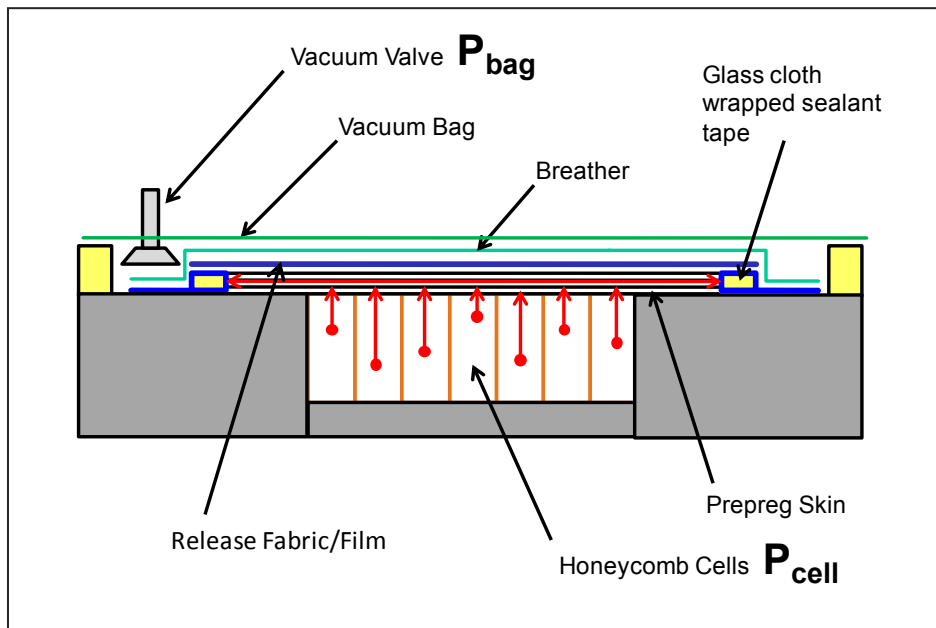


Figure 4.5: In-plane core pressure measurement test schematic.

4.1.3 Measurement System Validation

The performance of the test system was verified by performing a through thickness permeability test with a piece of sheet metal. The prepreg stack was replaced with a 1 mm thick, 200 mm square piece of sheet metal. The pressure inside the core was set to 80 kPa, and the bag pressure was set to full vacuum, and held for 55 minutes. The bag pressure was cycled twice from full vacuum to atmosphere to determine if the internal core pressure changed. The test results are shown in Figure 4.6. The results show that the internal core pressure

remained constant for the majority of the test, except for a few minor pressure fluctuations in the first 5 minutes. The little bump at the beginning of the test was caused by the opening of the ball valves to set the pressure inside the cavity and bag. Since there is no change in pressure inside the cells, any change in pressure during a test must be caused by the air flowing through the prepreg, into the vacuum bag.

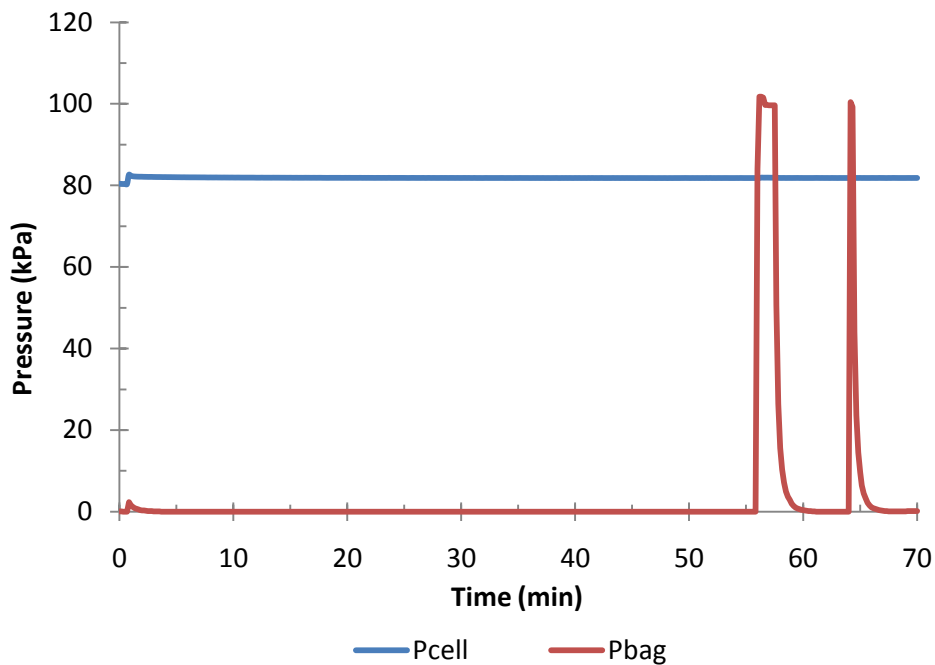


Figure 4.6: Jig leak test using sheet metal in place of prepreg.

The final verification was a leak test of the pressure pots. Full vacuum was drawn inside the pressure pots, and the system isolated by closing the ball valves. The pressure change was recorded over time, and the result of the test is shown in Figure 4.7. The test results indicate that there is an excellent seal in the measurement system, especially the system that measures P_{cell}. The pressure inside the P_{cell} pressure pot remained constant for over 1 hour, and only a slight rise in pressure was observed after 2 hours. The system that measure P_{bag} is less sealed than P_{cell}, this can be attributed to the lack of a ball valve between the

pressure pot and the quick disconnect fitting that connects the pot to the vacuum pump. It is not clear if the leak comes from the quick disconnect fitting, the seal between the vacuum transducer, or the pressure pot itself. Regardless, the vacuum pump will always be connected to this fitting during a test, and it is capable of overcoming this leak.

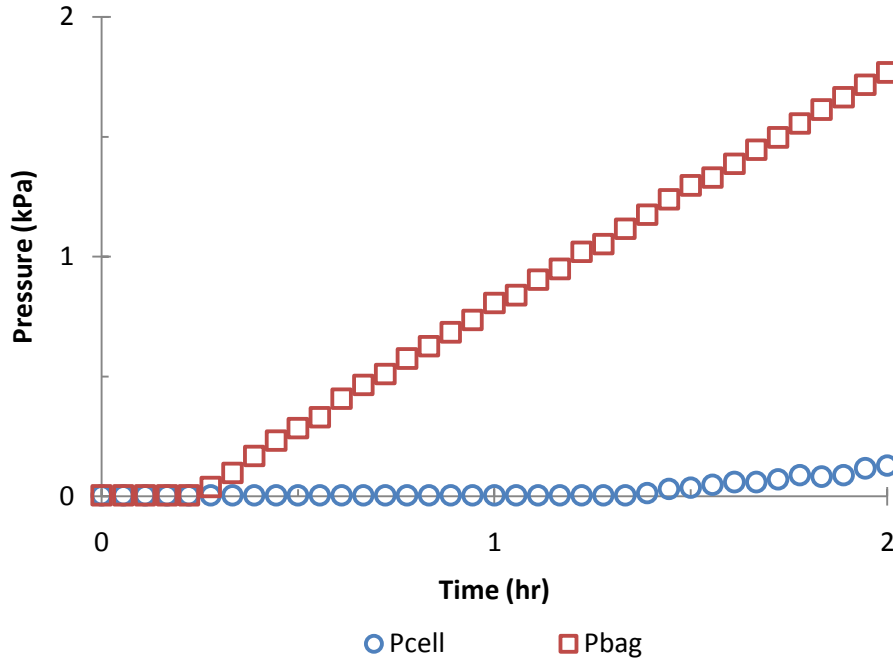


Figure 4.7: Leak test performance verification of the pressure pots.

4.1.4 Pressure Sensor Calibration

The pressure transducers that measure P_{cell} and P_{bag} were calibrated to a known reference using a 7-point calibration. An Omega high accuracy digital pressure gauge (model no. DPG7010-VAC) was connected to the same pressure pot as the pressure transducer being calibrated (Figure 4.8). The pressure in the pot was adjusted using a pressure regulator, and the reference value was input into LabView, along with the uncalibrated value from the pressure transducer. The difference between the reference and uncalibrated values were used by LabView to calibrate the pressure transducers so their output signal is equivalent to the

reference gauge. The pressure transducers were calibrated by first opening the Virtual Instruments Block Diagram in LabView. The DAQ assistant was opened, and the channel (in this case the pressure sensor) to be calibrated was selected. The vacuum level was increased in the pressure pot by approximately 12 kPa at each interval. Once the vacuum pressure had stabilized for 5 minutes, the reference and uncalibrated values were entered into LabView. This process was conducted for both sensors. Upon completion of calibration, the pressure pots were connected to each other, and the vacuum level was set to 50% vacuum. The reference gauge was also connected to the pressure pots, and the error recorded from the vacuum transducers was 0.01% for P_{cell} and 0.12% for P_{bag} .

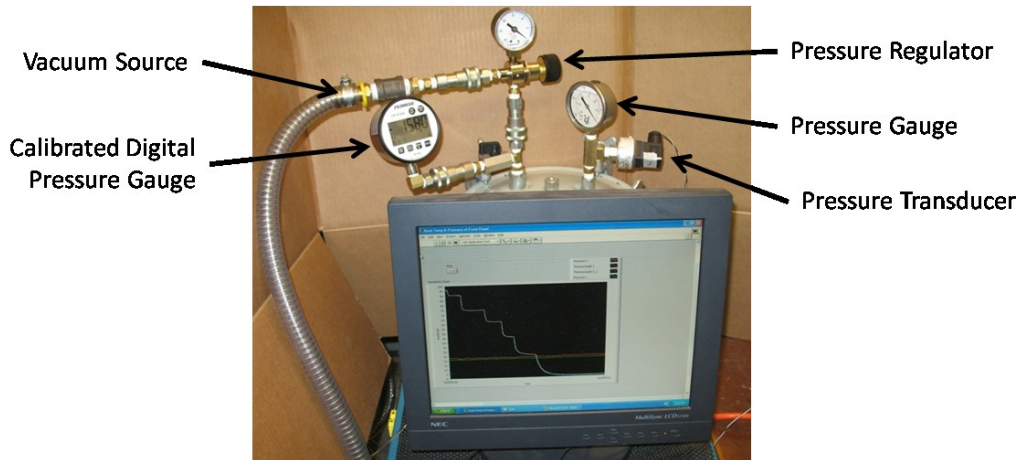


Figure 4.8: Pressure transducer calibration set-up.

4.2 Permeability Testing Procedure

The following procedure was used for both the through thickness and in-plane permeability tests. A release agent (ChemLease 70-90) was applied to the surface of the fixture, and inside the cavity to prevent the composite from sticking to the aluminum test fixture. The honeycomb core was cut to 150 mm square using a utility knife such that the core had less than a 1 mm gap between any edge and the cavity walls. The core was placed inside the cavity, and covered by the

prepreg stack. The prepreg plies were originally cut oversize, layed-up, and then cut to 200 mm square in order to have a flush edge. The following steps highlight the difference that occurred depending on whether the through thickness testing or in-plane test procedure was performed.

4.2.1 Through Thickness

The prepreg was placed over the core and the sealant tape was placed against the edge of the prepreg. The aluminum picture frame was installed between the alignment pins, and forced down with the toggle clamps, compressing the sealant tape and prepreg to form the edge seal. A piece of release fabric (peel ply) was cut to 150 mm square, and placed on top of the prepreg. To complete the bag, 2 plies of breather cloth were placed on top of the peel ply, followed by the vacuum bag. The permeability fixture is shown in Figure 4.9, with a cross section of the layup and bagging arrangement. Note that 6 of the 8 toggle clamps are removed for picture clarity.

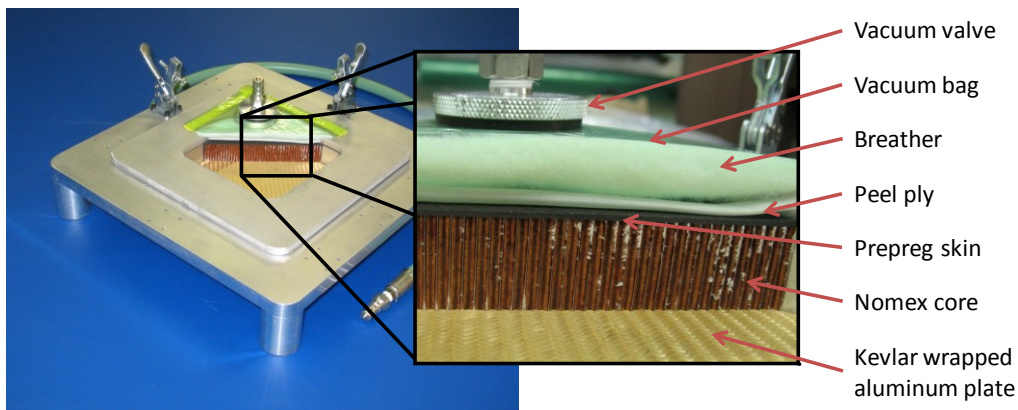


Figure 4.9: The permeability fixture configured for through thickness testing.

4.2.2 In-Plane

The prepreg was placed over the core and the edge breathing was placed around the perimeter of the prepreg. To build the edge breathing, strips of fiberglass cloth were cut to 200 mm x 50 mm. A strip of sealant tape was placed in the

middle, and the glass cloth folded over to cover the tape. The release film was cut to 175 mm square, and placed directly on top of the prepreg stack. The release film was cut to size such that it would cover only the prepreg and the sealant tape in the edge breathing; at least a 25 mm wide segment of the edge breathing was exposed directly to the breather cloth to allow a direct air path to the prepreg. To complete the bag, two plies of breather cloth were placed on top of the release film, followed by the vacuum bag. The permeability fixture is shown below in Figure 4.10. This test had no edge breathing, and the brown dots are the resin that flowed through the perforated (P3) release film, into the breather.

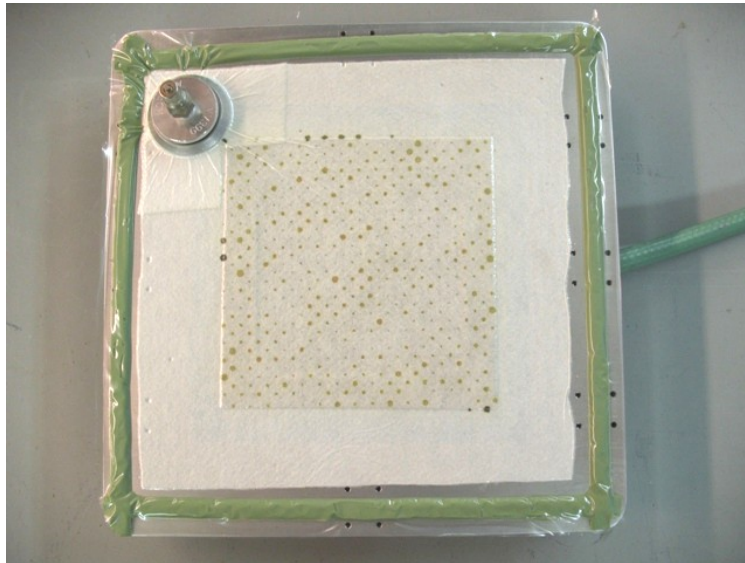


Figure 4.10: The permeability fixture after an in-plane test.

4.3 Test Matrix

When the air from the core reaches the skin, the bagging configuration will reveal if the air travels in either the through thickness direction, or the in-plane direction, or both. The effect of three different release fabric/films was investigated: 1:) polyester release fabric, 2:) fluoropolymer release film with no perforations but microporosities, and 3:) fluoropolymer release film with P3

perforation style. Since the polyester release fabric is very porous, the air would have no flow restrictions in the through thickness direction. With the fluoropolymer release films, the air will predominantly travel in the in-plane direction. Minor amounts of through thickness air flow could occur with the P3 bagging film. It was assumed that the small perforations would not dramatically influence the through thickness air flow, and therefore the tests with the perforated release film were considered in-plane. The following sections describe the test matrix for the through thickness and in-plane permeability configurations.

4.3.1 Through Thickness Permeability Tests

The through thickness permeability was the first series of tests performed. They were selected to validate the performance of the system and compare the results to the air permeability values to those found in literature [8]. The parameters of the test that was performed are presented in Table 4.1.

Table 4.1: The Through Thickness Test Matrix

<i>Test</i>	<i>No. Plies</i>	<i>Film Adh.</i>	<i>Edge Breath.</i>	<i>Release (type / plies)</i>	<i>RT Debulk (hr / kPa)</i>	<i>Full Vac Pressure Applied</i>	<i>Temp Cycle (°C / hr)</i>
1	4	None	None	1 / 1	1 / 5	Debulk	130 / 3

Release Ply Type:

1. Polyester release fabric

4.3.2 In-Plane Permeability Tests

The in-plane permeability tests were performed with two different release films. The first type was a non-perforated release film containing microporosites, which allows the air to flow in the through thickness direction, but not the resin. The second type was a perforated (P3) release film, which may allow more air to flow through the skin, but also a small amount of resin. The other parameters that were investigated include the number of plies N, the vacuum pressure cycle,

the temperature cycle, edge breathing, and the use of a film adhesive. The layup of the skin was $[0]_N$ for all the tests, where the 0-direction was parallel to the roll direction of the prepreg. Also, the vacuum pump was set between 10-20 kPa for all the tests, where 0 kPa is absolute vacuum. The time when full vacuum was applied during the cure cycle was varied between the room temperature debulking step, the temperature ramp, and the beginning of the dwell. Varying the position in the cure cycle when full vacuum was applied was used to determine if light vacuum pressure at room temperature would remove the entrapped air, and then increase the vacuum bag pressure at the beginning of the temperature ramp or dwell to 'lock in' the core pressure during cure. Finally, an edge breathing technique was investigated to see the influence on the skin quality. The edge breathing was similar to the one was used by *Repecka and Boyd* to improve the void content in out-of-autoclave prepreg [2]. The complete test matrix is shown in Table 4.2.

Table 4.2: In-Plane Permeability Test Matrix

<i>Test</i>	<i>No. Plies</i>	<i>Film Adh.</i>	<i>Edge Breath.</i>	<i>Release (type / plies)</i>	<i>RT Debulk (hr / kPa)</i>	<i>Full Vac Pressure Applied</i>	<i>Temp Cycle (°C / hr)</i>
1	4	None	Yes	3 / 2	0.5 / 50	Ramp	75 / 0.5 & 120 / 6
2	4	None	Yes	3 / 2	1 / 15	Debulk	75 / 0.5 & 120 / 6
3	4	None	Yes	3 / 2	3 / 15	Debulk	80 / 26
4	4	None	Yes	3 / 2	14 / 15	Debulk	180 / 2
5	4	None	Yes	3 / 2	1 / 15	Debulk	120 / 6
6	4	None	Yes	3 / 2	1 / 85	Dwell	120 / 6
7	4	None	None	3 / 2	2 / 15	Debulk	120 / 6
8	4	None	Yes	2 / 1	1.75 / 15	Debulk	75 / 0.5 & 120 / 6
9	2	Yes	Yes	2 / 1	1.5 / 15	Debulk	100 / 12
10	2	Yes	Yes	2 / 1	1 / 15	Debulk	75 / 0.5 & 120 / 6
11	2	Yes	Yes	2 / 1	1 / 15	Debulk	75 / 0.5 & 120 / 6
12	2	Yes	None	3 / 1	1 / 15	Debulk	100 / 12

Release Ply Types:

2. Polyester release fabric
3. Fluoropolymer release film with no perforations but microporosities, and

4.4 Permeability Results and Discussion

The data collected during the core pressure measurement tests included the temperature of the test fixture, and the pressures inside the core and vacuum bag. From this data, the permeability of the prepreg was calculated using Equation 2.2. The only difference in the calculation procedure was the length of the prepreg through which the air had to travel. The through thickness tests, the length the air had to travel was the thickness of the prepreg. In the in-plane tests, the length the air had to travel was a quarter of the length of the honeycomb core and the length of prepreg overlapping the fixture. The following sections present and describe the results of the through thickness and in-plane permeability tests.

4.4.1 Through Thickness Permeability Results and Discussion

The results of the through thickness test is shown in Figure 4.11. The test began with a room temperature de-bulk, where the through thickness permeability is constant, causing a constant decrease in the internal core pressure. When the resin softens during the temperature ramp, the permeability dramatically increases, and the high pressure air inside the core can easily flow through the 2 mm skin. The viscosity of the resin decreases from 9000 Pa·s at 25°C to 500 Pa·s at 60°C, and the resin begins to flow. By 80°C the resin has fully impregnated the prepreg, and this change in fibre bed architecture decreases the air flow. When the fibre bed becomes completely infused with resin, microchannels form allowing the remaining air to flow-out until the core pressure equals the vacuum pressure.

The through thickness configuration allows the core to be fully evacuated, preventing any lift-off of the skin from the honeycomb cells. Unfortunately, the porous peel ply allows some resin to flow out of the skin along with the air. This reduction in resin content created a skin with an unacceptably high void content, and therefore the use of peel ply as a bagging consumable was abandoned. The test did validate the fixture, and provide a point of comparison with other permeability research. The through thickness air permeability values were the same order of magnitude (10^{-18} m^2) as those in [8].

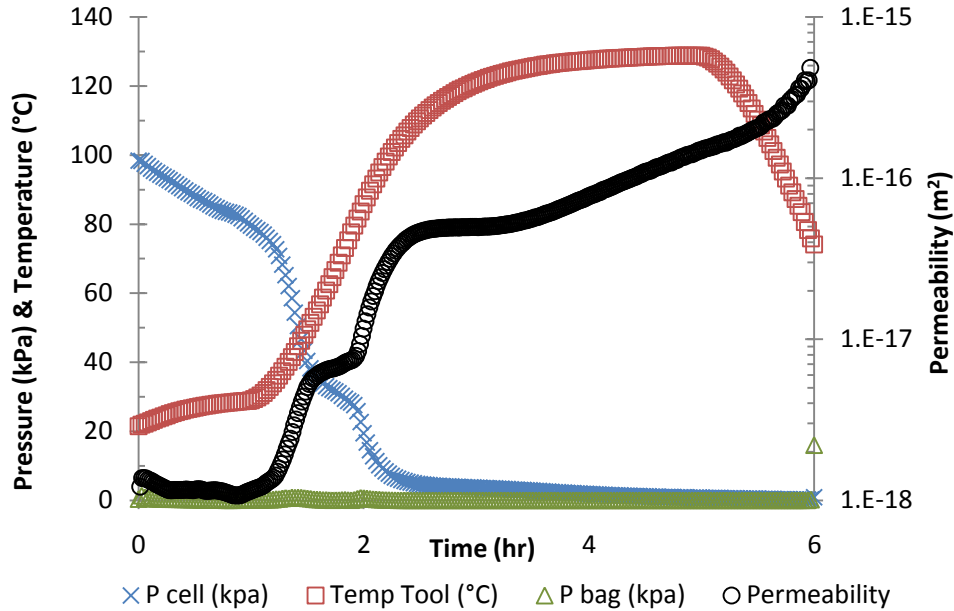


Figure 4.11: Through thickness air permeability test of 4 plies of MTM45-1/CF2426A, 1 ply of release fabric, and full vacuum applied at room temperature.

4.4.2 In-Plane Permeability Results and Discussion

The major differences between the through thickness and in-plane permeability tests are 1) the order of magnitude of the permeability, and 2) when the permeability is the highest during the cure cycle. The in-plane permeability is the highest during the room temperature debulk. The permeability is not constant at room temperature, even though the viscoelastic resin does not flow substantially to change the prepreg architecture. As described in section 2.2, the permeability measurement technique used in this research is based on falling pressure, not air flow rate, therefore as the air is removed from the core, the pressure changes, causing the permeability to change. Over time, the vacuum pressure collapses the interlaminar air channels, reducing the permeability of the prepreg. The permanent deformation of the prepreg is more pronounced for the in-plane permeability because the air must travel further distances to be evacuated.

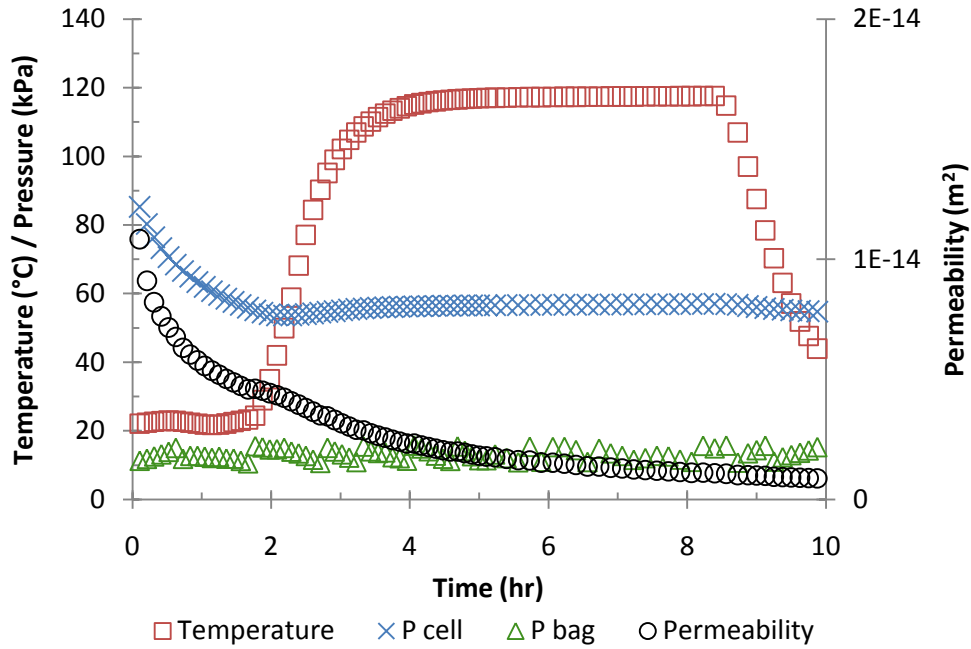


Figure 4.12: In-plane air permeability test of 4 plies of MTM45-1/CF2426A without edge breathing, 2 plies of P3 release film, and full vacuum applied at room temperature.

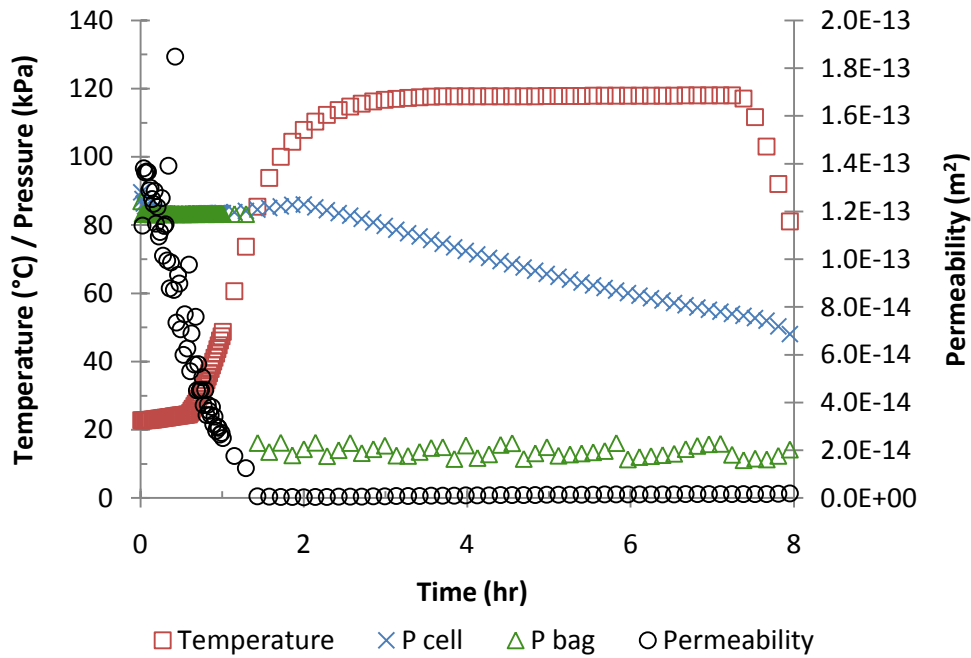


Figure 4.13: An in-plane permeability test of 4 plies of MTM45-1/CF2426A with edge breathing, 2 plies of P3 release film, and full vacuum applied at the start of the dwell.

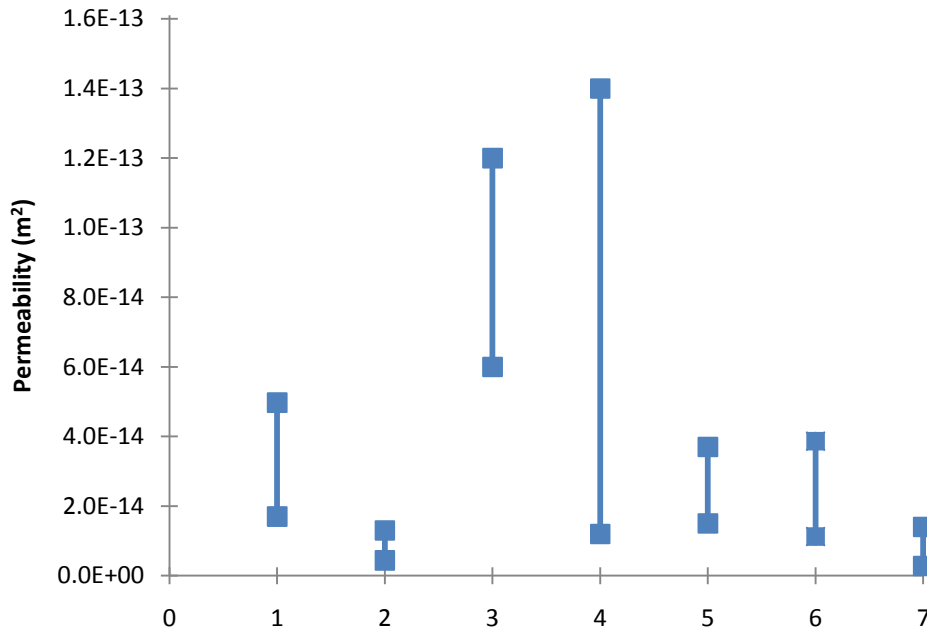
An example of an in-plane permeability test is shown in Figure 4.12. Most of the in-plane permeability tests had a consistent internal core pressure during the dwell because most tests were debulked at room temperature. In these cases, the permeability during the dwell is zero, however the pressure inside the core of test 6 and 12 decreased during cure. An example of the decreasing pressure from test 6 is shown in Figure 4.13. The reason for the air flow during the dwell of test 6 is that full vacuum pressure was applied at the beginning of the dwell, causing a large pressure gradient, and the air flowed through the skin during the dwell. A similar behaviour was observed in test 12 (available in Appendix B) because of the P3 release film and no edge breathing. Without edge breathing, the vacuum was unable to reduce the internal core pressure during the room temperature debulk. However, the single ply of perforated release film allowed the air to flow in the through thickness direction during the test.

Table 4.3: In-Plane Permeability Test Results

Test	Permeability (m^2)				Location in Cure Cycle	Dwell P_{cell} (kPa)	Void Content in Skin (%)
	RT Debulk		Cure Cycle				
	low	high	low	high			
1	6.0E-14	1.2E-13	1.0E-14	1.7E-14	Ramp	46	0.03
2	2.1E-14	8.4E-14	0	0	-	39	0.09
3	1.1E-14	2.4E-14	0	0	-	38	0.18
4	1.2E-14	3.9E-14	0	0	-	23	0.91
5	2.4E-14	5.2E-14	0	0	-	37	0.38
6	1.2E-14	1.4E-13	4.8E-16	1.7E-15	Dwell	85-51	0.11
7	4.4E-15	1.3E-14	0	0	-	56	0.15
8	1.5E-14	3.7E-14	0	0	-	41	0.42
9	4.7E-15	2.5E-14	0	0	-	47	0.04
10	1.5E-14	4.9E-14	0	0	-	38	0.02
11	1.4E-14	4.2E-14	0	0	-	37	0.03
12	2.8E-15	1.4E-14	1.0E-15	2.0E-15	Dwell	67-36	0.02

The permeability values from each test are summarized in Table 4.3, and the test data for all the permeability tests are available in Appendix B. In Table 4.3, the permeability values are first presented as a range (a high and low value) during the room temperature debulk. Second, if there was a pressure change during the ramp or dwell of the cure cycle, the permeability is reported, and the location in the cure cycle. The internal core pressure (P_{cell}) during the dwell is reported. If there was a pressure change during the dwell, the start and end values are reported. Finally, the void content in the skin was measured and is reported for each test. The technique used to measure the void content is presented in the following section 4.5.

The in-plane permeability tests were grouped together to identify any trends, and the results are presented in Figure 4.14. The permeability is higher when the applied vacuum pressure is lower because the compaction force is less. It should also be noted that the internal core pressure will equalize to the vacuum pressure used to debulk the panel. It could be advantageous to stage the application of the vacuum pressure to take advantage of the higher permeability at lower vacuum levels. For example, starting the debulking by applying 10 kPa, and increasing the vacuum at a specific time interval until full vacuum is reached. The other processing variables compared in Figure 4.14 include the film adhesive, the type of release film, and the use of edge breathing. The removal of edge breathing (conditions 2 vs. 1 & 5 vs. 6) from the bagging arrangement does reduce the permeability. The permeability of the stack is comparable when 2 plies of perforated release film are used, compared to 1 ply of non-perforated release film (condition 1 and 5). Finally, the film adhesive does not dramatically reduce the permeability (condition 5 and 6).



Conditions:

1. Full Vac Debulk, No film adhesive, 2 x P3 release film, Edge breathing
2. Full Vac Debulk, No Film Adhesive, 2 x Non-perf release film, No edge breathing
3. 50% Vac Debulk, No film adhesive, 2 x P3 release film, Edge breathing
4. 15% Vac Debulk, No film adhesive, 2 x P3 release film, Edge breathing
5. Full Vac Debulk, No film adhesive, 1 x Non-perf release film, Edge breathing
6. Full Vac Debulk, Film adhesive, 1 x Non-perf release film, Edge breathing
7. Full Vac Debulk, Film adhesive, 1 x P3 release film, No edge breathing

Figure 4.14: Room temperature debulking in-plane permeability ranges.

4.5 Void Content Results and Discussion

To determine the void content in the skin, three specimens were cut from each test panel on a water cooled saw with a diamond cutting blade. The specimens were 60 mm in length, and were sequentially polished using a 120, 320, 600, and finally 800-grit silicon carbide sand paper, mounted to a rotational grinder/polisher. The void content in the skin was determined for the samples using Image Tool 3.0 image processing software [52]. A visual representation of the steps used to determine the void content is shown in Figure 4.15. The complete image of the sample was scanned as a 24-bit colour image using a photo scanner with an optical resolution of 3200 dpi. The image was cropped to

isolate the composite skin, and then converted to grayscale. A manual threshold was used to adjust the contrast such that the voids were differentiated from the skin, and an area analysis was performed to determine the percentage of voids in the skin. In Figure 4.15, a close-up of the skin is presented to show the voids, but the complete 60 mm wide image is used during the image analysis process. It should be noted that this analysis approach is for comparative purposes, and only isolates the macrovoids greater than 50 μm in size. Since, the microvoids are not captured, the total void content in the skin is underestimated.

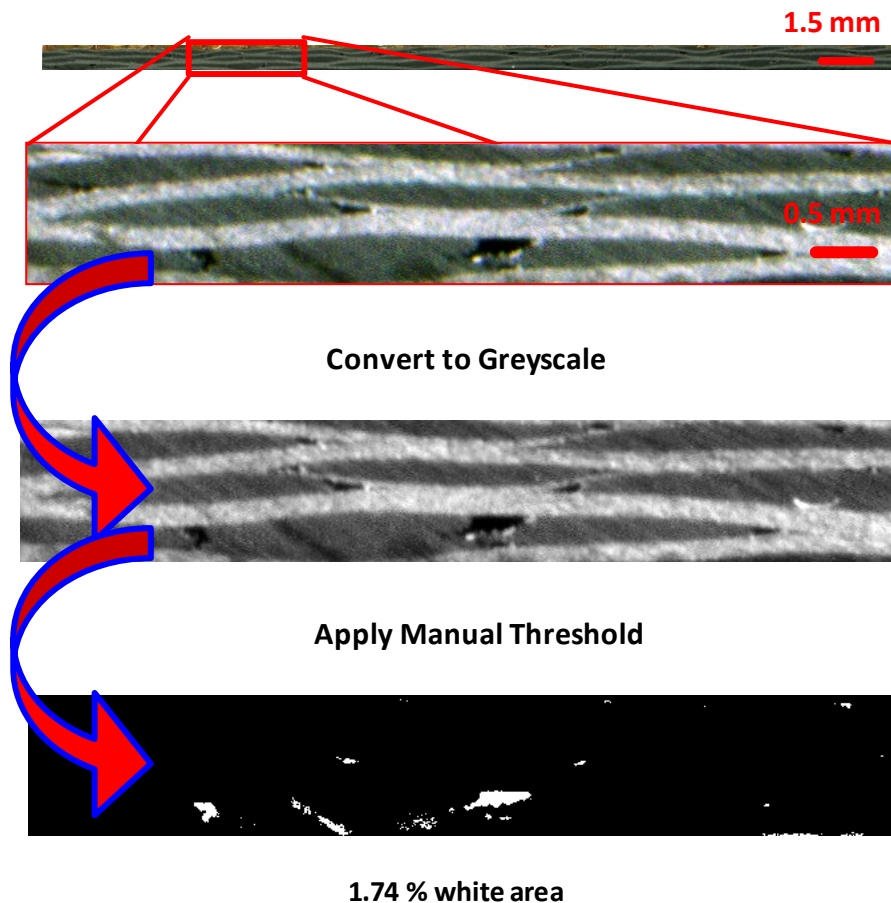


Figure 4.15: Process flow for the image analysis of the composite skin.

A plot of the internal core pressures versus the void content in the skin is shown in Figure 4.16. This plot indicates that a higher void content is likely to occur when a low internal core pressure is present. Furthermore, the internal core pressure for the majority of the tests was approximately 40 kPa, indicating that for this material system the in-plane permeability will approach zero near an internal core pressure of 40 kPa during a room temperature debulk.

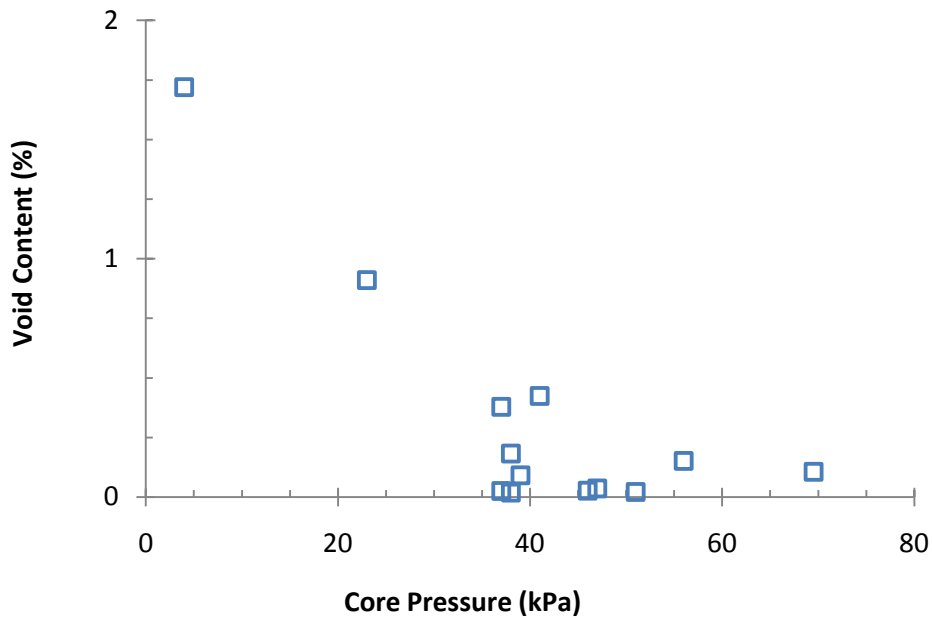


Figure 4.16: Void content as a function of the internal core pressure.

The quality of most of the panels was very good, with void contents less than 0.5%. However, the tests with an internal core pressure below 20 kPa had the worse quality skins. The test with the lowest internal core pressure was the through thickness permeability test. In that test, the release fabric allowed the resin to flow out of the skin, and was absorbed by the breather cloth, contributing to the highest void content. Since the initial resin content of the prepreg is 36%, the resin bleed caused sufficiently more voids to form in the skin, compared to the other tests. Moreover, the low internal core pressure reduces

the compaction of the skin. The ability for voids to nucleate and grow is present when the low skin compaction is coupled with the resin loss.

The lowest internal core pressure of the in-plane tests was observed in test 4. In test 4, the panel was debulked at room temperature overnight, creating a low internal core pressure. The panel was also cured at the highest tested temperature of 180°C, where more volatiles from the resin are escaping due to thermal degradation. The high temperature coupled with the low skin compaction creates an ideal void nucleation and growth environment. The other test variables were not clearly identified which configuration would lead to a better quality part at this scale. It is clear that a low internal core pressure increases the void content in the skin, even when all the prepreg resin is retained in the skin.

4.6 Summary

The through thickness and in-plane permeability of the prepreg were determined using the falling pressure measurement technique. The differences between the through thickness and in-plane permeability tests are summarized in Table 4.4. A surprising observation is that the film adhesive does not reduce the permeability of the layup. The relationship between the resin characterization, the prepreg permeability, and the quality of a composite sandwich structure is shown in Figure 4.17. The permeability will influence the internal core pressure, which will in turn affect the mechanical strength of the skin to core bond, and the porosity of the skin. The internal core pressure should be set to 40-50 kPa, which is controlled by the cure cycle and bagging configuration. The bagging configuration will determine the permeability (or how quickly the internal core pressure will reach the optimal range). When the “optimum” core pressure is achieved, the resin viscosity must be sufficiently low to flow-out, and prevent any further air from escaping the core. The resin viscosity is based on the resin characterization. The resin characterization also plays an important role in

predicting the cured part properties of the sandwich structure, such as the glass transition temperature.

Table 4.4: Comparison of Through Thickness and In-Plane Permeability

<i>Parameter</i>	<i>Through Thickness</i>	<i>In-plane</i>
Permeability		
Room temperature debulk	Constant (10^{-18} m^2)	Changing (10^{-14} m^2)
Temperature ramp	Increases	Decreases
Dwell	Zero	Dependent on bag & cure cycle
Internal Core Pressure		
Major pressure change	Temperature ramp	Room temperature

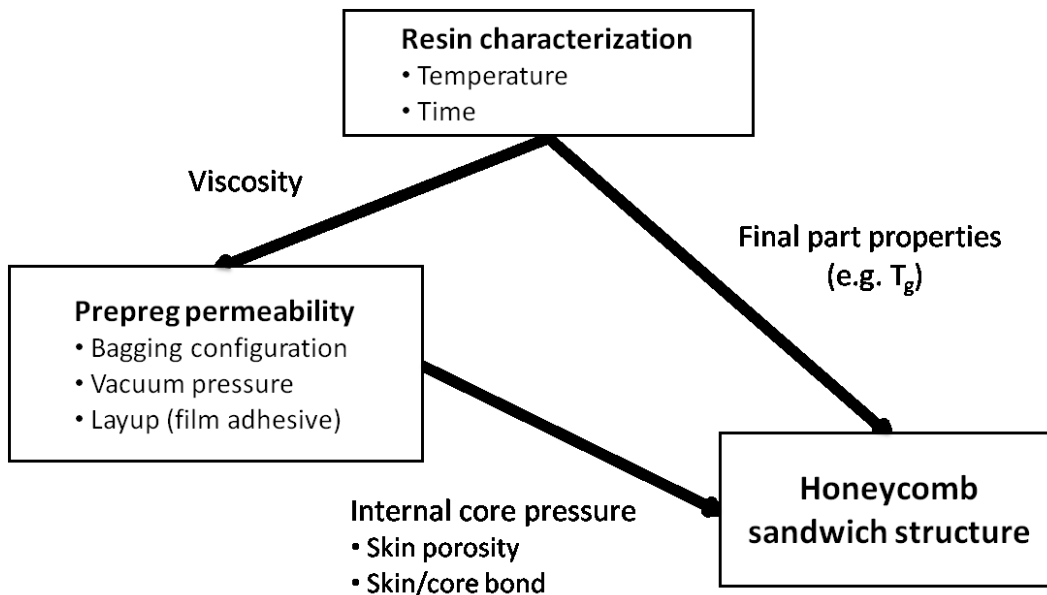


Figure 4.17: The relationship between the resin characterization, prepreg permeability, and the final part performance of the sandwich structure.

5 Representative Sandwich Panels

This chapter investigates the effect of scale-up, which may reveal processing issues that were not present in the small permeability panels manufactured in Chapter 4. Furthermore, the representative sandwich panels can be used to evaluate the effect of different cure cycles and bagging configurations on the mechanical performance. The following sections in this chapter describe the materials, test matrix, sandwich manufacturing method, qualitative testing (void analysis & hot water submersion tests), and mechanical testing of the representative panels.

5.1 Materials

The prepreg material was the same MTM45-1/CF2426A used in Chapters 3 and 4. The sandwich core was hexagonal Nomex honeycomb from Euro-Composites. The core was 25 mm thick, with a 3.175 mm cell diameter, and the core density was 72 kg/m³. A film adhesive was used to provide additional resin for bonding between the skin and core. The adhesives used were AF 163-2K from 3M Canada (London, ON), and FM300-2 from Cytac Engineering Materials (Anaheim, CA).

The consumable bagging materials were all supplied from Airtech International (Huntington Beach, CA). Perforated and non-perforated fluoropolymer release films (WL5200) were used to prevent the breather from sticking to the composite skin. Ultraweave 606 nylon breather was used to evenly distribute the compaction pressure, and remove air and volatiles from the composite. Finally, a Wrightlon WL7400 nylon film was used to complete the vacuum bag with a GS213 sealant tape.

5.2 Test Matrix

Five representative sandwich panels were manufactured in order to identify if the bagging configuration, debulking cycle, and cure cycle would impact skin quality and mechanical performance. The test matrix for the large sandwich panels is summarized in Table 5.1. All panels were cured under 10-15 kPa of vacuum, and only panel 5 was debulked at a lower pressure. The temperature ramp rate was constant at 2°C/min for every test.

Table 5.1: Sandwich Panel Test Matrix

<i>Panel</i>	<i>Film Adhesive</i>	<i>Edge Breathing</i>	<i>Release Film (type / plies)</i>	<i>RT Debulking (hr / kPa)</i>	<i>Temp Cycle (°C / hr)</i>
1	AF 163-2K	Yes	2 / 1	2 / 10	100 / 12
2	FM300-2M	Yes	2 / 1	12 / 10	100 / 12
3	FM300-2M	Yes	3 / 1	9 / 10	80 / 24
4	FM300-2M	None	2 / 1	2 / 10	80 / 2 & 140 / 2
5	FM300-2M	Yes	3 / 2	3 / 40	75 / 2 & 120 / 6

Release Ply Types:

2. Fluoropolymer release film with no perforations but microporosities, and
3. Fluoropolymer release film with P3 perforation style

Panels 1 and 2 were used to compare the difference between a short and long room temperature debulk on the skin quality (void content). Furthermore, panels 1 and 2 identify the difference in mechanical performance between the two film adhesives at the same cure temperature. Test panel 3 was used to identify the effect of a low temperature cure. Additionally, test panel 3 used the perforated release film to improve the air permeability because the viscosity of the resin would remain relatively high during cure. With the high viscosity, the resin would not easily flow into the breather, avoiding resin starvation of the skin. Panels 4 and 5 were used to explore the effect of a higher temperature, shorter cure cycle, on skin quality. Panel 4 was also used to determine the effect of no edge breathing on skin quality. Panel 5 was selected to observe the effect

on reducing the room temperature debulking pressure to increase the air permeability, by reducing the consolidation pressure. Two layers of perforated release film were used and placed such that the perforations did not align. The intention was that the perforations would increase the air permeability, but reduce the amount of resin flow because the perforations were not aligned.

5.3 Sandwich Panel Manufacturing Procedure

The representative sandwich panels were manufactured in a Blue M convection oven, on a flat aluminum tool plate of 60 cm x 90 cm. A release agent was applied to the tool to prevent the composite skin from sticking to the mould surface. During layup, two plies of prepreg were placed on the tool, followed by 1 ply of film adhesive Figure 5.1A, the honeycomb core Figure 5.1B, another ply of film adhesive Figure 5.1C, and finally 2 more plies of prepreg. After completion of the layup, the edges of the sandwich panels were cut such that all 4 plies were flush with the edge breathing Figure 5.1D. The release film was placed over the sandwich panel, and extended 1 cm onto the edge breathing, where the sealant tape ended. This technique ensured that the air passage between the breather and glass cloth was available. One layer of breather was cut to the size of the tool plate. One extra strip of breather was placed along the chamfer of the honeycomb, extending over the glass cloth edge breathing. The vacuum bag was installed with flaps at the locations of the core chamfers to ensure no loss of compaction pressure due to bag bridging Figure 5.1E.

The cured panel size was 65 cm x 45 cm, including a 5 cm edge band to close-out the core. The core was cut with a 45° chamfer using a table saw. The layup of the skin was $[0/90]_{2s}$, where 0° is the roll direction of the prepreg, and the 0° plies are parallel to the 65 cm side. The size of the panels is shown in Figure 5.2, along with the locations used for void analysis. The remainder of the panel was used to extract the climbing drum peel coupons. The peeling direction was parallel to the ribbon direction of the honeycomb core, as shown in Figure 5.2.

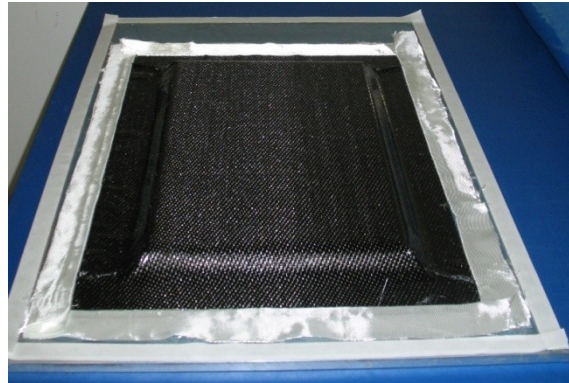


(A)

(B)



(C)



(D)



(E)

Figure 5.1: The steps in the sandwich structure layup process.

The lower prepreg plies and film adhesive (A), followed by the honeycomb core (B), the top layer of film adhesive (C), the top prepreg layers and edge breathing is installed when the part is placed on the tool (D), and the part vacuum bagged (E).

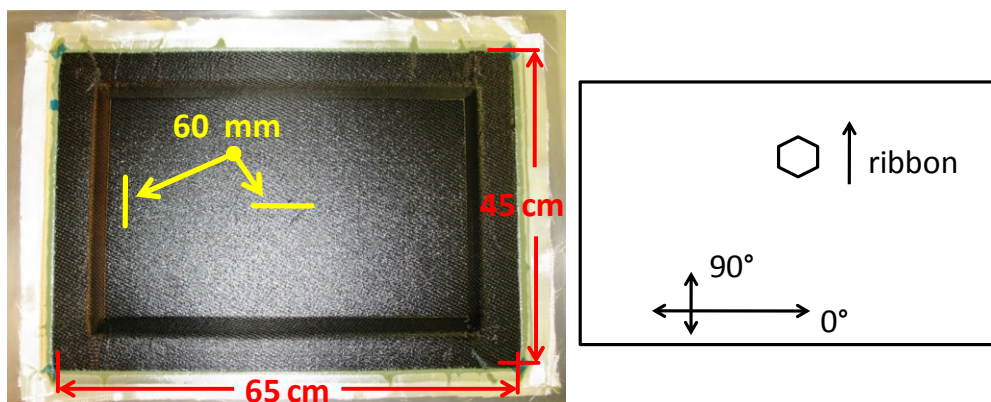


Figure 5.2: Representative sandwich panel (left), showing the microscopy locations, and the fibre and ribbon directions (right).

5.4 Void Content Analysis

The void content in the skin was determined for the five panels using the same technique as for the core pressure measurement tests, and the results are summarized in Figure 5.3. The average void content and one standard deviation are reported for each panel. The void content was taken at four locations. The bag and tool side at both the centre and one edge of the panel, as shown in Figure 5.2. Panels 1 and 2 had the best quality. The debulking time was varied to observe any effect on the void content; the void content of the skins was equivalent. For panel 3, the cure temperature was decreased to 80°C to see the effect of high resin viscosity on part quality. A single ply of perforated release film was used to help remove air in the through thickness direction. Almost no resin flowed from the skin into the breather cloth, helping to keep a low void content in the skin. In panel 4, the edge breathing was removed, and the cure cycle had 2 holds for 2 hours, one at 80°C and 140°C. At a final dwell temperature of 140°C, volatiles were escaping from the resin, and the resin was able to reach its minimum viscosity, which also led to a short gel time. The short gel time prevented the volatiles from being removed from the skin. The intermediate hold was successfully used with the permeability measurements (Chapter 4) to produce skins with a low void content, specifically in the 2-ply skin

panels. Unfortunately, the intermediate hold was unable to remove the entrapped air and volatiles without the edge breathing in the larger representative panels. For panel 5, the vacuum pressure was set at 40 kPa and held for 3 hours at room temperature in an effort to set the internal core pressure. The vacuum was increased to full before the temperature cycle started. Similar to panel 4, an intermediate hold was used before reaching the final cure temperature. Panel 5 had the most resin loss of all the panels due to the perforated release film and high dwell temperature. Some resin flowed in-between the 2 plies of perforated release film, reducing the amount of resin available to impregnate the dry fibres in the skin. The cured skin of panel 5 had the worst void content of all the panels.

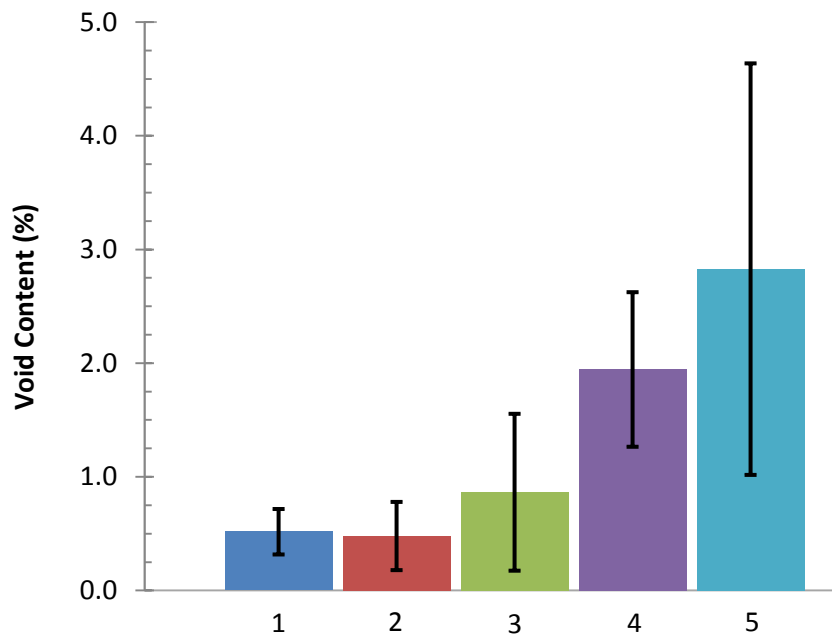


Figure 5.3: Void Content in the skin of the sandwich panels.

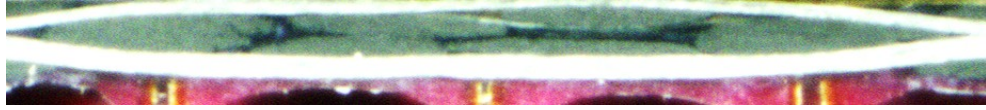


Figure 5.4: Cross section of the bag side in the centre of panel 1, showing the resin rich regions between the fibre tows.



Figure 5.5: Cross section of the bag side in the centre of panel 5, showing the voids.

Selected microscopy images at the centre of the bag side skins of panels 1 and 5 are shown in Figure 5.4 and Figure 5.5, respectively. The dark grey regions in between the fibre bundles are resin-rich regions in Figure 5.4, in contrast to the black areas that are voids in Figure 5.5. The image processing software is capable of discerning the difference in contrast level between the resin rich regions and the voids.

5.5 Hot Water Submersion Test

A non-standard test, the hot water submersion test, was performed to provide a qualitative comparison of the quality of the sandwich panel skins. A 40 mm x 75 mm section of sandwich panel was placed in a beaker of hot water (Figure 5.6), not boiling, and if bubbles formed on the surface, porosity existed in the skin. When the sample was placed in the hot water, the air inside the core expanded according to the ideal gas law. If no bubbles formed at the surface, the air remained in the core because the skin is sealed. If bubbles do form, passages exist for the air to escape, and possibly allow liquid into the core. Moisture ingress is a major concern for maintaining the structural integrity of the sandwich panel. If moisture, de-icing fluid, or hydraulic fluid enters the core of an aircraft sandwich structure during service, the quality of the adhesive bond between the skin and core will degrade over time.



Figure 5.6: Hot water submersion test setup.

5.5.1 Results and Discussion

The results from the hot water submersion tests are summarized in Table 5.2. Based on the visual observations of the experiment, panel 3 had almost no bubbles forming on the surface of the skin. A surprising result from this test was that the panels with higher void content had less bubbles forming on the surface. Panel 3 had a slightly higher void content than panels 1 and 2, and panel 5 had a considerably higher void content than panel 4. These results suggest that the moisture ingress resistance of the cured skins is not dependent on the void content. Furthermore, it may be preferable to have a sealed panel with more voids which are evenly dispersed throughout the skin opposed to a few voids that are closely joined to allow moisture to pass through. Finally, the amount of bubbles forming on the skin is proportional to the cure temperature. The least amount of bubbles occurred in panel 3, which was cured at the lowest temperature, and the most bubbles occur in panel 5, which was cured at the highest temperature. This indicates that void coalescence, occurs with greater ease at higher cure temperatures.

Table 5.2: Summary of Hot Water Submersion Tests

Bubble Formation on Surface	Panel
Least	3
	1 & 2
	5
Most	4

5.6 Climbing Drum Peel Testing

The climbing drum peel test is widely used in the aerospace industry to qualify incoming adhesives, and compare the performance of different adhesives. The test method does not provide a mechanical design value, such as fracture toughness, but does provide insight to the quality of the manufacturing process. In this research, the drum peel test was used to measure the peel resistance of the adhesive bond between the composite facing and the core of panels manufactured in Table 5.1. The following sections describe the preparation of the test coupons, the testing procedure, and a discussion of the test results.

5.6.1 Test Coupon Preparation

The test coupons were cut from the five panels such that the peeling direction was parallel to the ribbon direction of the honeycomb core (Figure 5.2). Four coupons were cut from each panel. Two of the coupons tested the peel strength of the tool side interface, and the additional two tested the bag side interface. The test coupons were cut to 80 mm wide and 310 mm long using a band saw with a composite specific cutting blade. The as-cut edges were jagged, as a result the coupons were sanded with 100-grit sandpaper until the edges were smooth and parallel. To allow clamping in the test fixture, the test coupons were cut with the band saw such that a 30 mm overhang of the peeling skin was available at

both ends of the coupon. The excess core was removed with an air grinder and an 80-grit sanding wheel. The surface was evenly sanded to ensure proper gripping in the knurled roller grip of the test fixture.

5.6.2 Experimental Procedure

The tests were performed according to ASTM standard D1781-98(2004) [53]. The test set-up is shown in Figure 5.7. An electromechanical testing machine was used with a test fixture built to the ASTM D1781 specification by Wyoming Test Fixtures (Salt Lake City, UT). The specimen was installed into the test fixture and visually aligned. The spherical bearing and the alignment clevis account for any minor misalignment. One end of the specimen was clamped tangentially to the surface of the drum, opposed to the ASTM standard, which was originally designed for aluminum skins. A string was placed through the centre of the drum to prevent damage to the test fixture in case the composite skin breaks during the test. If the composite skin broke during the test, the drum would fall onto the pin and clevis, damaging the drum and loading straps. The width of the specimen was measured using a digital vernier caliper at 3 locations prior to testing the specimen. The test was performed with a crosshead displacement of 50 mm/min, until a minimum 175 mm of peel had occurred. An example of a completed climbing drum peel test is shown in Figure 5.8.

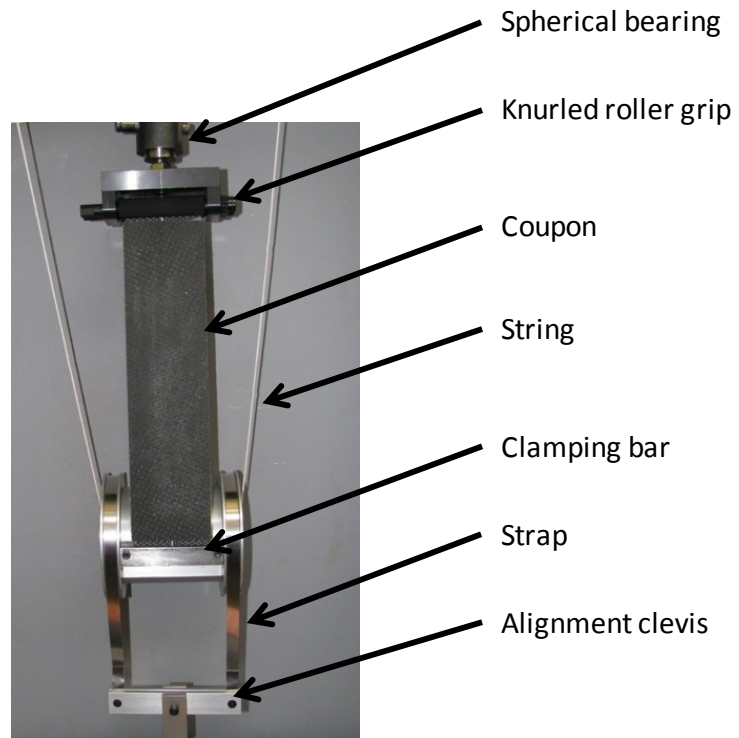


Figure 5.7: Climbing drum peel test setup.

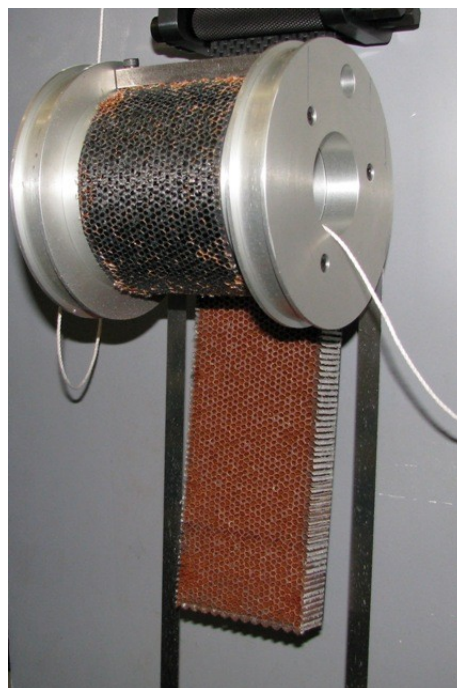


Figure 5.8: Completed climbing drum peel test.

5.6.3 Results and Discussion

The data that were recorded by the testing machine are the force required to peel the composite skin from the honeycomb core, and the displacement of the crosshead. An example of the recorded data is shown in Figure 5.9. The force required to wrap the composite skin around the drum is removed from the peel load, and an average peel load is used to determine the peel strength as specified in the standard [53]. The properties of the panels are summarized in Table 5.3. Included in the summary table is the degree of cure of the adhesive, the peel strength, and the failure morphology. The average peel strengths of the panels are presented in Figure 5.10, along with one standard deviation. The first panel constructed with AF 163-2K had the best peel strength. The peel strengths of the panels constructed with FM300-2M are proportional to the cure temperatures. From a comparative standpoint, the AF 163-2K has a higher peel strength with a lower degree of cure than the FM300-2. The AF 163-2K was visually observed to have better flow properties at lower temperature, compared to the FM300-2.

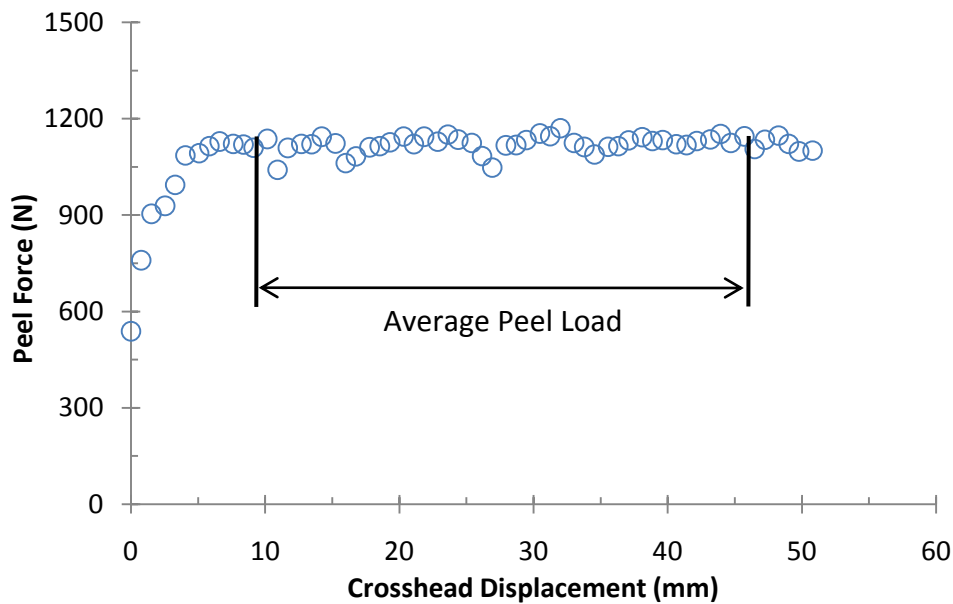
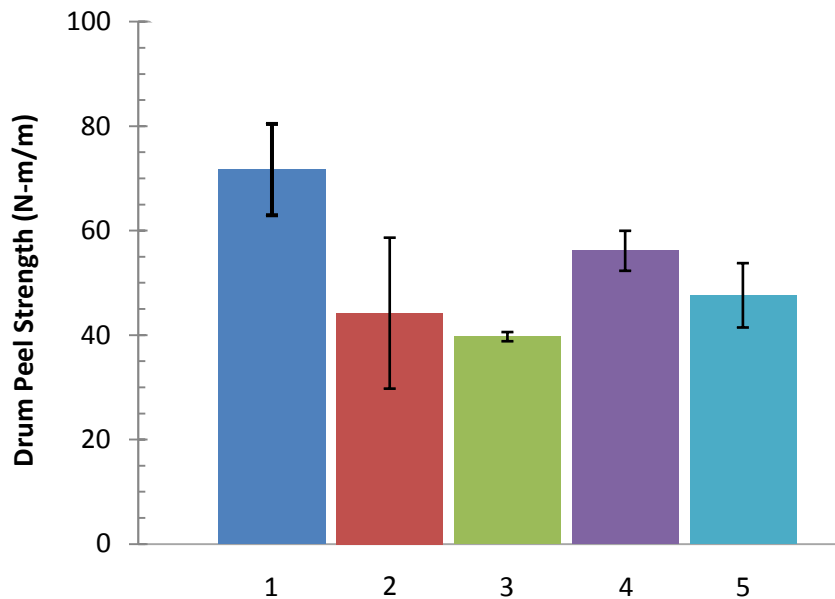


Figure 5.9: Typical climbing drum peel test data.

Table 5.3: Representative Panel Properties

<i>Panel</i>	<i>Cure Temp (°C)</i>	<i>Adhesive Degree of Cure (%)</i>	<i>Peel Strength (N-m/m)</i>	<i>Core Failure (%)</i>	<i>Adhesive Failure (%)</i>
1	100	91	71.68	82	18
2	100	83	44.19	8	92
3	80	69	39.69	6	94
4	140	99	56.13	86	14
5	120	93	47.61	90	10

**Figure 5.10: The average and one standard deviation of the climbing drum peel tests.**

The failure morphology of the tests gives an important insight into the quality of the joint between the skin and the core. The coupons failed in two different modes. The first mode was core failure and the second mode was adhesive failure. Core failure is the tearing of the core and a portion of the core remains attached to the peeled skin. Adhesive failure is the delamination of the

adhesive from the composite skin. Core failure is preferred since this indicated that the joint between the skin and core is stronger than one of the constituent materials. An example of a coupon with both core and adhesive failure is shown in Figure 5.11. The percentage of core and adhesive failure was recorded for each coupon, and the average is summarized in Table 5.3. The values were visually determined for each specimen by looking at the failure surface and assigning a percentage of core and adhesive failure, to within 10%. The test operator was consistent throughout the testing of the coupons, but the accuracy of the failure morphology should be considered to $\pm 10\%$. The FM300-2 has a higher percentage of core failure at an equivalent degree of cure than the AF 163-2, but a lower peel strength.

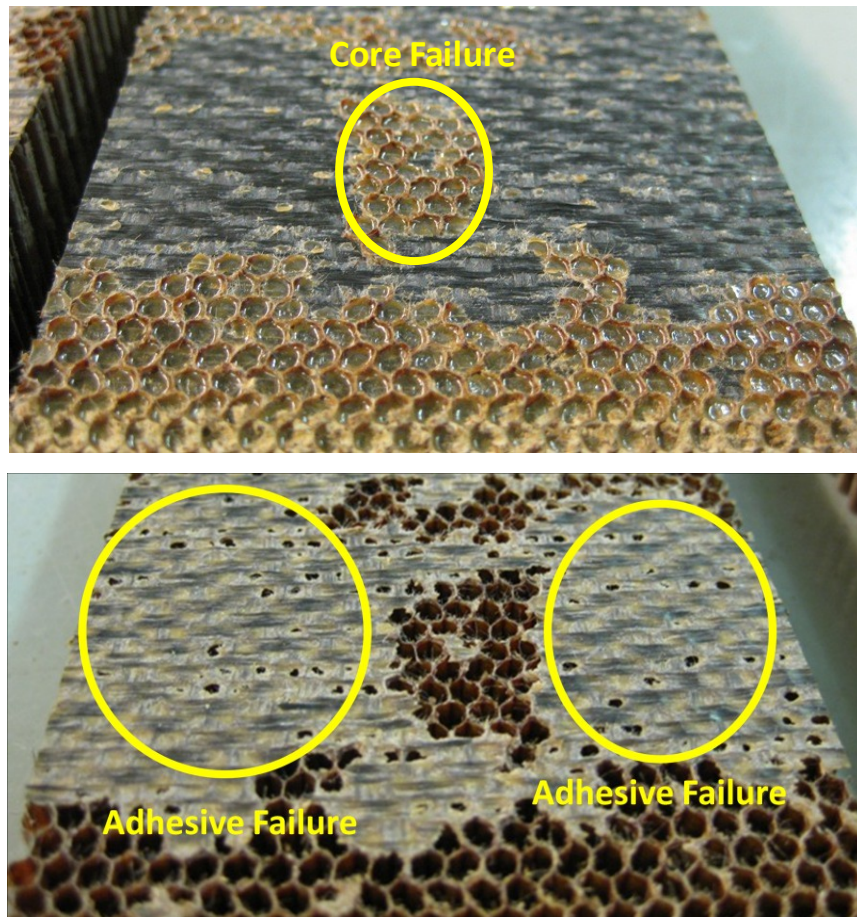


Figure 5.11: Example of core failure and adhesive failure from the same drum peel coupon.

5.7 Summary

Five panels were manufactured using conventional manufacturing techniques. The effect of cure cycle and bagging configuration were evaluated for void content, resistance to moisture ingress, and climbing drum peel strength. The panels that produced the best combination of the above were cured at full vacuum below 100°C. After curing at 100°C, the peel performance of AF 163 is better than FM300-2. The effect of post cure on peel strength was not performed.

6 Conclusion

The main objective of this work was to understand the critical parameters which affect sandwich structure quality manufactured using Out-of-Autoclave (OOA) prepreg. A secondary objective was to compare the performance of an OOA resin with an autoclave resin. A commercially available OOA prepreg (MTM45-1) with a public database was studied. The following conclusions can be drawn from this research:

1) The MTM45-1 resin was characterized

The resin characterization provides important information about the resin during the curing process. The resin is thermally stable until 110°C. However, the resin begins to flow at 80°C (a viscosity of 100 Pa-s), closing-off the air passages and reducing the permeability. The resin should be initially cured to gelation ($\alpha > 0.4$) below 110°C to avoid voids nucleating from volatiles. After gelation, the cure temperature can be increased to reduce the cure time of the material. However, the ramp rate should not exceed 0.5°C/min in order to avoid crossing the T_g and process temperatures. The fully cured T_g of the MTM45-1 is equivalent to second generation autoclave epoxies.

2) The prepreg air permeability was characterized

The air permeability of the prepreg was characterized for different flow directions, and bagging conditions. The in-plane permeability is considerably higher than the through thickness air permeability. Furthermore, a permeable release fabric (peel ply) is required for through thickness air flow. The peel ply allows the resin to flow out of the skin,

creating the highest void content, when compared to impermeable release films. In light of this, an impermeable release film was selected, and when coupled with edge breathing, the quality of the sandwich skin is excellent.

3) There exists an optimal internal core pressure

Completely evacuating the honeycomb core of the sandwich structure reduces the quality of the skin. An internal core pressure of 35 ± 5 kPa provides additional skin compaction pressure and does not flow into the skin during processing. This effect produces skins with a low void content.

4) Low temperature cures produce the best quality sandwich panels

When a low temperature cure cycle is coupled with the optimal bagging arrangement, the quality of the skin is better than a higher temperature cure cycle. Above 100°C , the void content is higher, and the voids coalesce, reducing the moisture ingress resistance of the panel.

5) AF 163 is better than FM300-2 at low cure temperatures

The peel strength of the AF 163 was higher than FM300-2 when both panels were cured at 100°C . It was visually observed that AF 163 flows better, and creates a better meniscus at the skin/core joint.

6.1 Future Work

A significant advance would be to measure the pressure inside the core of a panel cured with both skins. The technique should be applied to a large panel (1 m x 1 m) to determine if there are any pressure gradients in the panel during cure. Furthermore, a model could be developed that determines the compaction pressure of the skin based on the pressure inside the core, the applied compaction force, and the cell geometry and size. This model would be useful to understand how the cell size and geometry affect the quality of the sandwich. Finally, this process should be applied to a larger component with some curvature. Scale-up presents challenges that need to be overcome in order for OOA technology to replace the current autoclave process.

References

1. "Composites manufacturing", class notes for AERO 4608, Department of Mechanical and Aerospace Engineering, Carleton University, Fall 2005.
2. L. Repecka and J. Boyd, "Vacuum-bag-only-curable prepregs that produce void free parts," presented at the 47th International SAMPE Symposium, Long Beach, CA, May 2002.
3. P. Hubert, "Aspects of flow and compaction of laminated composite shapes during cure", PhD dissertation, the University of British Columbia, Vancouver, BC, Canada, 1996.
4. C. Ridgard, "Advances in low temperature curing prepregs for aerospace structures," presented at the 45th International SAMPE Symposium, Long Beach, CA, May 2000.
5. Scaled Composites, "SpaceShipOne Captures X-Prize," October 2004, http://www.scaled.com/projects/tierone/041004_spaceshipone_x-prize_flight_2.html.
6. J. Seferis, R. Hillermeier and F. Buehler, "Prepregging and autoclaving of thermoset composites," in *Comprehensive Composite Materials*, Vol. 2, A. Kelly and C. Zweben, Ed. Elsevier Science, 2000, p. 16.
7. S. Khan and H. Loken, "Bonding of sandwich structures the facesheet/honeycomb interface a phenomenological study," presented at the 52nd International SAMPE Symposium and Exhibition, Baltimore, MD, 2007.
8. S.S. Tavares, N. Caillet-Bois, V. Michaud and J.-A.E. Manson, "Non-autoclave processing of sandwich structures: the role of prepreg through thickness air permeability," presented at the 16th International Conference on Composite Materials, Kyoto, Japan, 2007.

9. V. Michaud, S.S. Tavares, A. Sigg, S. Lavanchy, and J.-A.E. Månson, "Low pressure processing of high fiber content composites," presented at the 8th International Conference on Flow and Processes in Composite Materials, Douai, France, 2006.
10. G. Bond and J. Luner, "Design of experiments evaluation of processing parameters for non-autoclave composite prepreg," presented at SAMPE 09, Baltimore, MD, 2009.
11. G. Bond, J. Griffith, G. Hann, C. Bongiovanni and J. Boyd, "Non-autoclave prepreg manufacturing technology," presented at the Fall SAMPE Technical Conference, Memphis, TN, 2008.
12. C. Ridgard, "Out of autoclave composite technology for aerospace, defence, and space structures," presented at SAMPE 09, Baltimore, MD, 2009.
13. K. Mitani, K. Wakabayashi and H. Shigetsugu, "A new low temperature curing prepreg," in *Proceedings of the Fourty-Sixth International SAMPE Symposium*, 2001, pp. 2293-2302.
14. K. Jackson, "Low temperature curing materials: the next generation," *SAMPE Journal*, vol 34, pp. 23-31, September/October 1998.
15. M. Steele and T. Corden, "New prepreps for cost effective, out-of-autoclave tool and component manufacture," *SAMPE Journal*, vol. 40, pp. 30-34, March/April 2004.
16. ACG MTM46 Intermediate Service Temperature Vacuum Processable Prepreg, PDS 1191/01.08/2, The Advanced Composites Group, Heanor, Derbyshire, UK.
17. ACG MTM44-1 Matrix Resin, PDS 1189/01.08/3, The Advanced Composites Group, Heanor, Derbyshire, UK.
18. ACG MTM45-1 Matrix Resin, PDS 1205/11.07/3, The Advanced Composites Group, Heanor, Derbyshire, UK.

19. ACG VTM 260 Series Variable Temperature Moulding Prepreg System, PDS 1154/05.08/6, The Advanced Composites Group, Heanor, Derbyshire, UK.
20. Cycom 5215 Modified Epoxy Resin, Out of Autoclave Processing, Technical Datasheet 082602 revision 6/11/02, Cytec Engineered Materials, Anaheim, CA.
21. Cycom 5320 Toughened Epoxy for Structural Applications, Out-of-Autoclave Manufacturing, Information Sheet Revision 1.3 – 03.18.09, Cytec Engineered Materials, Anaheim, CA.
22. Cytec 754 Modified Epoxy Resin, Technical Datasheet 080602, Cytec Engineered Materials, Anaheim, CA
23. EP142-C510-50 Carbon Reinforced Epoxy Prepreg, PDS EP142-C510-50-1-0907, Gurit, Zullwil, Switzerland.
24. ST 95 Carbon Structural SPRINT, PDS-- ST 95carbon-3-0309, Gurit, Newport, Isle of Wight, UK.
25. HexPly M36 Epoxy Matrix, Product Data, Hexcel
26. HexPly M9/M10 Epoxy Matrix, Product Data, Hexcel
27. S.S. Tavares, V. Michaud and J.-A.E. Månson, "Semipregs: how through thickness air permeability and resin flow correlate during vacuum-bag only cure," in Proceedings of the 9th International Conference on Flow Processes in Composite Materials, Montreal, QC, 2008.
28. Gurit Materials and Technology for Composite Processing, online reference, <http://www.gurit.com/page.asp?section=00010001002800110004sectionTitle=SPRINT+is+Gurit%27s+unique+composite+technology>, accessed May 2009.
29. K.J. Ahn, J.C. Seferis, J.O. Price and A.J. Berg, "Permeation measurements through prepreg laminates," *SAMPE Journal*, vol. 27, pp. 19-26, November/December 1991.

30. J.W. Putnam and J.C. Seferis, "Prepreg gas permeation as a function of fiber orientation and aging time," *Journal of Advanced Materials*, vol. 26, pp. 35-41, April 1995.
31. J.-D. Nam, J.C. Seferis, S.-W. Kim and K.-J. Lee, "Gas permeation and viscoelastic deformation of prepregs in composite manufacturing processes," *Polymer Composites*, vol. 16, pp. 370-377, October 1995.
32. S.B. Shim and J. Seferis, "Thermal and air permeation properties of a carbon fibre / toughened epoxy based prepreg system," *Journal of Applied Polymer Science*, vol. 65, pp. 5-16, July 1997.
33. A.W. Alteneder, D.J. Renn, J.C. Seferis and R.N. Curran, "Processing and characterization studies of honeycomb composite structures," in *the proceedings of the 38th International SAMPE Symposium and Exhibition*, 1993, pp. 1034-1067.
34. P. Jouin, D. Pollock and E. Rudisill, "Effects of processing variables on the quality of co-cured sandwich panels," in *Composite Materials: Testing and Design*, Vol 10, G.C. Grimes ed., ASTM Special Technical Publication, Philadelphia: ASTM International, 1992, pp. 293-307.
35. R. Okada and M.T. Kortschot, "The role of the resin fillet in the delamination of honeycomb sandwich structures," *Composites Science and Technology*, 62 (2002), pp, 1811-1819.
36. S. M. Grove, E. Popham and M.E. Miles, "An investigation of the skin/core bond in honeycomb sandwich structures using statistical experimentation techniques," *Composites Part A: Applied Science and Manufacturing*, 37 (2006), pp. 804-812.
37. S.B. Shim, J.C. Seferis and W. Hudson, "Different lay-up procedure influences on final porosity distribution in a carbon/toughened epoxy structural composite system," in *Proceedings of the Twenty-ninth International SAMPE Technical Conference*, 1997, pp. 495-504.

38. C. Slough, "Weight loss determined from mass spectrometry trend data in a thermogravimetric/mass spectrometer system," TA Instruments Application Brief No. 306.
39. B. Cassel, "How Tzero technology improves DSC Performance Part IV: MDSC enhancement," TA Instruments Application Brief No. 282.
40. D. McRae and S. Hunt (private communication), 2009.
41. K. Cole, "New approach to modeling the cure kinetics of epoxy amine thermosetting resins. 1. Mathematical development," *Macromolecules*, vol. 24, pp. 3093-3097, May 1991.
42. M. Parker, Test Methods for Physical Properties, in *Comprehensive Composite Materials*, Vol. 5, A. Kelly and C. Zweben, Ed. Elsevier Science, 2000, pp. 10-27.
43. K. Menard, *Dynamic Mechanical Analysis A Practical Introduction*, New York: CRC Press, 1999.
44. F. Morrison, *Understanding Rheology*, New York: Oxford University Press, 2001.
45. Kenny, J.M., Apicella, A. and Nicolais, L., "A model for the thermal and chemorheological behavior of thermosets I: processing of epoxy based composites," *Polymer Engineering and Science*, Vol. 29, pp. 973-983, 1989.
46. TA Instruments, "Characterization of epoxy reinforced glass by DSC and DMA," TA Instruments Thermal Solution 66.
47. ASTM Technical Staff, "Standard test method for glass transition temperature (DMA Tg) of polymer matrix composites by dynamic mechanical analysis (DMA)," Standard D 7028-07, Jan 2008.
48. S. Kalpakjian and S. Schmid, *Manufacturing Engineering and Technology*, 4th Ed., Toronto: Prentice-Hall, pp. 185, 2001.
49. A. DiBenedetto, "Prediction of the glass transition temperature of polymers: a model based on the principle of corresponding states," *Journal*

- of Polymer Science, Part B (Polymer Physics)*, Vol. 25, pp. 1949-69, September 1987.
50. Cytec Engineered Materials Technical Staff, *Cycom 5276-1 Toughened Epoxy Resin*, Cytec Industries, Tempe, Arizona, 2002.
 51. Hexcel Prepreg Technical Staff, *HexPly 8552 Epoxy Matrix*, Hexcel Corporation, Stamford, Connecticut.
 52. UTHSCSA ImageTool, downloaded 30 March 2009, available at <http://ddsdx.uthscsa.edu/dig/itdesc.html>. Last revision 22 February 2002.
 53. ASTM Standard D1781, 1998 (2004), "Standard Test Method for Climbing Drum Peel for Adhesives," ASTM International, West Conshohocken, PA, www.astm.org.

Appendix A - DMA Test Data

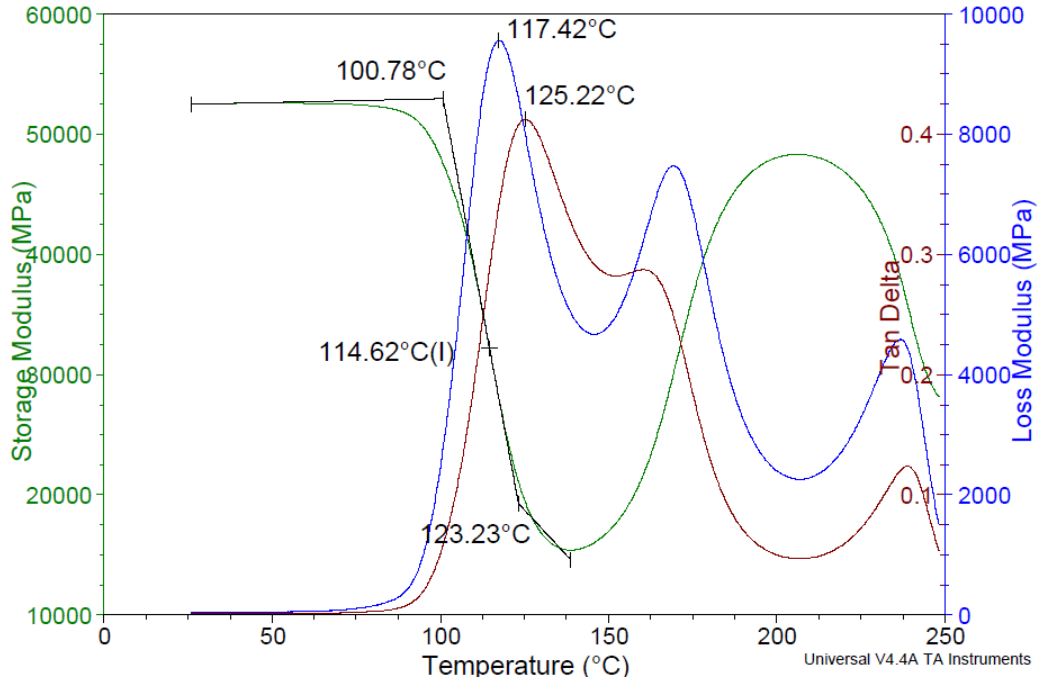


Figure A.1: DMA test results of two plies of MTM45-1/CF2426A which was cured at 80°C for 24 hours.

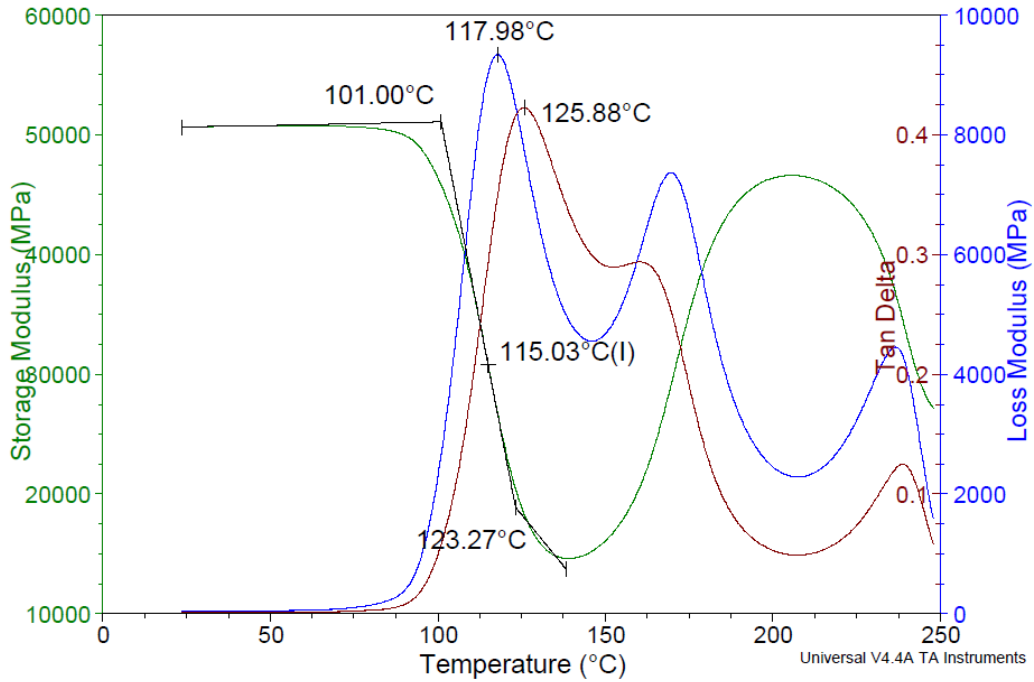


Figure A.2: DMA test results of two plies of MTM45-1/CF2426A which was cured at 80°C for 24 hours.

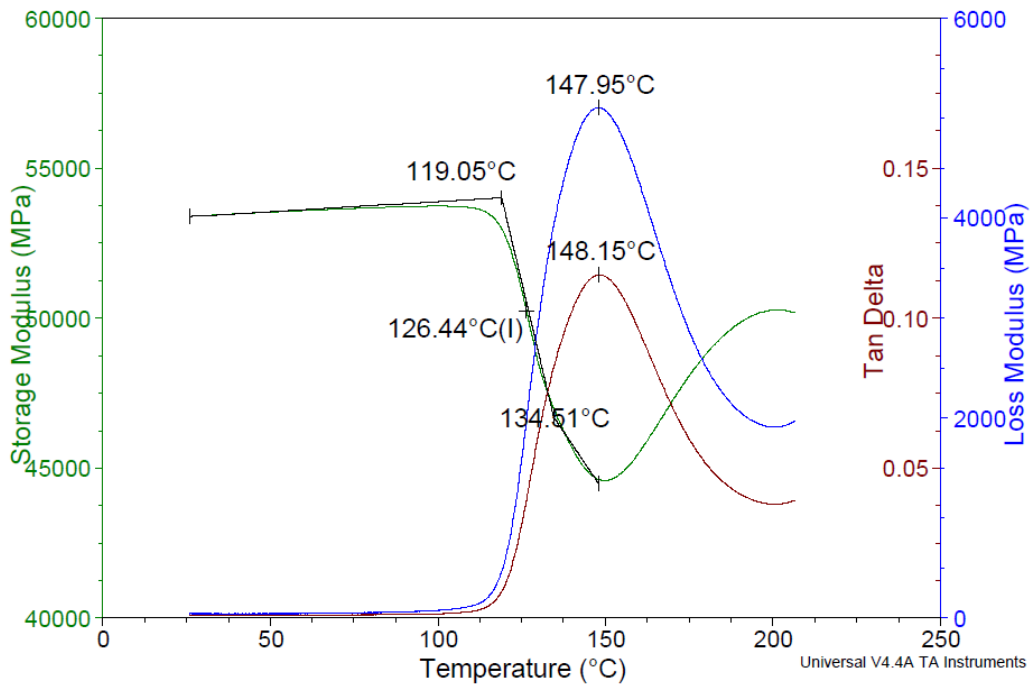


Figure A.3: DMA test results of two plies of MTM45-1/CF2426A which was cured at 100°C for 12 hours.

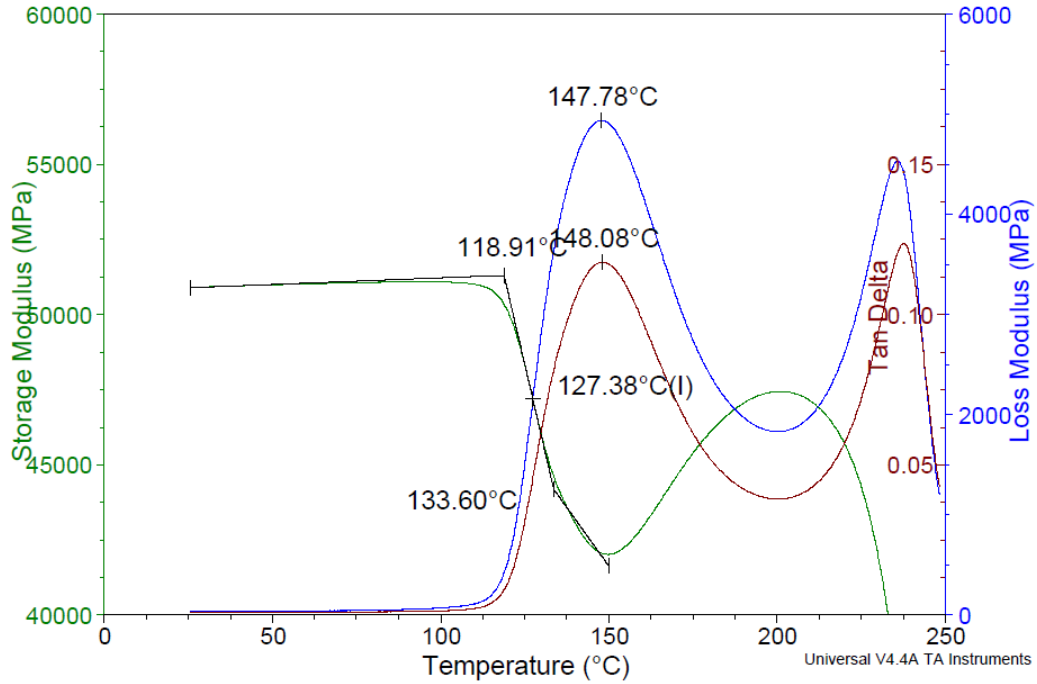


Figure A.4: DMA test results of two plies of MTM45-1/CF2426A which was cured at 100°C for 12 hours.

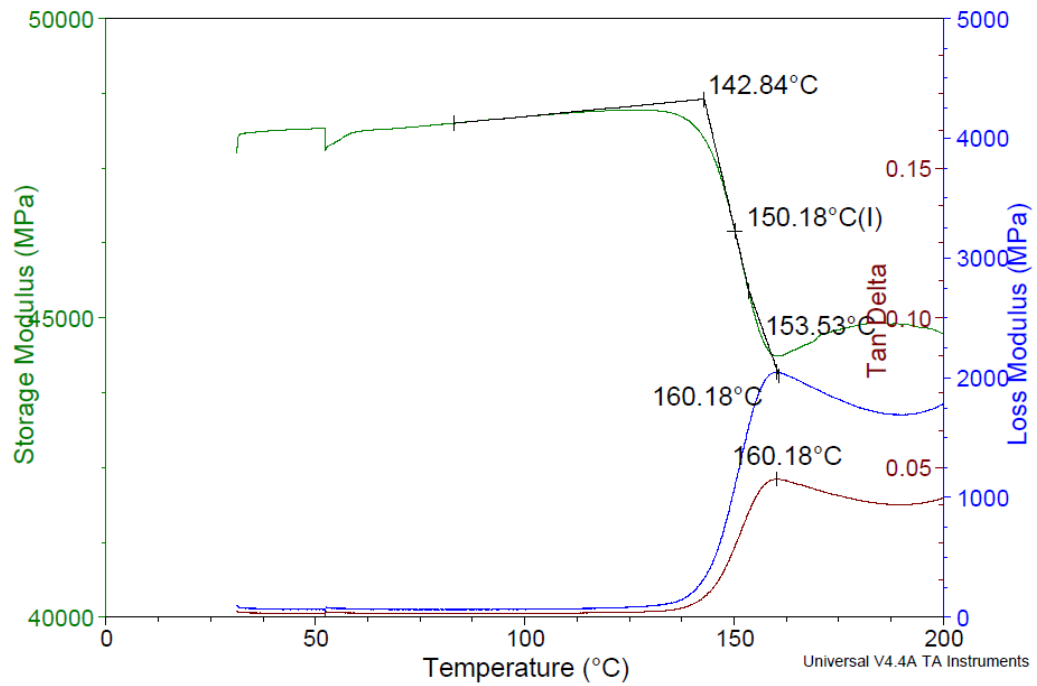


Figure A.5: DMA test results of two plies of MTM45-1/CF2426A which was cured at 120°C for 6 hours.

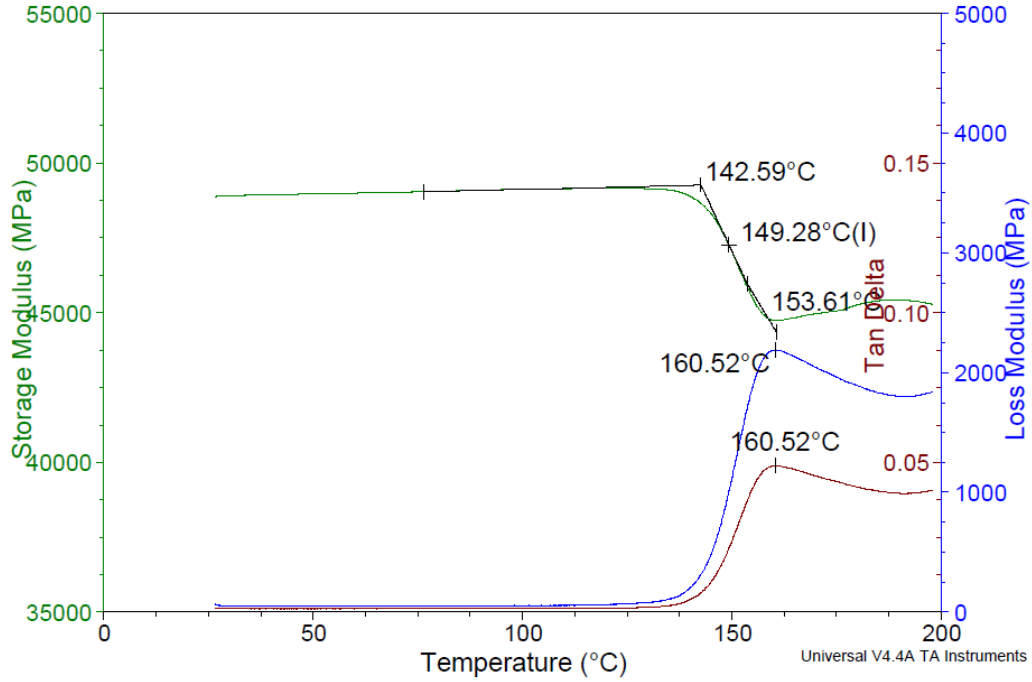


Figure A.6: DMA test results of two plies of MTM45-1/CF2426A which was cured at 120°C for 6 hours.

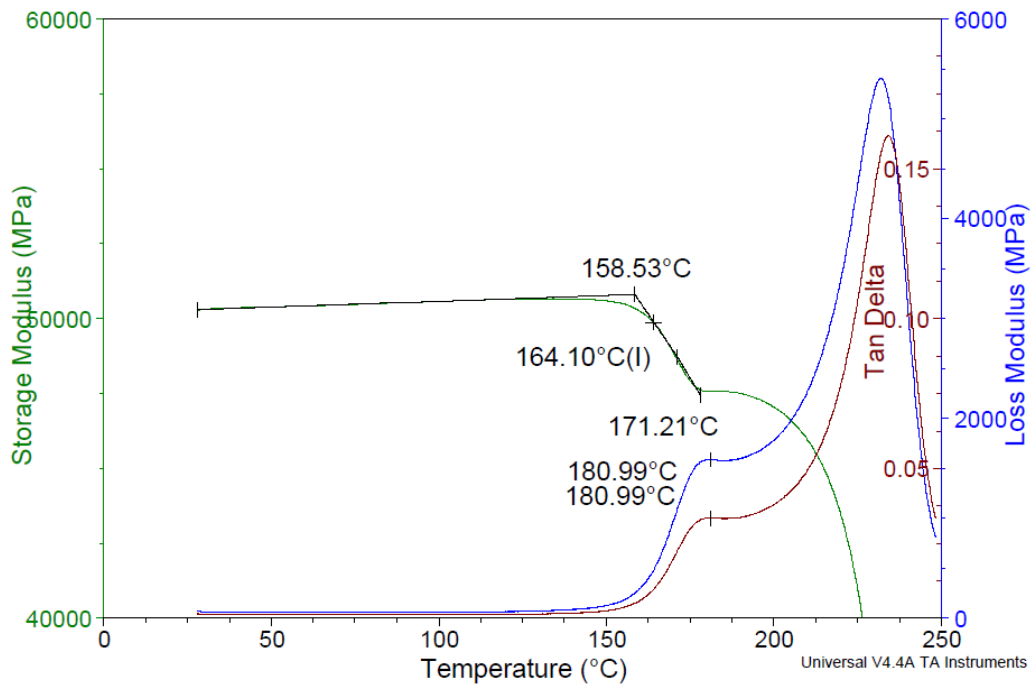


Figure A.7: DMA test results of two plies of MTM45-1/CF2426A which was cured at 140°C for 2 hours.

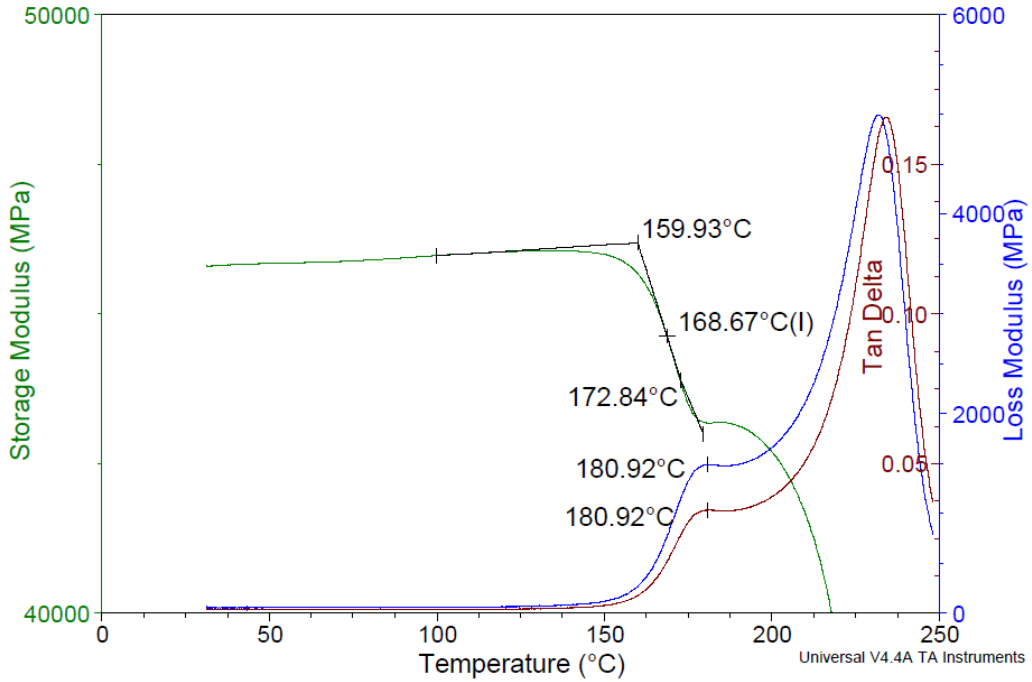


Figure A.8: DMA test results of two plies of MTM45-1/CF2426A which was cured at 140°C for 2 hours.

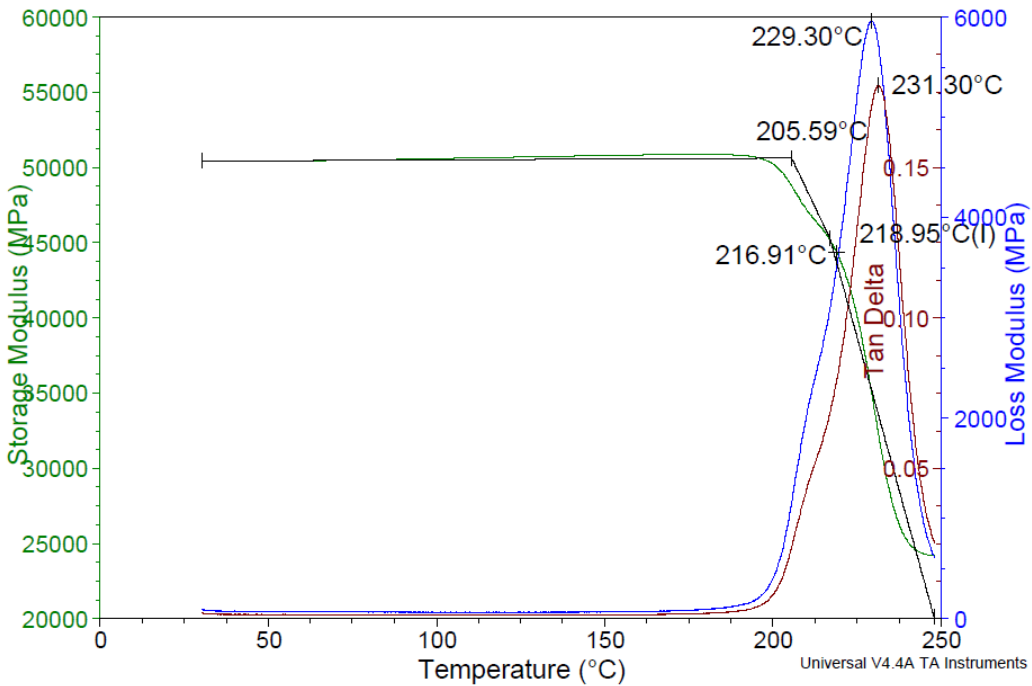


Figure A.9: DMA test results of two plies of MTM45-1/CF2426A which was cured at 180°C for 2 hours.

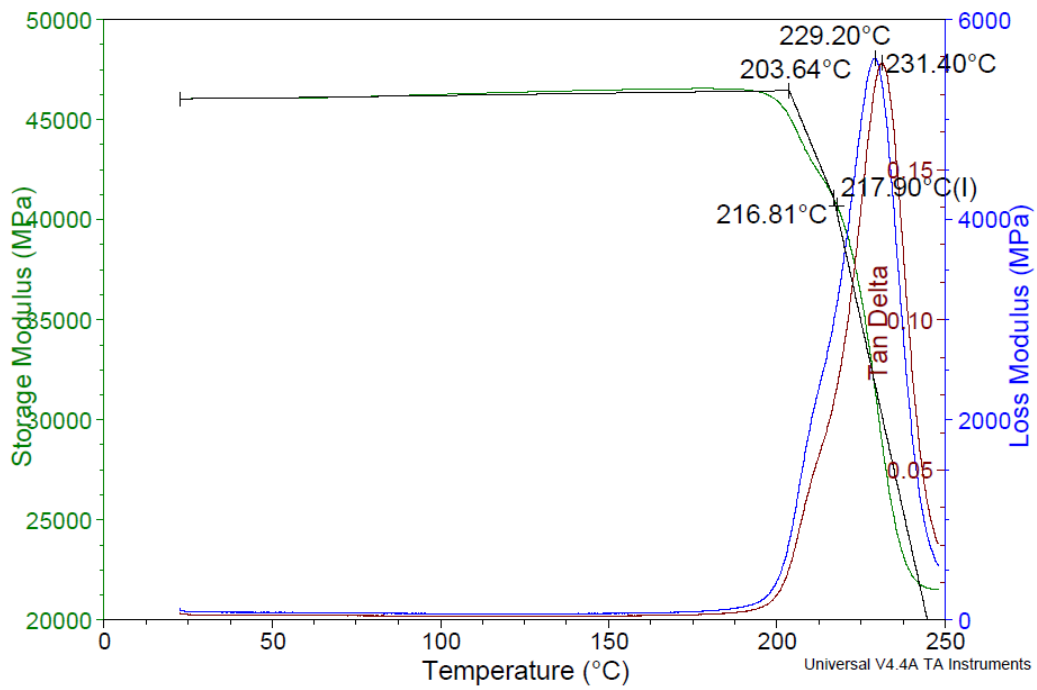


Figure A.10: DMA test results of two plies of MTM45-1/CF2426A which was cured at 180°C for 2 hours.

Appendix B – Permeability Test Data

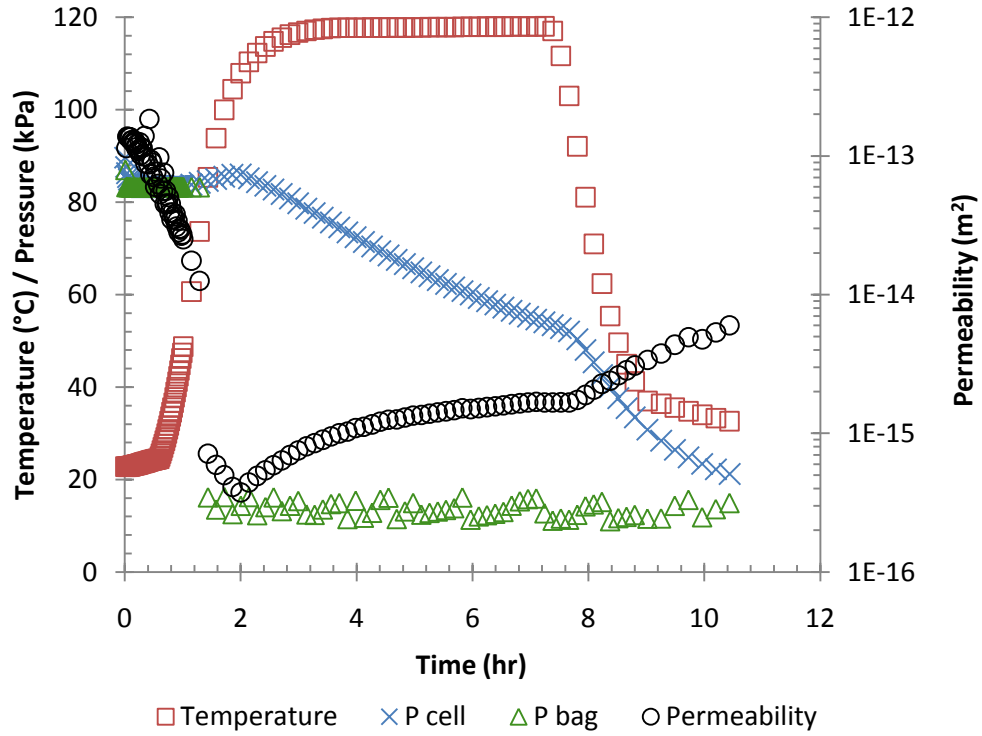


Figure B.1: Through thickness permeability test of 4 plies MTM45-1 prepreg with 1 layer of peel ply.

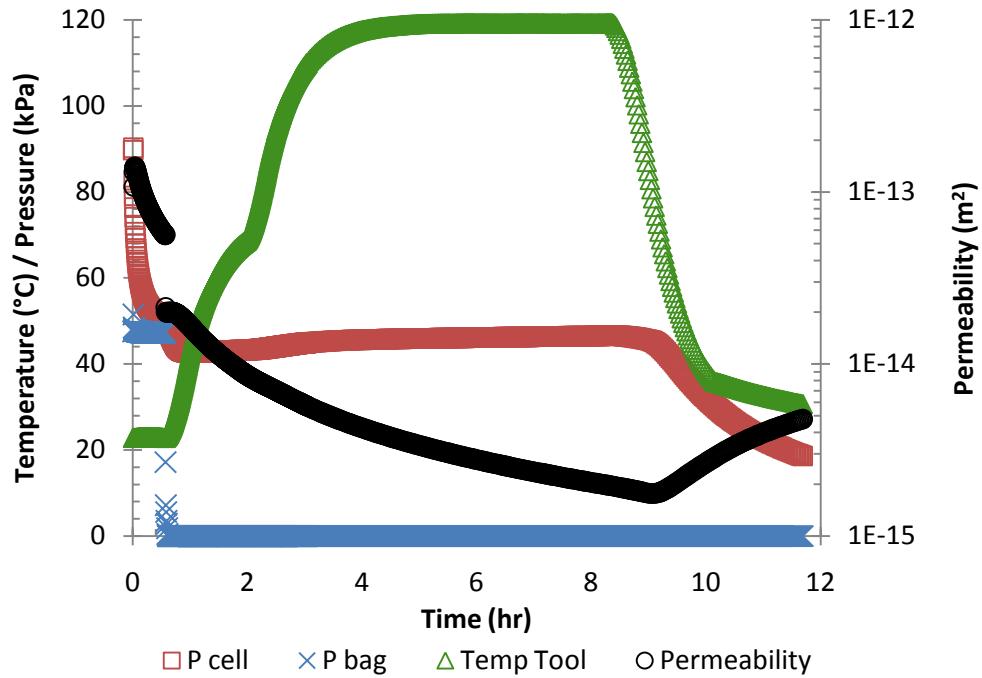


Figure B.2: In-plane permeability test 1. Layup consisted of 4 plies of MTM45-1 prepreg. Bagging configuration was 2 plies P3 release film with edge breathing.

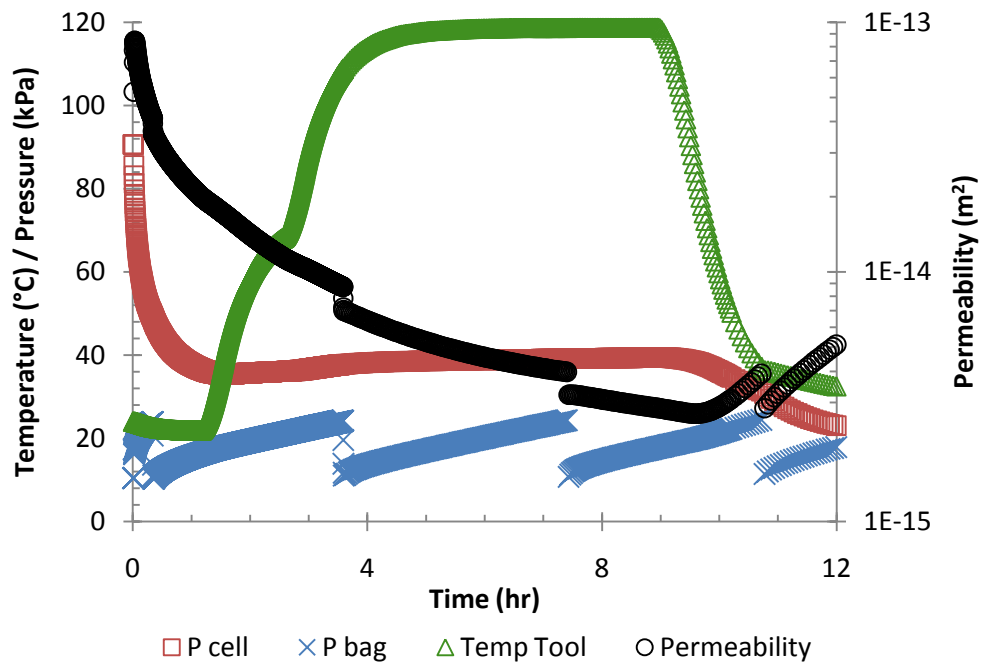


Figure B.3: In-plane permeability test 2. Layup consisted of 4 plies of MTM45-1 prepreg. Bagging configuration was 2 plies P3 release film with edge breathing.

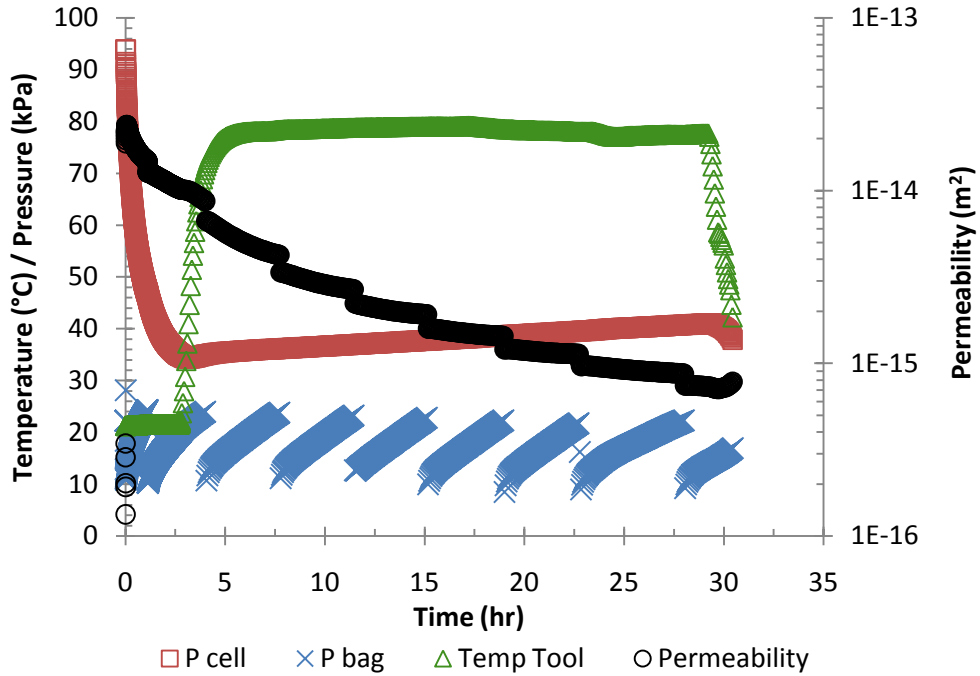


Figure B.4: In-plane permeability test 3. Layup consisted of 4 plies of MTM45-1 prepreg. Bagging configuration was 2 plies P3 release film with edge breathing.

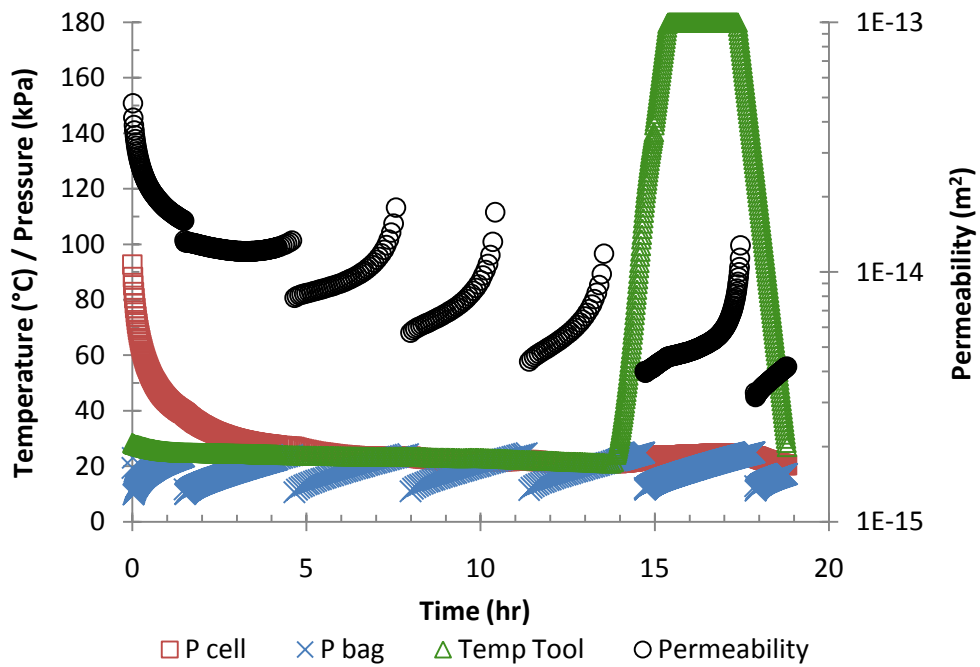


Figure B.5: In-plane permeability test 4. Layup consisted of 4 plies of MTM45-1 prepreg. Bagging configuration was 2 plies P3 release film with edge breathing.

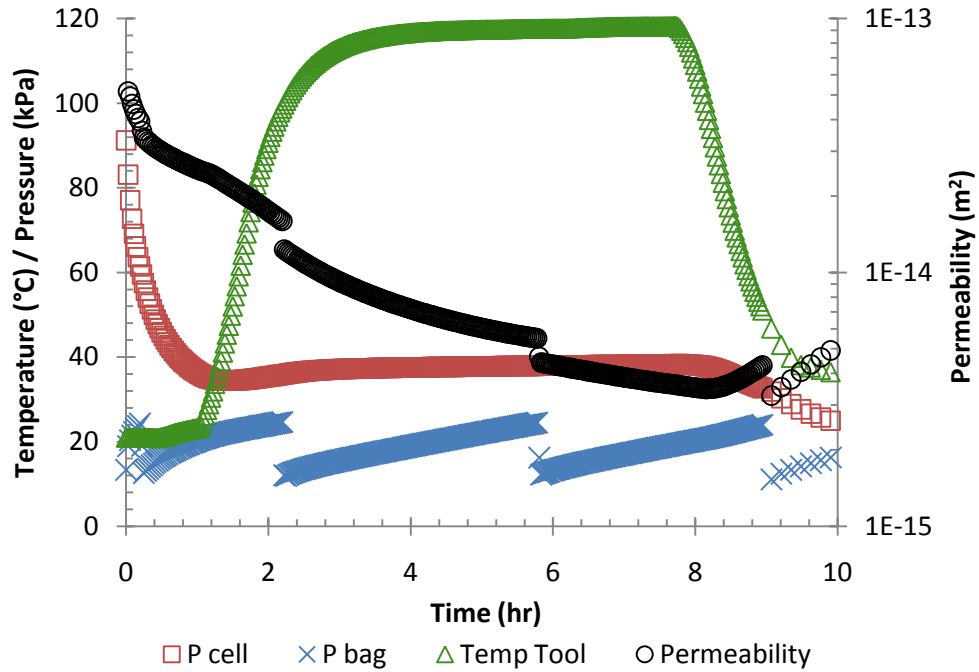


Figure B.6: In-plane permeability test 5. Layup consisted of 4 plies of MTM45-1 prepreg. Bagging configuration was 2 plies P3 release film with edge breathing.

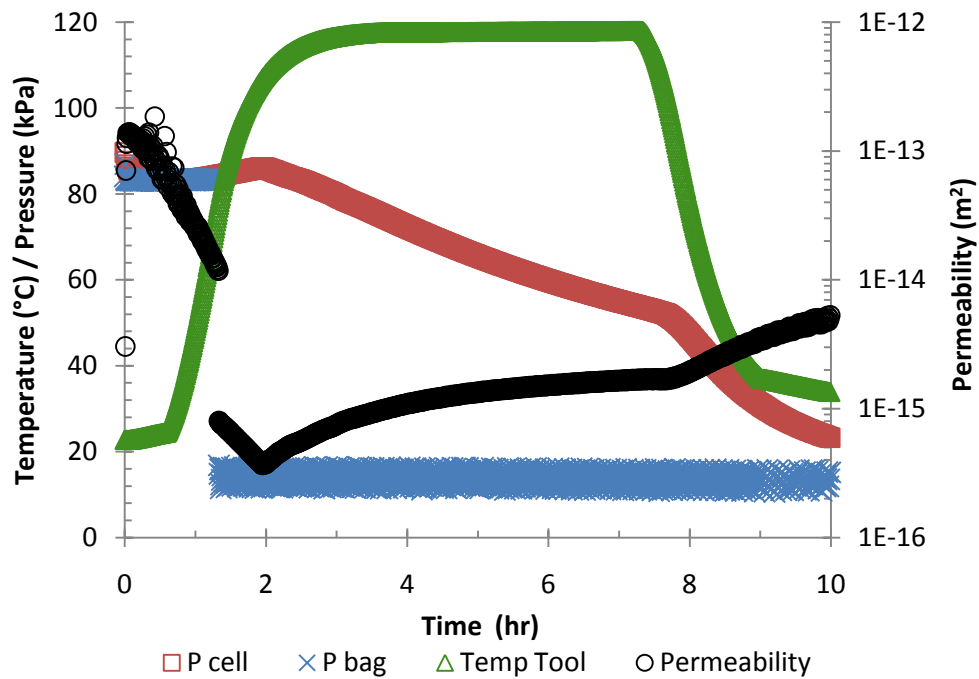


Figure B.7: In-plane permeability test 6. Layup consisted of 4 plies of MTM45-1 prepreg. Bagging configuration was 2 plies P3 release film with edge breathing.

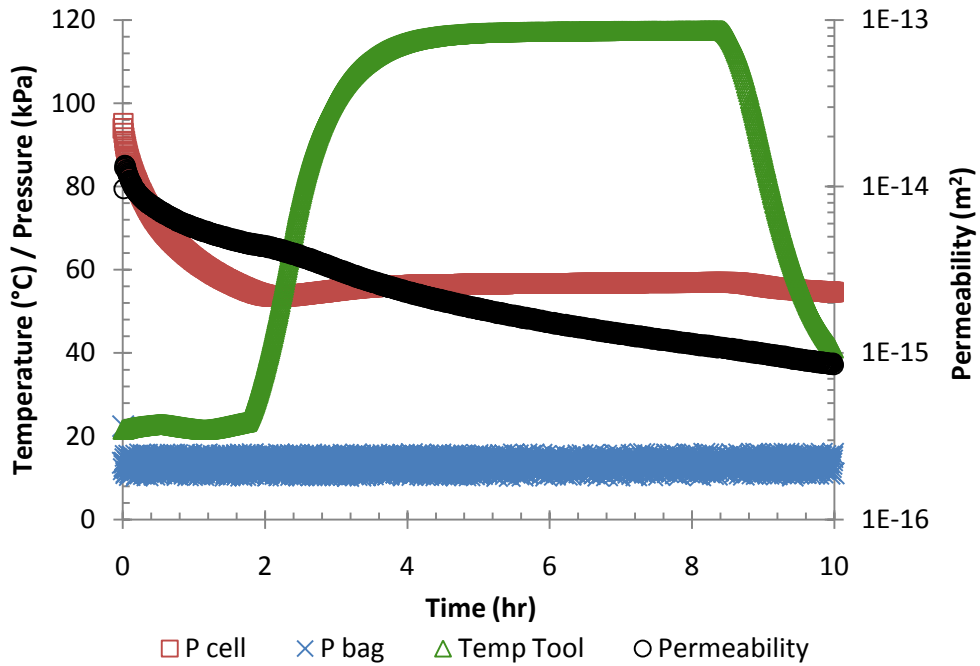


Figure B.8: In-plane permeability test 7. Layup consisted of 4 plies of MTM45-1 prepreg. Bagging configuration was 2 plies P3 release film *without* edge breathing.

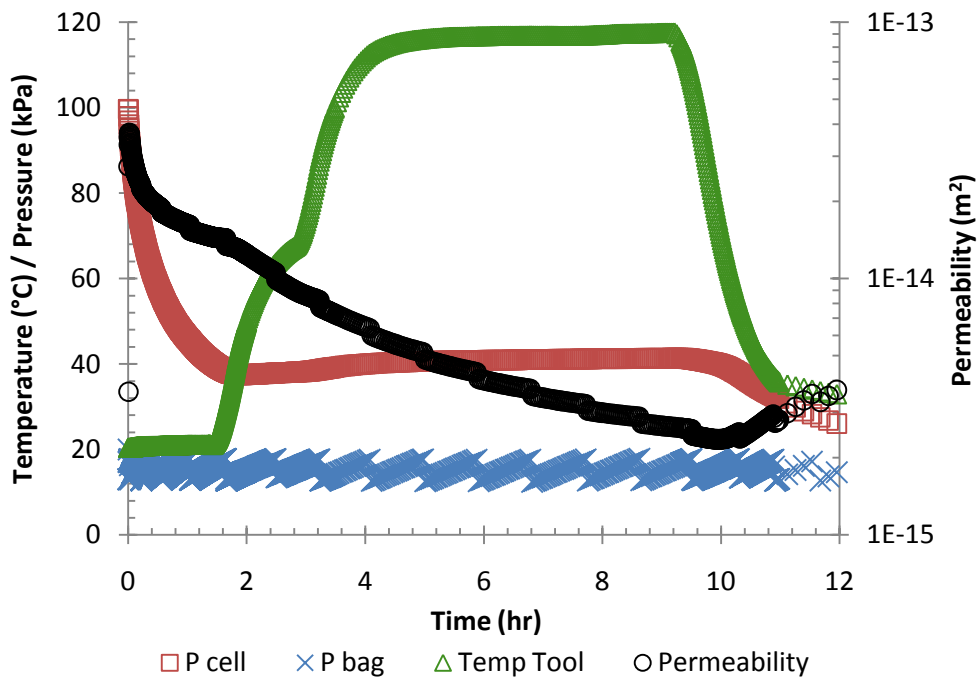


Figure B.9: In-plane permeability test 8. Layup consisted of 4 plies of MTM45-1 prepreg. Bagging configuration was 1 ply non-perf release film with edge breathing.

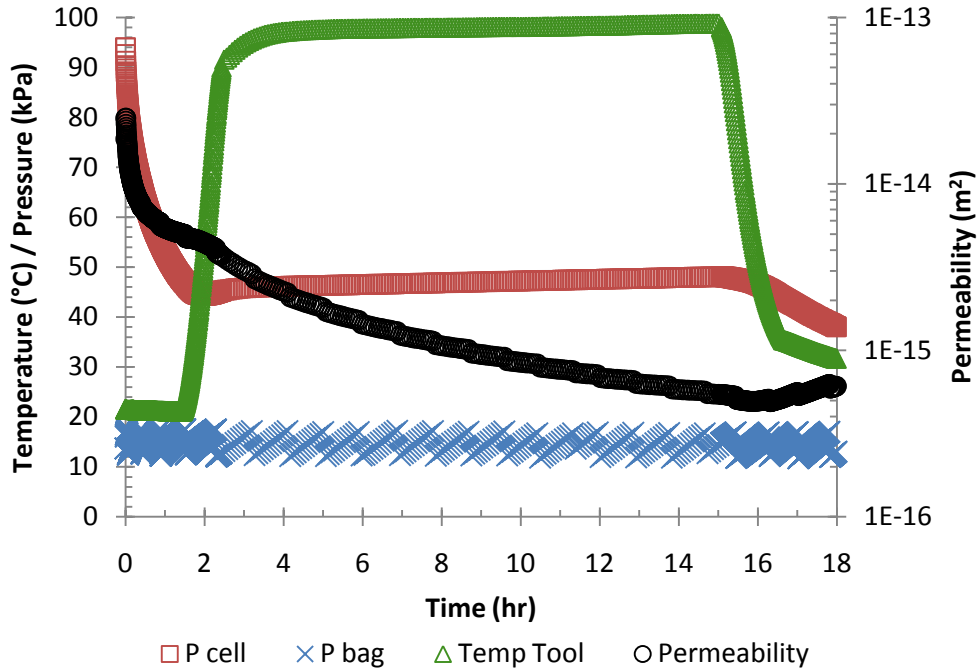


Figure B.10: In-plane permeability test 9. Layup consisted of 2 plies of MTM45-1 prepreg and 1 ply of AF 163 film adhesive. Bagging configuration was 1 ply non-perf release film with edge breathing.

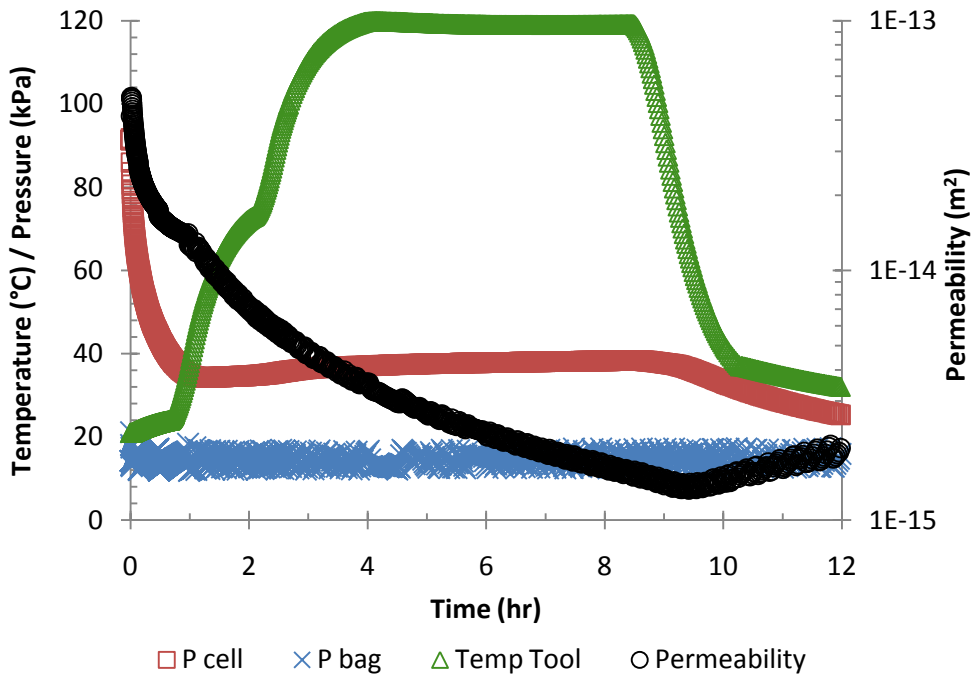


Figure B.11: In-plane permeability test 10. Layup consisted of 2 plies of MTM45-1 prepreg and 1 ply of AF 163 film adhesive. Bagging configuration was 1 ply non-perf release film with edge breathing.

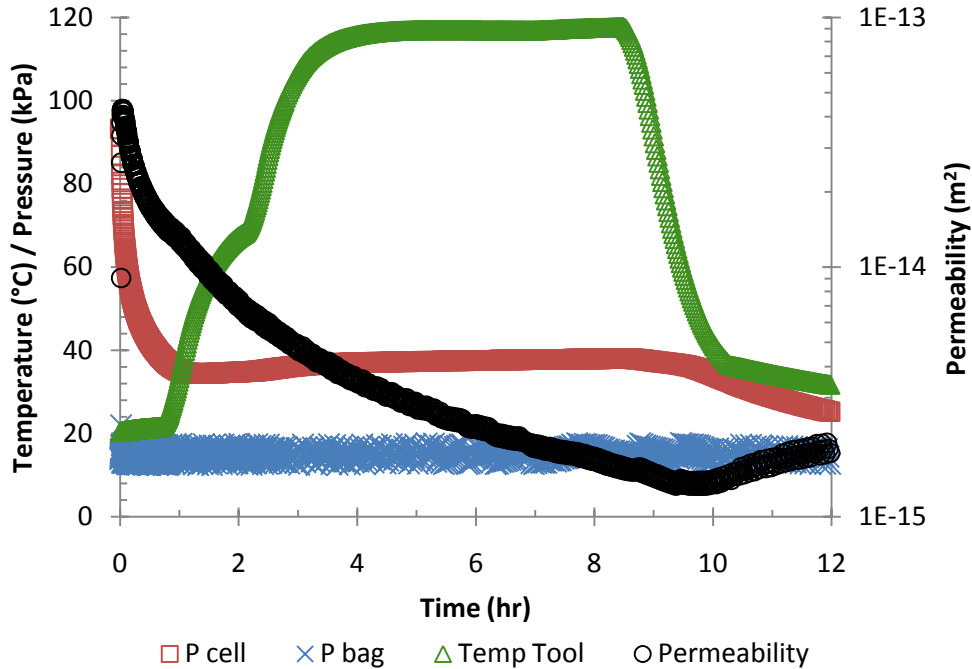


Figure B.12: In-plane permeability test 11. Layup consisted of 2 plies of MTM45-1 prepreg and 1 ply of FM300-2 film adhesive. Bagging configuration was 1 ply non-perf release film with edge breathing.

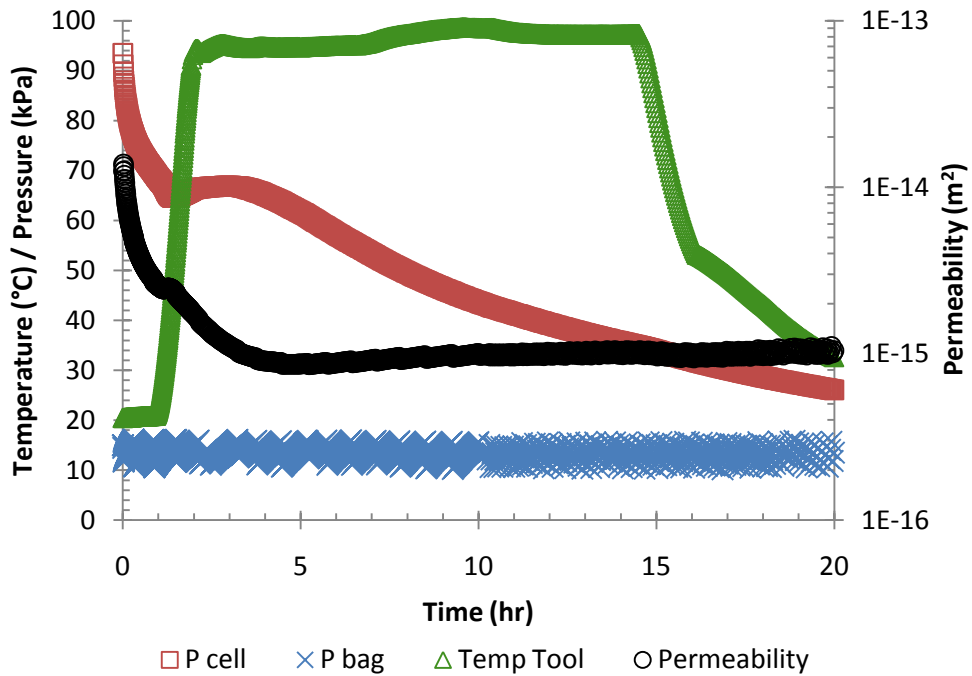


Figure B.13: In-plane permeability test 12. Layup consisted of 2 plies of MTM45-1 prepreg and 1 ply of FM300-2 film adhesive. Bagging configuration was 1 ply P3 release film *without* edge breathing.